BIOPHYSICAL AND BIOANALYTICAL ANALYSIS OF THE IRON-OME IN MITOCHONDRIA ISOLATED FROM *Saccharomyces cerevisiae*

A Dissertation

by

JESSICA HOPE GARBER MORALES

Submitted to the Office of Graduate Studies of
Texas A&M University
in partial fulfillment of the requirements for the degree of

DOCTOR OF PHILOSOPHY

May 2010

Major Subject: Chemistry

BIOPHYSICAL AND BIOANALYTICAL ANALYSIS OF THE IRON-OME IN MITOCHONDRIA ISOLATED FROM *Saccharomyces cerevisiae*

A Dissertation

by

JESSICA HOPE GARBER MORALES

Submitted to the Office of Graduate Studies of
Texas A&M University
in partial fulfillment of the requirements for the degree of

DOCTOR OF PHILOSOPHY

Approved by:

Chair of Committee,	Paul A. Lindahl
Committee Members,	David Russell
	Gyula Vigh
	James Hu
Head of Department,	David Russell

May 2010

Major Subject: Chemistry

ABSTRACT

Biophysical and Bioanalytical Analysis of the Iron-ome in Mitochondria Isolated from *Saccharomyces cerevisiae.* (May 2010)

Jessica Hope Garber Morales, B.S., Virginia Commonwealth University

Chair of Advisory Committee: Dr. Paul A. Lindahl

An integrative biophysical and bioanalytical approach to studying the Fe distribution in isolated mitochondria was developed. This procedure involved large-scale growths, the inclusion of a chelator in isolation buffers and an anaerobic isolation protocol. Electron microscopy confirmed that mitochondrial membranes were intact and that samples were largely devoid of contaminants. The Fe-ome—the sum of all Fe species in mitochondria--was studied using a combination of EPR, Mössbauer Spectroscopy, Electron Absorption, ICP-MS and Protein analysis.

Isolated mitochondria were packed prior to analysis to improve the S/N ratio. The residual buffer content of sample pellets was determined by use of a radio-labeled buffer. There was essentially no difference in the packing efficiency of mitochondria isolated from respiring and fermenting cells. The determined packing factor, 0.80, was used to calculate concentrations of individual species in neat mitochondria.

The Fe-omes of mitochondria isolated from cells grown on respiring, respirofermenting and fermenting media were determined. Neat mitochondria contained ~ 750 μM Fe, regardless of whether the cells had been grown on respiring or fermenting media. The Fe distribution of respirofermenting samples (which can undergo respiration and fermentation simultaneously) was nearly identical to that of respiring mitochondria. Fermenting samples had a very different Fe-distribution.

Nearly 40 % of the iron in respiring mitochondria was present in respiratory complexes including cytochrome c, cytochrome bc_1, succinate dehydrogenase, and cytochrome c oxidase. Fermenting mitochondria contain an Fe-ome dominated by non-protein centers. Approximately 80 % of the Fe was present as a combination of nonheme HS Fe^{2+}, nonheme Fe^{3+} and Fe^{3+} nanoparticles. These centers were present in roughly equal amounts. The remaining 20 % of the Fe was present as respiratory complexes which have concentrations ~ ½ to $^1/_3$ that of respiring mitochondria.

A model is presented in which the nonheme HS Fe^{2+} species serves as a feedstock for Fe/S and heme biosynthesis. When the cell is growing on respiring media, this metabolic reservoir diminishes as respiratory complexes are constantly synthesized. Under fermentative growth, the metabolic pool increases due to the reduced demand for respiration-related prosthetic groups.

DEDICATION

For my husband who can be both incredible and incredibly aggravating all at the same time. And who, just when I needed it most, went out to buy us a couch and came back with a puppy instead. I would not have finished this document without your support, encouragement, understanding and patience.

And for my parents who taught me the importance of both family and humor as well as the inevitable integration of the two. I love you guys!

ACKNOWLEDGEMENTS

This dissertation would not have been possible without the constant encouragement and guidance of many individuals. It is an honor to be able to formally thank them here.

I would like to thank my advisor, Paul Lindahl. His enthusiasm for science and his determination in research are truly inspiring. It was amazing to work on a project that developed so rapidly and for someone so open to new directions. I am immensely grateful for his insights to grant writing, encouragement for participation at conferences and his open door policy. I am indebted for the many opportunities he has given to me. Thanks so much, Paul!!!

I would also like to thank my committee; Professors Gyula Vigh, David Russell and James Hu. Their advice and insights offered over the past few years have been indispensible. Their suggestions helped develop the proteomics aspects of this projects. Thank you all so much for your mentoring and your guidance!

I am indebted to the other members of the Lindahl group who contributed in one way or another to this work. I would specifically like to mention Ren Miao and Gregory Holmes-Hampton who have worked closely with me and who have contributed greatly to the design and implementation of many experiments. They always keep a sunny disposition that makes it a pleasure to work along-side them. I am sure that wherever I end up, I will miss their singing. In addition,

I would like to thank Ivan Surovtsev, Allison Cockrell, Jinkyu Park, Sean McCormick and Nema Jhurry. I really appreciate their support and advice.

Other valuable contributions originated from Professor Eckard Münck's Lab at Carnegie Mellon University. The assistance in obtaining Mössbauer spectra on their high field instrument was very helpful. In addition I could not have interpreted Mössbauer spectra without the assistance of Dr. Yi Lu or Yisong (Alex) Guo. I would also like to thank Ysong Guo and Professor Michael Hendrich (Carnegie Mellon University) for their assistance in interpreting EPR spectra.

I would also like to thank my family and friends for their understanding and support. I know there were times when I was virtually unreachable while I 'lived' in lab. Thank you all for not only understanding, but encouraging my growth. I am fairly certain that I would not have been able to make it through some of my roadblocks without the advice and weekly conferences with my friends and fellow graduate students Shelley and Chris. You guys are the best! I don't know what I would have done without Laura or Brittany who made it possible for me to stay at work late while they took care of Bear and made dinner for us all. You are awesome! I would also like to thank the girls who participated in the GG and GA events that kept me focused and recharged.

I would like to acknowledge the Welch Foundation, the National Science Foundation and the National Institute of Health for their financial support. The opportunities and interactions provided by these grants were indispensible. The

NIH's Chemistry Biology Interface financially supported me for two years. More importantly, this program introduced me to a great group of individuals and taught me how to interact with scientists in other fields. The NSF G-K12 teaching grant financially supported me for one year and allowed me to bring my research to G-K12 classrooms. My participation in both of these training grants continually renewed my love for science and kept me motivated in research. I could not have finished this dissertation without either opportunity.

Most importantly, I would also like to thank God for giving me the strength, determination and confidence to finish this document. It has been remarkable to study some of the details of His Creation.

TABLE OF CONTENTS

CHAPTER Page

CHAPTER Page

LIST OF FIGURES

FIGURE Page

FIGURE Page

LIST OF TABLES

NOMENCLATURE

OM	Outer membrane
IM	Inner membrane
IMS	Inner membrane space
M	Matrix
ETC	Electron transport chain
ATP	Adenosine triphosphate
EPR	Electron paramagnetic resonance
LS	Low spin
HS	High spin
ROS	Reactive oxygen species
NADH	Nicotinamide adenine dinucleotide
ISC	Iron sulfur cluster
BPS	Bathophenanthroline disulfonic acid
EXAFS	Extended X-ray absorption fine structure
CIA	Cytosolic iron sulfur cluster assembly machinery
ISC	Iron sulfur cluster
ER	Endoplasmic reticulum
OD_{600}	Optical density at 600 nm
YPD	Yeast extract, peptone, dextrose media
RPM	Revolutions per minute

PMSF	Phenylmethanesulfonylfluoride
EGTA	Ethylene glycol tetraacetic acid
HEPES	4-(2-Hydroxyethyl)-1-piperazineethanesulfonic acid
RCF	Relative centrifugal force
S/N	Signal to noise ratio
CPM	Counts per minute
DRC	Dynamic reaction cell
BSA	Bovine serum albumin
BCA	Bicinchoninic acid
ESR	Electron spin resonance
ICP-MS	Inductively coupled plasma mass spectrometry
NHHS	Non-heme high spin
R	Respiring
RF	Respirofermenting
F	Fermenting
WCR	Whole cell respiring
WCF	Whole cell fermenting
T	Telsa

CHAPTER I

INTRODUCTION

The Importance of Mitochondria in Eukaryotic Respiration

Mitochondria are organelles essential for nearly all eukaryotic cells. Physiologically they have four architectural compartments/components; the outer membrane (OM), the inner membrane (IM), inner membrane space (IMS) and the matrix. See Figure 1-1. The OM is highly porous and contains porins which allow molecules and nutrients smaller than ~ 5 kDa to flow in and out freely (1). Most metabolites will therefore have the same concentration in the IMS as in the cytosol (1). Larger molecules and proteins that need to transport through the membranes require the assistance of the translocase of the outer membrane (TOM) (2-4). Proteins are usually directed to the mitochondria by sequences of amino acids. Although these are usually present as precursor sequences, large, multimeric or multi-spanning proteins will sometimes contain internal sequences (3, 5-6). Sequences of IM and matrix-directed proteins are recognized and bound by receptors of the TOM complex which then mediates translocation across the outer membrane (2, 7).

The IM is highly invaginated and its folds, or cristae, consist primarily of protein. Most inner membrane proteins are responsible for oxidative phosphorylation or are part of the electron transport chain (ETC) (8). Proteins

---

This dissertation follows the style of *The Proceedings of the National Academy of Science*.

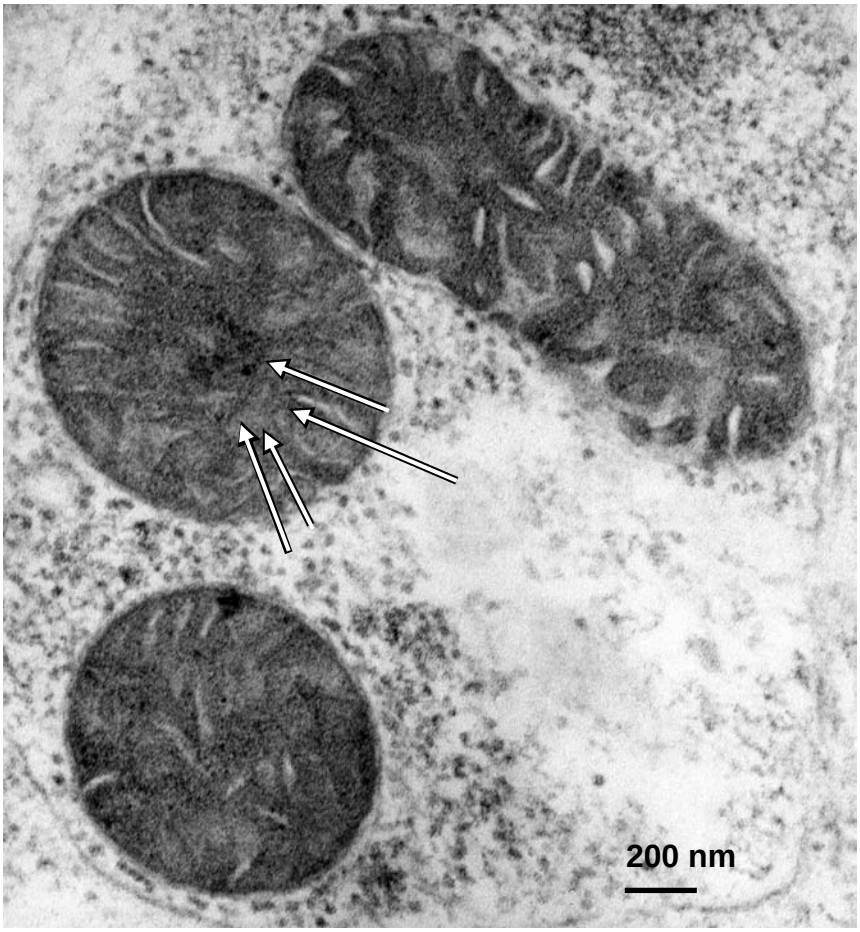

Figure 1-1. Mitochondria isolated from *Caenorhabditis elegans*. Electron micrograph of a sample isolated and prepared in our lab. This image is displayed since visualization of structural components is often more difficult in yeast samples. Arrows indicate the outer membrane, inner membrane, inner-membrane space, and the matrix. Size discrepancies are typical in mitochondrial samples.

housed in the IM also regulate traffic to the matrix since nearly all molecules require a translocase to permeate the compartment. There are two translocase complexes of the inner mitochondrial membrane, Tim22 and Tim23 (9-12). These translocases work with the TOM complex to import proteins from the cytosol. Tim23 recognizes presequence-containing proteins and mediates their insertion to the IM or translocation into the matrix (9-10). The insertion of proteins into the IM sometimes requires the protein to first be inserted into the matrix (10). Tim23 requires both a presequence-translocase-associated-motor-complex (PAM) and a membrane potential (Δψ) to completely import proteins into the matrix even when such import is a precursor to membrane integration (9). It is thought that the Δψ activates the opening and closing of the pores for each complex as proteins are imported to the matrix or IM (9, 13). Tim22 recognizes multi-spanning proteins with internal targeting sequences and inserts them into the IM using the IM membrane potential (13-16).

The potential across the IM is approximately 200 mV which helps in regulating transport of nutrients and proteins (17-18). The membrane potential allows positively charged amino acid sequences of IM proteins to form matrix-exposed loops which promote docking into the IM (19). The membrane potential promotes contacts of the precursor proteins with the Tim22 complex, signaling one or the other side of the pore to close so insertion can be completed as the protein moves through the complex (13).

The Δψ is responsible for regulating several important processes. For example, it prevents translocation of metabolites and molecules that would interfere with mitochondrial homeostasis. Chelators such as negatively charged ethylene glycol tetra acetic acid (EGTA) cannot pass through the IM to sequester essential metal ions from the mitochondrial matrix (20). Disruption of the membrane potential causes molecules to flow freely through the IM thereby inhibiting oxidative phosphorylation (4, 20-22). Dissipated Δψ prevents protein import since the opening/closing of pores of the translocases cannot be activated (9, 13, 23). Both mitochondrial aging and exposure to oxidative stress correlate to loss and eventual dissipation of the membrane potential (17-18, 24-25). The Δψ deficiency is associated with both mitochondrial structural damage and an efflux of matrix solutes (17, 25).

Mitochondria are often present as sausage shaped vesicles approximately 3 μm in length and 1 μm in diameter (22). Stevens (26) discovered that mitochondria may also be present as larger tubular networks although smaller, sausage shaped mitochondria are still present. Mitochondria constantly undergo fission and fusion during the cell cycle which results in significant size variations (27). This process of fission and fusion may serve as a way of exchanging genetic information (22).

Mitochondrial Pathways

Mitochondria are responsible for several vital processes including the citric acid cycle, Fe metabolism and oxidative phosphorylation. Oxidative phosphorylation is utilized by eukaryotes because it is such an efficient means of energy production. A series of proteins (also called respiratory complexes) located in or along the mitochondrial inner membrane transfer electrons from donors to oxygen resulting in the production of water and an electrochemical gradient which is used to drive ATP production (22, 28).

Although oxidative phosphorylation is highly conserved, there are a few differences in yeast from other eukaryotes. Yeast mitochondria lack a Complex I (22, 28-30). Succinate dehydrogenase or Complex II of the electron transport chain removes electrons from succinate and sends them to CoQ (31). Complex III, also called cytochrome bc1, accepts electrons from CoQ and donates them to cytochrome c. It also helps to form the proton gradient that is used by respiratory Complex V to produce ATP (21, 32). Complex IV, also known as cytochrome c oxidase (Cox1) uses 4 electrons from cytochrome c and 4 protons to convert molecular oxygen to two molecules of water (33-34). Many of the proteins involved in oxidative phosphorylation contain Fe.

Fe Prosthetic Groups

There are two dominant types of Fe prosthetic groups in mitochondria, including Fe/S clusters (Figure 1-2) and hemes (Figure 1-3). Iron sulfur clusters

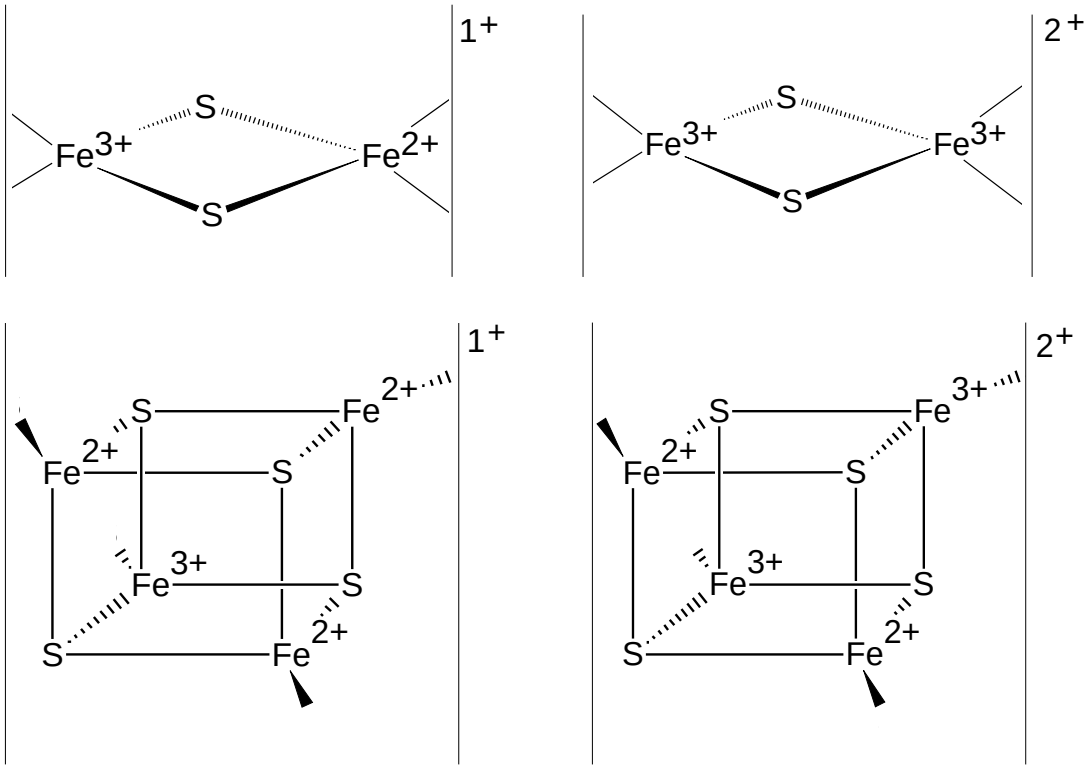

Figure 1-2. Types of Fe/S clusters. $[Fe_2S_2]$ (Top) and $[Fe_4S_4]$ (Bottom) clusters are displayed in their oxidized (Right) and reduced (Left) forms.

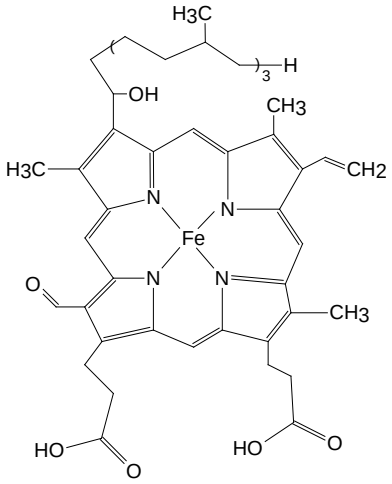

Heme *a*

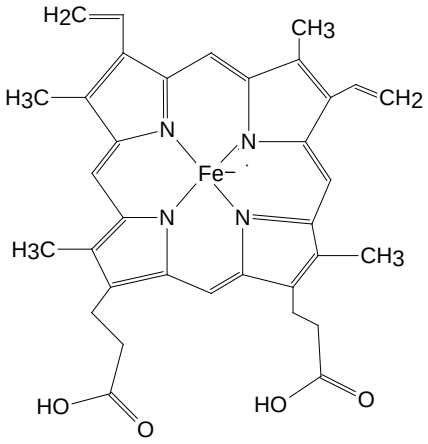

Heme *b*

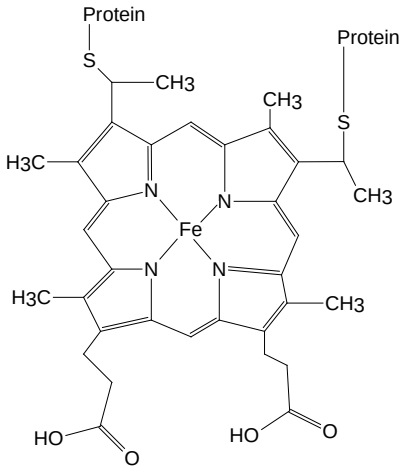

Heme *c*

Figure 1-3. Heme centers.

can be of three main types: $[Fe_2S_2]$, $[Fe_3S_4]$ and $[Fe_4S_4]$. $[Fe_2S_2]$ clusters are coordinated either by four cysteine ligands or by two cysteine and two histidine ligands. The reduced state of the cluster $[Fe_2S_2]^{1+}$ contains one Fe^{3+} and one Fe^{2+} while the oxidized cluster $[Fe_2S_2]^{2+}$ contains two Fe^{3+} ions. The reduced cluster typically has a ground state electron spin S = ½, which gives rise to EPR signals with g_{ave} = 1.94 (35-36). $[Fe_4S_4]$ clusters are also usually ligated by cysteines. Reduced clusters $[Fe_4S_4]^{+}$ contain a Fe^{3+} ion and three Fe^{2+} ions while the oxidized cluster $[Fe_4S_4]^{2+}$ contains two ferric and two ferrous ions, all of which are spin-coupled. Oxidized clusters have spin S = 0 while reduced clusters have the EPR active S = ½ and S = $^3/_2$ with signals visible in the g = 2.0 region (35-37). Oxidized $[Fe_4S_4]$ clusters can sometimes lose one Fe to form $[Fe_3S_4]$ clusters. In this type of cluster three of the iron ions are coordinated by cysteines, while the labile iron is typically coordinated by water (38-39). Most Fe/S cluster proteins participate in redox reactions, but proteins containing clusters with a labile Fe can be an exception. The $[Fe_4S_4]$ cluster of aconitase, for example, can actually bind the substrate directly (38, 40-42). In the inactive $[Fe_3S_4]$ cluster form, the labile Fe is absent, preventing substrate binding. In this state, one of the sulfide ions bridges all three remaining Fe atoms (35-36, 39, 41). Oxidized $[Fe_3S_4]^{+}$ clusters contain three ferric ions while the reduced cluster $[Fe_3S_4]^{0}$ contains one ferrous ion and two ferric ions [(35-36)]. The oxidized cluster is also EPR active. Observed g values, spin states and other known properties are listed in Table 1-1.

Table 1-1. Known Fe-containing mitochondrial proteins.

Protein (gene)	Gene	location	Prosthetic Group	$E^{0'}$ (mV, NHE)	Electronic and Magnetic Properties
Succinate dehydrogenase	*Sdh2*	IM(facing M) (43)	Fe_2S_2	0 (44)	S = 0 $[Fe_2S_2]^{2+}$ and S = ½ $[Fe_2S_2]^{1+}$ (g = 2.026, 1.935, 1.912) (44-45)
Succinate dehydrogenase	*Sdh2*	IM (facing M) (43)	Fe_3S_4	+ 60 (44)	S = ½ $[Fe_3S_4]^{1+}$ (g = 2.01) and S = 2 $[Fe_3S_4]^{0}$ (45)
Succinate dehydrogenase	*Sdh2*	IM (facing M) (43)	Fe_4S_4	- 260 (44)	S = 0 $[Fe_4S_4]^{2+}$ and S = ½ $[Fe_4S_4]^{1+}$ (g = 2.064, 1.992, and 1.847 and magnetic interactions affording features at 2.27 and 1.63) (44)
Succinate dehydrogenase	*sdh3:* *sdh4*	IM (43)	Heme b	+ 60 (45) (but this is for non-Sc enzyme which has novel cys)	S = ½ Fe^{3+} (g = 3.63) (46) and S = 0 Fe^{2+}
Cytochrome bc_1	*rip1*	IM (facing IMS) (47-48)	Fe_2S_2 (Reiske)	+285 (49-50)	S = 0 $[Fe_2S_2]^{2+}$ and S = ½ $[Fe_2S_2]^{1+}$ (g = 2.02, 1.90, 1.80) (51)
Cytochrome bc_1	*cob1*	IM (47-48)	Heme b_H	- 45 (- 35 to + 25) (48)	S = ½ Fe^{3+} (g = 3.45) (52) and S = 0 Fe^{2+}
Cytochrome bc_1	*cob1*	IM (47-48)	Heme b_L	- 150 (-95) (48)	S = ½ Fe^{3+} (g = 3.78) (52) and S = 0 Fe^{2+}
Cytochrome bc_1[T9]	*cyt1*	IM (47-48)	Heme c_1	+ 230 (est) (53)	S = ½ Fe3+ (g = 3.33 or 3.35) (52, 54) and LS Fe^{2+}
cytochrome c isoform I	*cyc1*	IMS (33)	Heme c	+ 290 (55)	S = ½ Fe^{3+} (g = 3.06; 2.26, 1.25) (56) and S = 0 Fe^{2+}
cytochrome c isoform II	*cyc7*	IMS (33)	Heme c	+286 (57)	S = ½ Fe^{3+} (g = 3.2; 2.05, 1.39) (56) and S = 0 Fe^{2+}
cytochrome c peroxidase	*ccp1*	IMS (58)	Heme b	- 182 (59)	S = 5/2 Fe^{3+} (g = 6.60, 5.23 (5-CN) and g = 6.13, 5.81 (6-CN) (60) and S = 2 Fe^{2+}
Cytochrome c oxidase	*cox1*	IM (61)	Heme a	+ 320 (62)	S = ½ Fe^{3+} (g = 3.03, 2.21, 1.45) (63-64) and LS Fe^{2+}
Cytochrome c oxidase	*cox1*	IM (61)	Heme a_3:Cu_b	+ 350 (65)	Fully Oxidized: EPR-silent Fe^{3+} spin-coupled to Cu^{2+} with J ~ 1 cm^{-1}
					Intermediate: S = 5/2 Fe^{3+} (g = 6.4, 5.3)[116] mixed with (g = 6.0) when Cu^{1+} (64)
					Fully Reduced: HS Fe^{2+}: Cu^{1+} (63)
Fe/S Scaffold Protein	*Isu1*	M (66)	Fe_2S_2	(probably low)	S = 0 $[Fe_2S_2]^{2+}$ (67)
Fe/S Scaffold Protein	*Isu1*	M (66)	Fe_4S_4	(probably low)	S = 0 $[Fe_4S_4]^{2+}$ (67)
Fe/S Scaffold Protein	*Isu2*	M (66)	Fe_2S_2	(probably low)	S = 0 $[Fe_2S_2]^{2+}$ (67)
Fe/S Scaffold Protein	*Isu2*	M (66)	Fe_4S_4	(probably low)	S = 0 $[Fe_4S_4]^{2+}$ (67)
Fe/S Scaffold Protein	*Isa1*	M (68)	Fe_2S_2	(probably low)	S = 0 $[Fe_2S_2]^{2+}$ (67)
Fe/S Scaffold Protein	*Isa1*	M (68)	Fe_4S_4	(probably low)	S = 0 $[Fe_4S_4]^{2+}$ (67)
Fe/S Scaffold Protein	*Isa2*	M (63) or IMS (68)	Fe_2S_2 (putative) (63)	(probably low)	S = 0 $[Fe_2S_2]^{2+}$ (67)
Fe/S Scaffold Protein	*Isa2*	M (63) or IMS (68)	Fe_4S_4 (putative) (63)	(probably low)	S = 0 $[Fe_4S_4]^{2+}$ (67)

Table 1-1. Continued.

Protein (gene)	Gene	location	Prosthetic Group	$E^{0'}$ (mV, NHE)	Electronic and Magnetic Properties
Fe/S Scaffold Protein	*Nfu1*	M (66)	Fe_2S_2	(probably low)	S = 0 $[Fe_2S_2]^{2+}$ (67)
Fe/S Scaffold Protein	*Nfu1*	M (66)	Fe_4S_4	(probably low)	S = 0 $[Fe_4S_4]^{2+}$ (67)
biotin Synthase	*Bio2*	M (69)	Fe_2S_2	-140 (70)	S = 0 $[Fe_2S_2]^{2+}$ and S = 1/2 $[Fe_2S_2]^{1+}$ (g = 2.01, 1.96, 1.88; and g = 2.00, 1.94, 1.85) (71-72)
biotin Synthase	*Bio2*	M (69)	Fe_4S_4	- 440 (70)	S = 0 $[Fe_4S_4]^{2+}$ and S = ½ $[Fe_4S_4]^{1+}$ (g = 2.042, 1.937, and 1.937) (73)
					or (g = 2.035, 1.937, 1.937) (14) (or g = 2.044, 1.944, 1.914 and S = 3/2) (72)
lipoic acid synthase	*Lip5*	M (74)	Fe_2S_2	- 430 (73)	S = 0 $[Fe_2S_2]^{2+}$ and S = ½ $[Fe_2S_2]^{1+}$
lipoic acid synthase	Lip5	M (74)	Fe_4S_4	- 505 (73)	S = 0 $[Fe_4S_4]^{2+}$ and S = ½ $[Fe_4S_4]^{1+}$ (g = 2.039, 1.937, and 1.937) (75)
Dihydroxyacid dehydratase	*Ilv3*	M (putative) (76)	Fe_4S_4 (putative)	(dithionite-reducible) (77)	S = 0 $[Fe_4S_4]^{2+}$ and S = 3/2 $[Fe_4S_4]^{1+}$ (g = 5.2, 4.7) (76-77)
Frataxin homolog	*Yfh1*	M (78)	2 Mononuclear Fe's (79)	(probably high)	S = 5/2 Fe^{3+} and Fe^{2+} (79-80)
Catalase A	*Cta1*	M (81)	Heme b	- 226 (est (82))	S = 5/2 Fe^{3+} (g = 6.48, 5.10) (83)
flavocytochrome b_2	*cyb2*	IMS (58)	Heme b_2	- 3 (84)	S = ½ Fe^{3+} (g = 2.99, 2.22, 1.47) (85) and S = 0 Fe^{2+}
Ferrechelatase	*hem15*	IM (facing M) (86)	Mononuclear Fe	---	S = 2 Fe^{2+} (d = 1.36 mm/s; DEQ = 3.04 mm/s) (87)
heme Monooxygenase	*cox15*	IM (88)	Heme a (61, 89)	+ 242 (61)	S = ½ Fe^{3+} (g = 3.5) and S = 0 Fe^{2+}, (61)
heme Monooxygenase	*cox15*	IM (88)	Heme b (61, 89)	+ 85 (61)	S = ½ Fe^{3+} (g = 3.7) and S = 0 Fe^{2+}, (61)
carboxylate monoxygenase	*Coq7*	IM (90)	Fe-O-Fe (91-92)	+ 48 and - 135 (93)	(putative) S = 0 $[Fe^{2+}\,Fe^{2+}]$, S = ½ $[Fe^{3+}\,Fe^{2+}]$ (g = 1.95, 1.86, 1.77) and S = 4 $[Fe^{2+}\,Fe^{2+}]$ (94)
Aconitase	*Aco1*	M (41)	Fe_4S_4 and Fe_3S_4	- 450, - 268,	S = 0 $[Fe_4S_4]^{2+}$ and S = ½ $[Fe_4S_4]^{1+}$ (g= 2.06, 1.93, 1.86) (95)
				+ 100 (42)	S = ½ $[Fe_3S_4]^{1+}$ (g = 2.024, 2.016, and 2.004) and S = 2 $[Fe_3S_4]^{0}$
					S = ½ $[Fe_4S_4]^{3+}$ and S = 0 $[Fe_4S_4]^{2+}$
Homoaconitase	*Lys4*	M (96)	Fe_4S_4 and Fe_3S_4	Similar to aconitase (96)	Similar to aconitase (96)
			(Putative)		
Ferredoxin	*Yah1*	M (97)	Fe_2S_2	- 353 (98)	S = 0 $[Fe_2S_2]^{2+}$ and S = ½ $[Fe_2S_2]^{1+}$ (g = 2.024, 1.937, 1.937) (98)
flavohemoglobin	*Yhb1*	M (99) (and cytosol)	Heme b	- 230 to - 320 (100)	S = 5/2 Fe^{3+} (g = 5.75, and 6.47, 5.22) (101)

Heme prosthetic groups have an iron atom coordinated at the center of a protoporphyrin IX ring. The iron is coordinated by the four planar N atoms of the ring and has two (axial) binding sites left for coordination to either protein amino acid donor atoms or to an exogenous ligand. Hemes usually contain one axial protein side chain (histidine or cysteine, most commonly) coordinated to the Fe atom, although there are situations when the heme is bound axially by two protein side chains (102). Hemoproteins are responsible for a variety of functions including electron transfers, biosynthesis, regulation, catalysis, and the transport of gases (102).

Yeast mitochondria contain three types of heme: heme *a*, heme *b* and heme *c* which differ by the functional groups located at the C3, C8 and C18 positions. Heme *b* has vinyl groups on C3 and C8 and a methyl group on C18. In heme *c* there are covalent thioether groups on C3 and C8. Heme *a* has a formyl group at C18 and a hydroxyfarnesyl group at C3 (102). Yeast mitochondria contain only LS heme *c* centers which have S = ½ (Fe^{3+}) or S = 0 (Fe^{2+}) and reduction potentials ranging from +230 to +290 mV vs. NHE (55, 57). Heme *a* and heme *b* are found in yeast as either HS or LS with corresponding (Fe^{3+}) S = $^5/_2$ or S = ½ and (Fe^{2+}) S = 0 (60-61, 63-64). Heme *a* has a potential ranging from +250 to +350 mV (61, 64). Heme *b* has potentials ranging from -200 to +85 mV (60-61). Details for the prosthetic groups of specific proteins including potentials and g values of EPR signals are listed in Table 1-1.

Fe-Containing Proteins

Yeast mitochondria contain at least 20 Fe-containing proteins, all of which have vital roles in metabolic pathways. These proteins are listed in Table 1-1. Several proteins involved in oxidative phosphorylation, including Respiratory Complexes II-IV, contain Fe. Succinate dehydrogenase contains a LS heme *b* in its Sdh3:Sdh4 subunit in addition to the [Fe_2S_2], [Fe_3S_4] and [Fe_4S_4] clusters in Sdh2 (31, 45, 103). Cytochrome bc1 contains two LS heme *b's* (Cob1), heme *c* (Cyt1) and a [Fe_2S_2] cluster (Rip1) (47-48). LS Heme *c* centers are found in both cytochrome c isoform I (Cyc1) and isoform II (Cyc7) (33, 56). Cox1 has two heme *a* centers; one is LS heme *a*, while the second is HS heme a_3 (56, 61, 63-65).

Fe-containing proteins may also funnel electrons and substrates into the ETC. Heme monoxygenase (Cox15) is responsible for converting heme *b* centers to heme *a* centers which are then incorporated into Cox1 (104-105). Cox15 contains a heme *b* center in addition to any bound heme *a* (89, 106). Carboxylate monoxygenase (Coq7), one of the proteins responsible for Coenzyme Q biosynthesis, contains a Fe-O-Fe center (107-108).

Enzymes responsible for scavenging and detoxifying reactive oxygen species (ROS) often contain Fe centers. The two proteins responsible for detoxifying hydrogen peroxide, catalase (Cta1) and cytochrome c peroxidase (Ccp1), each contain a HS heme *b* (59-60, 109-110). Flavohemoglobin (Yhb1),

which is responsible for the detoxification of nitric oxide, also contains a HS heme *b* (99, 111-112).

Several other metabolic pathways involve Fe-containing proteins. Flavocytochrome b2 (Cyb2), a protein in the IMS responsible for a step in lactate metabolism, contains a LS heme *b* (113). Dihydroxyacid dehydratase (Ilv3), a protein involved in amino acid biosynthetic pathway, appears to contain a [Fe_4S_4] cluster (76, 114). Biotin synthase (Bio2), which catalyzes the last step of the biotin synthetic pathway, contains both a [Fe_2S_2] and a [Fe_4S_4] cluster (69). Biotin is a cofactor in gluconeogenesis as well as in fatty acid and leucine metabolism (69). Lipoic acid synthase (Lip5), a [Fe_2S_2] and [Fe_4S_4] containing protein, catalyzes the production of lipoic acid, an essential cofactor for many enzymes including pyruvate dehydrogenase (73-74).

Understandably, many of the proteins involved in Fe metabolism also contain Fe. Yfh1 carries two mononuclear Fe's to either Hem15 or Isu1/2 for Fe metabolism (115-116). The scaffold proteins involved in Fe/S cluster synthesis, including Isu1, Isu2, Isa1, Isa2, and Nfu1 may each contain both [Fe_2S_2] and [Fe_4S_4] clusters or an intermediate form of the Fe/S clusters being assembled (66, 68, 117). Ferredoxin (Yah1), a [Fe_2S_2] containing protein, accepts electrons from NADH and donates them to either Cox15 for heme *a* synthesis or to an unknown component of the ISC to aid the formation of Fe/S clusters on the Isu1/2 scaffold (97, 118).

One family of [Fe_4S_4] cluster-dependent enzymes catalyzes isomerization reactions by using both a hydration and a dehydration step. Aconitase (Aco1), an enzyme in the citric acid cycle, catalyses the isomerization of citrate to isocitrate, through the intermediate cis-aconitate (40). Homoaconitase (Lys4) is part of the lysine biosynthetic pathway and catalyzes the conversion of homocitrate to homoisocitrate via the intermediate homoaconitate (96). Homoaconitase also contains a [Fe_4S_4] which can be converted to an [Fe_3S_4] upon oxidation (96). ETF dehydrogenase (Cir2) which has similarities to other oxidoreductases, and is even part of a supramolecular complex with other mitochondrial dehydrogenases, contains a [Fe_4S_4] cluster (119-120).

Fe Metabolism

Although oxidative phosphorylation is generally viewed as the most important function of mitochondria, Fe metabolism is also critical (121-124). Iron is an essential metabolite utilized in many proteins involved in oxidative phosphorylation and the electron transport chain. Without Fe or the associated processes involving the import and regulation of Fe in mitochondria, these proteins could not function properly. Fe stores can also lead to toxic side effects. For example, high mitochondrial Fe concentrations are often associated with the misincorporation of Fe into proteins (125). Mitochondria must find a balance in maintaining a concentration of biologically useful Fe while preventing toxic side

effects. Therefore regulation of Fe-trafficking and Fe metabolism is essential for healthy mitochondrial function.

Fe Import

The first step in mitochondrial Fe metabolism is Fe import. Lange *et al.* (126) found that only ferrous ions can be imported into mitochondria although the exact Fe complex imported is still not known. Mrs3 and Mrs4 are thought to be two high affinity iron importers located in the inner mitochondrial membrane (127-128). Cells with decreased expression of Mrs3/4 exhibit low mitochondrial iron concentrations when grown on Fe-depleted media (127). Additionally Fe/S cluster and heme containing protein activity is diminished (128). Over-expression of these two proteins results in the protein activity being restored (128). Growing Mrs3/4-deficient cells on Fe-replete media has no impact on Fe/S cluster or heme activity, indicating there is at least one other Fe import pathway (128).

Mft1 and Mft2 [also called Mmt1 and Mmt2] are also thought to be mitochondrial Fe importers. Lange *et al.* (126) found that cells grown on Fe-limiting media grow slower and have lower mitochondrial Fe accumulation than cells grown under Fe-replete conditions. Over-expressing Mft1 and Mft2 resulted in a 2-5 fold increase in mitochondrial Fe. Radioactive Fe^{2+} could be transported across the inner mitochondrial membrane and incorporated directly into heme centers (126). In fact, the rate-limiting step appears to be Fe import,

suggesting the Fe is utilized immediately from the inner membrane and not from a storage protein or reservoir of Fe in the matrix. Interestingly Fe imported by Mft1 and Mft2 does not seem to have an impact on heme synthesis, which may indicate that the iron imported by these proteins is utilized for Fe/S biosynthesis (122, 126, 129).

Fe Storage

Fe levels inside mitochondria must be regulated. High Fe concentrations are associated with mitochondrial defects. Cells must sense Fe concentrations and use that information to import and store Fe complexes for mitochondria (121-123). However, it is not clear what specific Fe-complexes are imported or stored although it has been hypothesized that the Fe is coordinated by ligands of low molecular weight (130-133). This raises the question of how Fe complexes are stored and what function those store(s) have.

Stored Fe complexes may contribute to a metabolic reservoir inside mitochondria (125, 134-137). This reservoir may consist of multiple Fe complexes or states. One hypothetical pool consists of ferrous Fe that is “bioavailable,” which has been defined as the ability of Fe to replace Mn ions in manganese superoxide dismutase (Sod2) in Mtm1-depleted cells (125). Fe in this form has the reactive properties necessary to interact with proteins and metabolites and to be utilized or inserted into apo-proteins. The Fe is chelated by unknown small molecules, possibly amino acids (133). Although some

portion of mitochondrial Fe is always present in this bioavailable state, it appears to be a small portion. Occasionally Fe homeostasis is disrupted by genetic mutations (such as through mutations in Mtm1, Ssq1 and Grx5) allowing Fe to accumulate (125). Control of this ferrous reservoir is crucial to avoid Fe toxicity.

It is uncertain what portion of wild-type mitochondrial Fe is part of the labile pool. Tangeras *et al.* (138) incubated isolated mitochondria in bathophenanthroline sulfonate (BPS) which strongly chelates mononuclear Fe^{2+} (138). The labile Fe was estimated to be nearly 25 % of the total mitochondrial Fe (138). Similar estimates have been obtained by digesting isolated mitochondria for ICP-AES analysis (134). Interestingly addition of 0.1 mM Fe to the media reproducibly caused this labile pool to increase five-fold (134). The dramatic increase in mitochondrial Fe in response to addition of Fe to media is surprising. Due to the toxic nature of Fe overload, it seems intuitive that Fe concentrations should be low and tightly regulated.

Lower estimations of the labile pool have been made using fluorophores which accumulate in mitochondria and chelate Fe^{2+} (135-137). Fluorescence is quenched by Fe chelation allowing the presence of fluorescence to indicate when sufficient indicator to exceed the amount of labile Fe had been added. The addition of a stronger chelator permeable to the mitochondrial membrane restores fluorescence that had been quenched by Fe-binding (135-137). These studies indicate that chelatable Fe is present in rat liver mitochondria at approximately 12-17 μM. Assuming these mitochondria contain 4 mM total Fe,

Petrat *et al.* (135) concluded that the labile Fe was present at approximately 0.4 % of the total Fe.

One disadvantage of the fluorescence studies is that they destroy the Fe complexes of interest during detection. To gain the most information about the labile Fe, it would be beneficial to keep samples intact while neither destroying the Fe complexes nor disrupting the *in vivo* state of the mitochondria. Additionally, it would be beneficial to determine whether the detected Fe is from the mitochondria themselves or whether it is adventitiously bound.

Isolation protocols have been designed to remove adventitious Fe but there are still variations in the size of labile Fe detected in samples (139). As mentioned above, addition of Fe to media results in higher mitochondrial labile Fe (134). This could indicate that the chelators included in isolation buffers are not able to remove adventitious Fe or it could simply reflect the actual variations in samples. If the samples themselves contain variable amounts of labile Fe, it has significance for mechanisms of Fe regulation. However, there may be an effect on the size of the labile Fe pool by carbon source, media nutrients and other factors. Further analysis of this labile Fe pool is necessary to determine the portion of mitochondrial Fe in this state and whether the amount of this Fe is variable under different growth conditions.

There is a second pool of Fe that has been termed “biounavailable” because it is unable to replace Mn ions in Sod2 even under Mn-starving conditions (125, 140). Although this type of Fe may be present under wild-type

conditions, it is not known what portion of mitochondrial Fe is in this state. It has been hypothesized that biounavailable Fe can accumulate under genetic mutations just like the labile Fe pool (125). Cells depleted in the yeast frataxin homolog (Yfh1p) have an accumulation of mitochondrial Fe while exhibiting wild-type activity of Sod2p (115, 125, 141-142). Mössbauer spectra of Yfh1p-depleted cells exhibit a broad quadrupole doublet typical of high spin ferric iron bound to either oxygen or nitrogen atoms (142). High field Mössbauer spectra show features typical of a broad distribution of magnetically nonequivalent ferric ions (142). EPR and EXAFS confirmed the Fe was most likely present as iron phosphate nanoparticles. It is unclear whether the biounavailable Fe in wild-type cells is present as nanoparticles or some other form. Additional research is needed to characterize the non-labile Fe pool.

Fe/S Cluster and Heme Biosynthesis

Fe/S cluster and heme biosynthesis both occur in the mitochondria. Imported or stored Fe can be incorporated into these centers . This process is depicted in Figure 1-4. Fe/S cluster biosynthesis can occur in either the mitochondria or cytosol. However, the maturation of cytosolic or nuclear Fe/S cluster proteins still requires the involvement of the mitochondrial Fe/S cluster biosynthesis (ISC) (126, 129, 143-147). The mitochondrial ISC machinery exports an unknown component for cytosolic Fe/S cluster assembly (CIA)

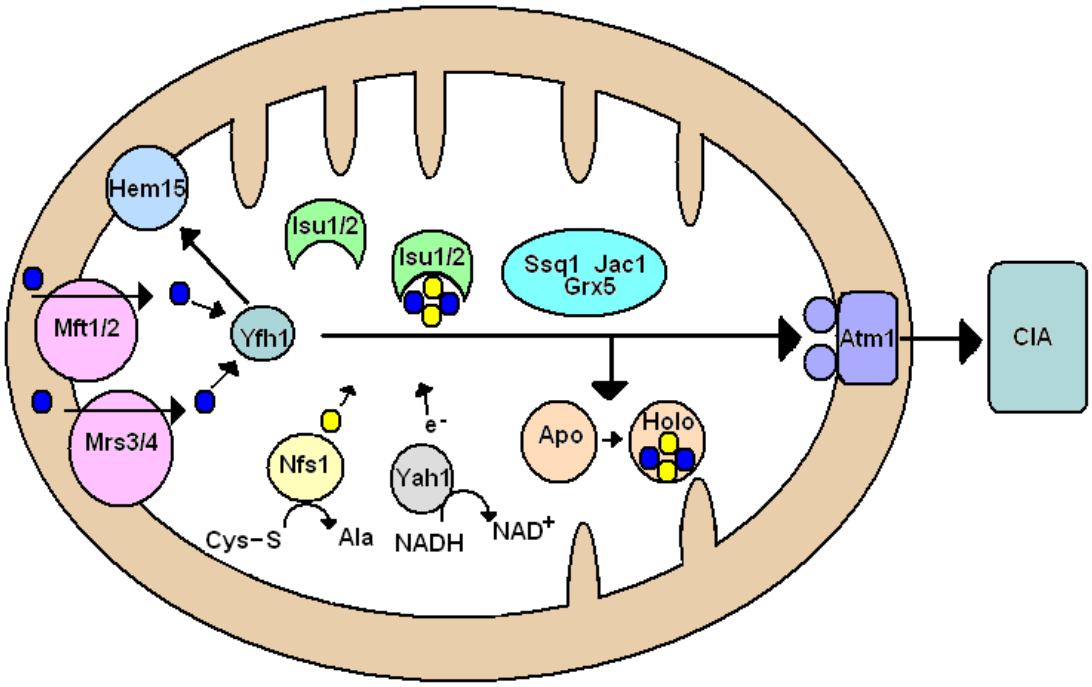

Figure 1-4. Mitochondrial Fe metabolism. Fe is imported and chelated by Yfh1p which delivers Fe to Isu1/2p for Fe/S cluster biosynthesis. It may also deliver Fe to either Hem15p for heme biosynthesis, but this is still debated in literature. Nfs1p converts a cysteine to an alanine to donate S to the Isu1/2 scaffold. Yah1p accepts electrons from NADH. Once the cluster has formed on the scaffold, the Ssq1/Jac1/Grx5 complex associates with Isu1/2p. The cluster is incorporated into apo-proteins. Atm1p exports an unknown compound for use in cytosolic Fe/S cluster assembly.

through the exporter Atm1p (144). Preventing either export through Atm1p or the interaction between Atm1p and the CIA has disastrous defects in cytosolic Fe/S cluster proteins. Interestingly, Atm1p-depleted mitochondria do not contain Fe/S clusters (148). Mitochondrial ISC machinery is therefore responsible for all cellular Fe/S clusters.

Fe/S cluster biosynthesis requires a source of sulfur, usually cysteines, as well as a source of Fe. The Fe atoms must be brought together with the sulfur atoms into the proper arrangement by chapperones and scaffold proteins. Ferrous Fe is imported into the mitochondria and chelated by the yeast frataxin homolog Yfh1, a small protein which can bind two ferrous ions (79, 115). Yfh1p is known to interact with the scaffold protein Isu1 and the cysteine desulfurase Nfs1 in an iron-dependent manner (116, 142, 145). Yfh1 transfers the iron to Isu1/2 (116). Isu1/2 serves as a platform on which Fe/S clusters form (143). Activity of both mitochondrial and cytosolic Fe/S cluster proteins is greatly diminished in the absence of Isu1 indicating its role in the synthesis of all cellular Fe/S clusters (143). Figure 1-4 shows the Fe/S cluster biosynthetic pathway.

Once nascent Fe/S clusters are formed, Isu1/2 interacts with Jac1p, a chaperone protein, which mediates the interaction of the Isu1/Isu2/Jac1 complex to Ssq1 (149). Cells with reduced expression of Jac1p have low activity of Fe/S cluster proteins but accumulate Fe/S clusters on Isu1/2 indicating the Fe/S clusters can neither be transferred to apo-proteins nor exported (149). The Jac1p/Ssq1p complex is responsible for transferring the Fe/S clusters to either

apo-proteins or to molecules for export to the cytosolic Fe/S cluster assembly pathway.

While mitochondria are the foundation of all cellular Fe/S cluster biosynthesis, they are also essential for heme biosynthesis. The last step of heme biosynthesis occurs in the mitochondrial inner membrane when Ferrochelatase (Hem15p) delivers Fe from the matrix to protoporphyrin IX (142). Hem15 can only use Fe that was already loaded into the mitochondrial matrix and not any free Fe in the IMS (142). The yeast frataxin homolog (Yfh1p) has been shown to interact with Hem15, though the physiological significance of this is unclear (126, 142). Since Yfh1p is also responsible for Fe delivery to Isu1 of the mitochondrial ISC, it may have a regulatory role in determining whether imported Fe is delivered for Fe/S cluster or heme biosynthesis (115-116, 141-142).

The incorporation of Fe into protoporphyrin IX may be a GTP-dependent process (150-151). Yhm1 (also called Ggc1), is a GTP/GDP carrier protein (150). Yhm1-depleted cells have increased cellular and mitochondrial iron import but low cytosolic iron levels (142, 152). They also exhibit increased mitochondrial and cytosolic Fe/S cluster proteins (142) but a decreased activity in heme protein levels (although this defect was not as severe as in Yfh1-depleted mitochondria) (150). In addition to accumulating Fe, Ggc1-depleted mitochondria also have high GDP levels with low GTP concentrations (151). Expression of a human GTP carrier protein almost completely restored wild-type

characteristics indicating matrix GTP levels may have a role in the delivery of Fe to Hem15 for heme synthesis and export (150).

Fe Export

Once Fe centers are manufactured, they may be exported for use in cytosolic or nuclear proteins. Whether Fe is exported as Fe/S clusters or as chelated ions in trafficking proteins is unknown (122, 144, 153). One exporter of the as-of-yet unknown Fe component may be Atm1p (144).

Atm1p from the ATP Binding Cassette (ABC) transporter is known to be an importer of metal complexes in other organisms. However, in yeast mitochondria the ATPase domain is located in the matrix and so Atm1p should function as an exporter (144, 153). Atm1p-depleted cells exhibit low cytosolic iron concentrations and defects in the CIA. Atm1-depleted mitochondria hyper-accumulate HS nonheme Fe^{2+}, Fe nanoparticles and have high levels of oxidative damage (144, 148, 153). However, when Atm1 deficient cells were grown anaerobically, mitochondria exhibited wild-type levels of hemes and Fe/S clusters and did not hyper-accumulate Fe (148). The cytosolic Fe/S cluster protein activity could not be recovered. This indicates that the component Atm1p exports is likely utilized in the CIA (148). See Figure 1-4.

Atm1-replete cells exhibit normal levels and activities of cytosolic Fe/S cluster proteins as long as the mitochondrial ISC machinery functions properly. Mutations in Nfs1 or Isu1 inhibit the CIA (121, 144-145, 154). Preventing the

mitochondrial localization of Nfs1 by mutations in the protein's presequence causes dramatic defects in both the ISC and CIA even when the protein functions normally (145). Nfs1's absence in mitochondria is accompanied by accumulation of free Fe (144). This Fe could not be delivered to the CIA. Both mitochondrial and cytosolic Fe/S cluster protein activities were recovered by directing murine Nfs1 to Nfs1-depleted human cells (144). This indicates both Isu1 and Nfs1 must be localized to the mitochondria to promote the CIA. Kuhnke *et al.* (153) further demonstrated that the ATPase activity of Atm1p was selectively stimulated by substrates containing sulfhydryl groups (including $[Fe_2S_2]$ clusters, peptides with cysteine groups and other thiol containing molecules. This result may also indicate that the Fe component Atm1 exports to the CIA may contain sulfur although it is unclear what form that sulfur is in (148).

Fe and ROS Toxicity

Mitochondria must import, transport, store, utilize and export Fe while regulating its redox state, ligands and concentrations. The challenge is that Fe can be both biounavailable and toxic due to its chemical properties in aqueous environments (123, 155). Ferric Fe is largely insoluble and cannot be easily chelated at biological pH (pH ~ 7). Ferrous Fe is soluble but can easily undergo Fenton chemistry resulting in the production of reactive oxygen species (ROS), one of the major contributors to mitochondrial dysfunction (22). ROS are

responsible for DNA damage, initiating apoptosis (cell death), inactivating enzymes and oxidative signaling (22).

The three most common ROS are superoxide, hydrogen peroxide and the hydroxyl radical. Until recently it was believed that mitochondrial ROS production came solely from the ETC. Respiratory Complexes III-IV can leak electrons to molecular oxygen forming superoxide or hydrogen peroxide (32, 156-157). This type of ROS production occurs during normal respiration, but increases when the ETC is disrupted by inhibitors. Alternatively, ROS production also increases when the ETC is functioning at a capacity too high for the corresponding ATP production such as through substrate (ADP) depletion (32, 157). In this case the ETC continues to transport electrons, but with an increased chance for the reduced proteins to leak electrons to molecular oxygen forming superoxide (32, 156-157). Superoxide can be converted to hydrogen peroxide by an electron and leaked protons that would otherwise form the proton gradient.

Almost as soon as they were discovered, researchers began questioning the reactivity of mitochondrial Fe species. Mutations causing Fe build-up are often associated with oxidative damage and dysfunctions caused by ROS. In fact, it is well known that ferrous Fe can react with molecular oxygen to produce superoxide. Additionally if hydrogen peroxide is present, Fe^{2+} ions have a more toxic side effect. In the presence of reduced Fe, hydrogen peroxide can be reduced to form a hydroxyl radical in the Fenton reaction (22). This leads to two

paradoxes for mitochondria. Mitochondria need to produce enough energy (ATP production) for cellular function while regulating the ETC so that electrons are not leaked to molecular oxygen. In addition, mitochondria are the primary location of Fe metabolism which means Fe must be imported and kept for Fe/S cluster and heme biosynthesis while preventing Fe^{2+} accumulation in the matrix. Mitochondria may be able to prevent Fe toxicity by sequestering imported ferrous ions from the ability to undergo the Fenton reaction.

Once ROS are produced, there are several enzymes that scavenge and detoxify ROS including superoxide dismutase, cytochrome c peroxidase and catalase. Superoxide dismutase (Sod2) catalyzes the dismutation of superoxide to hydrogen peroxide and molecular oxygen (32, 125, 140). Catalase (Cta1) decomposes hydrogen peroxide to water and oxygen (81, 109-110). Peroxidases, such as cytochrome c peroxidase (Ccp1) reduce hydrogen peroxide to water (58-60). Interestingly all three of these enzymes contain Fe emphasizing the paradox between toxic Fe concentrations and detoxifying Fe proteins. Cta1p and Ccp1p both contain heme *b* while Fe has been shown to replace Mn in the active site of Sod2 under high Fe concentrations (125, 134, 140). In addition to scavenging enzymes, there are numerous antioxidant molecules (such as vitamin E) and repair mechanisms to address inactivated proteins and damaged DNA (32, 81, 96, 156). These processes are essential for the detoxification of ROS in mitochondria.

This balance between needed and toxic Fe may be achieved by maintaining a set level of free Fe as well as sequestering that Fe in a way which prevents its ability to undergo Fenton chemistry (130-133). Since mitochondria have to store Fe for metabolic processes (such as the bioavailable HS Fe^{2+}), it holds that some ROS production may be coming from this accumulated Fe. There may be a reason that some of the nonheme Fe in samples (biounavailable pool) is in a state that prevents its mis-incorporation into enzymes. Perhaps this allows Fe accumulation without providing free ferrous Fe. This may also implicate an equilibrium between the two types of nonheme Fe in mitochondria.

Fe-Associated Diseases

Mitochondrial dysfunctions are closely linked to numerous human diseases and disorders including heart disease, anemia, aging and ataxia (158-161). Defects in Fe metabolism is involved in Friedrich's Ataxia, Parkinson's Disease and Sideroblastic Anemia (158-162). In Friedrich's Ataxia, the yeast frataxin homolog (Yfh1p) is depleted causing a build-up of amorphous precipitated Fe (141-142, 163-164). A build-up of precipitated Fe is also seen in a small part of the brain, the substantia nigra, in Parkinson's Disease (165-166). Typical Fe complexes are disrupted by favored production of Fe complexes that are more likely to undergo Fenton reactions in Alzheimer's Disease (167-168).

Patients with Sideroblastic anemia accumulate Fe that is unable to be incorporated into hemoglobin (169-170).

The inability of diseased cells to utilize Fe in the proper pathways has severe symptoms for the cells and organisms involved including decreased respiration, ataxia, neurodegenerative traits and even death (158-161). It is therefore important to establish a wild-type distribution of Fe and establish trends to further evaluate mechanisms associated with these conditions.

The Importance of Using a Systems Biology Approach to Study Fe Metabolism

The information accumulated on the cell as a model system began with the meticulous identification and characterization of individual proteins and their activities (171-172). But in order to understand a system, it is necessary to integrate this information. The “omics” suffix was coined with the ultimate goal of incorporating multiple datasets into a comprehensive analysis of a system. The earliest example of this is found in ‘genomics’. In the late 1970’s researchers began sequencing genes to understand the storage, maintenance and expression of an organism’s hereditary information. By the mid-1990’s the entire genome of organisms were being sequenced (173). Furthermore, the invention of DNA microarrays led to exponential amounts of information being available. The incorporation of this information into databases (ATCC, Yeast Genome Database etc) for public use has been beneficial to many research fields.

The next step in understanding cells as a system was to investigate the gene products. This process is complicated since proteins are constantly being translated, modified and degraded. The methods for identification would have to account for these variations. Proteomics originated in the mid-1990's when 2-D electrophoresis was used to identify large numbers of proteins at a time (174). Since then, numerous other methods for proteomic studies have been implemented. Enzyme-linked immunosorbent assays and matrix-assisted laser desorption/ionization are two popular methods for determining which proteins are present in a mixture. Fluorescent tags have been added to each gene in yeast in order to investigate the relative concentrations and locations of proteins (175-176). Protein networks of interactions have also been investigated as a means of understanding cell processes. Most recently, the metabolome of cells became a subject of interest as researchers began to investigate metabolites to identify and understand biomarkers for conditions and diseases. The integration of these three types of studies is necessary for the comprehensive analysis of the cell (177).

The success of the "omics" studies in interpreting cellular processes and identifying mechanisms led us to question why a similar study had not been done on metal ions, such as Fe. The development of a method to study the Fe-ome would help interpret mechanistic details related to Fe metabolism. Although we ultimately want to understand the Fe-ome of entire cells, the number of components involved and the low concentrations of many of those

components make that goal unrealistic. Indeed the resolution of many of our biophysical methods would not be able to handle either of those issues. Analysis of an individual organelle is a more realistic goal and would still provide information on an intact cellular 'system'. Incorporation of multiple organelle studies can be pieced together at a later time.

Mitochondria were the logical choice for the first system in which to study the Fe-ome. Mitochondria are the site where much Fe metabolism occurs, as well as the site of essential processes governed by Fe-containing proteins. In order to obtain mechanistic details and to determine trends in Fe metabolism it is necessary to evaluate intact mitochondria. This will preserve the *in vivo* state of the organelle and allows the entire system to be studied without disrupting interactions, redox states or concentrations. The ultimate goal of most chemists is to understand a system completely on the molecular level. The number of components in our system, including the quantity of Fe-containing proteins, the different metal complexes, and the countless interactions and pathways involved makes that goal unrealistic for our purposes. Instead we endeavored to obtain information on a broad scale by evaluating trends in Fe metabolism by investigating the Fe distribution. While the traditional approach of studying individual proteins has yielded a wealth of knowledge, we were interested in how the system functions as a whole.

Developing an Approach to Study the Fe-ome

In order to investigate trends in Fe metabolism, we must be able to see the total Fe in our samples: the "Fe-ome" of mitochondria. In order to do this we utilized an integration of numerous biophysical studies to gain information about that system. We employed Mössbauer Spectroscopy, Electron Paramagnetic Resonance, Electron Absorption, Electron Microscopy as well as metal and protein analysis. Integrating the information gained from each type of analysis allowed a more comprehensive assessment of the Fe in our samples than has ever been obtained previously.

Mössbauer Spectroscopy is a vital tool in our Fe-ome analysis. This is because the total Fe in a sample can be evaluated—there is no "Mössbauer-silent" Fe. Furthermore, the spectral features are proportional to the amount of Fe in each state. Mössbauer Spectroscopy allows the separation of Fe complexes into classes of Fe centers; such as HS heme, HS nonheme Fe, $[Fe_2S_2]^+$ and $[Fe_2S_2]^{2+}/[Fe_4S_4]^{2+}$ clusters. There are some limitations with this method as it is impossible to distinguish between low spin heme and $[Fe_4S_4]^{2+}$ clusters. Nonetheless we will begin our analysis of the mitochondrial Fe-ome with Mössbauer Spectroscopy because it can give us the broad picture of the Fe present.

Lesuisse *et al.* (142) was the first to publish a Mössbauer spectrum of intact mitochondria from *S. cerevisiae*. Yfh1-depleted mitochondria showed a doublet corresponding to accumulated iron (III) phosphate, but the wild-type

spectra was completely devoid of any signals (142). This indicates that the wild-type sample was not concentrated enough for Mössbauer studies. This is most likely because traditional growth and isolation parameters were designed for micro-scaled experiments. A single Mössbauer sample requires at least 200 µL of packed mitochondria—approximately 10-fold more than most protocols were designed to produce. We designed a protocol that will provide enough sample material for several macro-scale analyses. Once we achieve the conditions necessary to observe Mössbauer spectra of mitochondria, we will have a depiction of the relative amounts of Fe centers present.

One disadvantage to Mössbauer Spectroscopy is that magnetic Fe contributes to a broad feature that spans much of the spectrum's baseline. Although we can determine the relative proportion of paramagnetic Fe, we cannot characterize or quantify individual components (such as between cytochrome bc1's Reiske protein and succinate dehydrogenase's $[Fe_2S_2]^+$ cluster). In order to evaluate individual paramagnetic species, we relied on EPR. A few recent studies have attempted to use EPR to study intact mitochondria. Bulteau *et al*. (38) treated mitochondria with hydrogen peroxide to observe damaged aconitase. They were unable to detect signals from cytochrome bc1's Reiske center, succinate dehydrogenase or cytochrome oxidase (38). EPR studies were also performed on rat mitochondria to evaluate whether calcium or manganese ions had an effect (178). Weak signals have even been seen in mitochondria isolated from human placenta (179). These studies were not able

to obtain strong signals from multiple components in mitochondria and samples were usually isolated aerobically, preventing the preservation of the sample's redox state. Just as with Mössbauer samples, EPR samples will have to be prepared in a way that provides a sufficient signal to noise ratio so that reliable spectra can be obtained.

Mössbauer Spectroscopy can determine the amount of HS heme in a sample, but it is impossible to determine which type of heme (heme *a*, heme *b* or heme *c*) is contributing to the HS heme feature. Electron Absorption Spectroscopy can easily distinguish between each heme type. Furthermore, concentrations of each heme center can be determined by using standard curves obtained from isolated proteins containing one type of heme. Knowing the concentrations of the total heme content in a sample as well as the portion of HS heme (obtained by Mössbauer) will allow us to determine the portion of Fe in LS heme centers. Since this type of heme overlaps with diamagnetic Fe/S clusters, we will be able to determine the portion of Fe in those Fe/S clusters as well. We are also interested in the presence of the Fe pools. If such pools are present, Electron Microscopy can evaluate that Fe to determine what elements are chelating the Fe to give information on the state of the Fe in the pool(s).

Although mitochondria and mitochondrial dysfunctions have been studied for more than fifty years, there is still a wealth of information to learn. Mössbauer of wild-type cells has never been obtained. Although EPR and Electron Absorption studies of individual proteins have been completed before,

data from multiple techniques has never been integrated so comprehensively. We aim to investigate the Fe-ome of mitochondria by integrating data collected from several biophysical methods. The main limitation of our analysis is that for most Fe-containing species, it is impossible to draw conclusions on the per-species basis. Instead we will be focusing on *groups* of Fe centers. We can use the molecular and supra-molecular information gained from our integrated analysis to draw conclusions about mechanisms of Fe metabolism and gain new physiological insights.

Objectives for the Dissertation

Our study is novel in that we are isolating intact organelles to attempt a more systems-biology approach. In addition, we strive to maintain the biological states of the organelle by isolating mitochondria anaerobically. Finally we seek to incorporate information from Electron Paramagnetic Resonance, Mössbauer Spectroscopy, Electron Microscopy, Electron Absorption, respiration assays, protein and metal analysis to obtain a more integrated analysis. This allows us to gain more quantitative analysis on the organelle than ever before obtained. We describe the Fe-ome of intact mitochondria from S. *cerevisiae*.

This dissertation will discuss the:

- Development of an integrative biophysics-based approach to study the Fe-ome (Chapter II).

- Fe-ome of isolated mitochondria collected from cells grown on respiring and fermenting carbon sources (Chapter III).
- The discovery of Fe pools in mitochondria.
- The determined concentrations of some Fe species in mitochondria.

CHAPTER II

METHODOLOGY AND PROTOCOLS[*†]

Introduction

As described in the Introduction, the goal of the project was to probe the Fe-ome of isolated mitochondria. None of the established isolation procedures addressed the requirements of preparing mitochondrial samples for our integrated analyses. We had two categories of problems to deal with. First—how could we obtain samples that were pure, intact and representative of the *in* vivo state of the organelle? Second—how could we use established biophysical and bioanalytical techniques to investigate the entire Fe-ome (or at least as much as possible) of our samples? A protocol was developed that addressed both problems.

Several modifications to existing isolation protocols were necessary. Our analyses required a substantially larger sample volume than previous studies employed. Our lab uses custom-built 25 L bioreactors to obtain enough cells (to yield enough mitochondria) for our series of experiments. Several steps of the protocol had to be adjusted for handling large sample volume (see below).

---

[*] Part of this chapter is reprinted with permission from "Electron paramagnetic resonance and Mössbauer spectroscopy of intact mitochondria from respiring Saccharomyces cerevisiae*"* by Hudder,BN.; Morales, JG.; Stubna, A.; Münck, E.; Hendrich, MP.; and Lindahl PA. *Journal of Biological Inorganic Chemistry*, 12, 1029-1053, [2007]. Elsevier Inc.

[†] Part of this chapter is reprinted with permission from "Chapter 15 isolation of *Saccharomyces cerevisiae* mitochondria for Mössbauer, EPR, and electronic absorption spectroscopic analyses." by Lindahl PA.; Morales JG.; Miao, R.; and Holmes-Hampton GP. 456. 26-285 *Methods Enzymology.* [2009]. Elsevier Inc.

We endeavored to maintain the *in vivo* state of the organelle by keeping our samples in a refrigerated (5 °C) MBraun glove box with an inert Argon atmosphere (~ 1 ppm O_2) during all isolation steps. Several Fe containing proteins including biotin synthase (180), aconitase (181) and lipoic acid (73) are oxygen sensitive. There is evidence that the mitochondrial matrix is anaerobic. Although oxygen is consumed by the mitochondrion, it is likely that its consumption is fast relative to its diffusion across the matrix allowing the matrix to remain essentially anaerobic (182-183). Isolating mitochondria anaerobically allows the *in vivo* state of the organelle to be preserved while preventing protein and membrane degradation caused by oxygen exposure. Additionally, maintaining our samples in an anaerobic environment, limits ROS production which may damage proteins and membranes and would likely give an altered Fe distribution.

Previously published protocols did not include a chelator in isolation buffers. In order to probe the Fe-ome of mitochondria, it is necessary to know that the metal ions present are contained within the mitochondria themselves. We needed to remove adventitiously bound metal ions from our samples without compromising Fe centers inside isolated mitochondria. We utilized EGTA, a chelator that cannot enter the mitochondrial membrane.

Sample integrity was another concern. Aliquots of isolated proteins can be frozen and thawed repeatedly until samples are consumed. Treating organelles the same way would damage membranes and result changes in the

state of the mitochondria. Isolated organelles are susceptible to aging—which involves protein degradation and membrane ruptures. Therefore samples of sufficient volume must be isolated and immediately analyzed.

To interpret results from our analyses the purity and integrity of our samples needed to be characterized in a simple yet insightful way. This is especially important since mitochondrial samples generally contain some contamination. Brito *et al* (184) found that the ER actually tethers to mitochondria which means ER contamination of mitochondrial samples is likely. Characterizing the relative amounts of cellular contamination in mitochondrial samples provides information of the relative purity of the mitochondria for use in interpreting results.

Electron microscopy allows the visualization of samples and contaminants. Mitochondria vary in size and this distribution can be viewed by this method. Additionally sample contamination by broken membranes, cell spheroplasts, vacuoles and bacteria are also visible. Furthermore, membranes can be visualized and characterized in a qualitative manner since intact membranes will have sharp lines while damaged membranes will often look blurry. A large number of electron micrographs were collected on our samples. In fact, after each adjustment to isolation procedures, several replicates were taken for electron micrographs to evaluate sample integrity and purity.

In addition to purity assays, functionality of samples was tested. Individual enzyme activities can be determined but this is an inadequate

estimate of sample health since only ~ 1-4 proteins of the ~ 800 total proteins are tested. A slightly more effective experiment involves evaluating isolated mitochondrial respiration activities. This assay has the ability to determine how well samples couple oxygen consumption to ATP production. Aged mitochondria or samples with damaged membranes will not maintain the proton gradient necessary to couple oxygen consumption to ATP production. This uncoupled respiration is indicative of the level of damage in isolated samples. The coupling ratio (the ratio of the rate of coupled to uncoupled respiration) is often determined to demonstrate the viability of mitochondria (185). We incorporated this assay into many of our early sample preparations to determine whether our samples were consistent with previously published respiration/functionality assays.

The large number of Fe containing species in mitochondria means that there is a distinct possibility that each individual species is relatively dilute. In order to detect as many Fe components as possible, it is necessary to concentrate our samples. Dilute mitochondrial solutions would not have a S/N ratio necessary to resolve spectral features. Furthermore, we wanted to determine absolute concentrations (concentrations of species in neat mitochondria). All papers, that we are aware of, report concentration data for mitochondrial species in relative terms (μM / mg protein). In order to determine absolute concentrations, samples need to be packaged in a way that can address both of these issues. Samples were packed by centrifugation. This

provides the high S/N ratio necessary for spectroscopic analysis. Furthermore, electron microscopy and respiration assays showed that repeated packing did not cause significant damage to samples.

Since samples were packed with low force (10,000 x g), it was likely that some interstitial buffer remained in the mitochondrial pellets. It is necessary to know the exact percent of that included buffer in order to determine the absolute concentrations of Fe species in neat mitochondria. An experiment utilizing radiolabeled buffer was designed to determine the pellet composition. Samples were packed using conditions shown to be gentle, yet effective. The sample pellet was resuspended in radiolabeled buffer and centrifuged again. The dilution of the radioisotope into interstitial buffer provided a means to calculate the volume of mitochondria occupying sample pellets. This allowed us to establish a packing constant for use when calculating absolute concentrations from spectral features.

Evaluation of the Fe-ome requires the integration of several biophysical techniques. We decided to center our study around Mössbauer Spectroscopy because of its ability to simultaneously distinguish the total Fe in a sample into distinct categories. The collection and analysis of all Mössbauer spectra were done in collaboration with Eckard Münck's lab at Carnegie Mellon University. Mössbauer spectroscopy takes advantage of the Mössbauer effect: gamma radiation emitted by a source can be absorbed by atoms of the same isotope (186). The resulting absorption will differ based on the chemical environment of

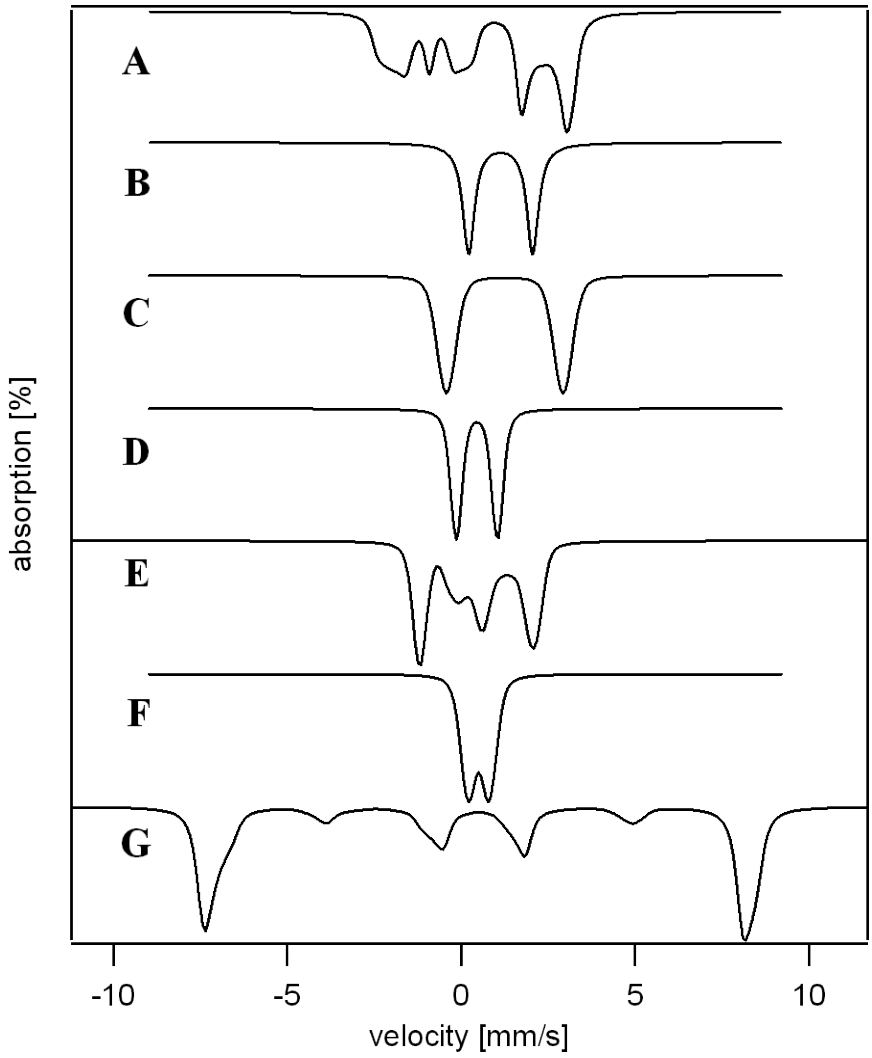

Figure 2-1. Simulations of typical Mössbauer features. Spectra are of; A, Isolated Reiske protein; B, HS reduced heme; C, HS Fe^{2+} nonheme (NHHS); D, the central doublet; E, central doublet in the presence of an 8T magnetic field; F, Fe(III) nanoparticles; and G, HS Fe(III) in the presence of an 8T magnetic field.

the Fe atoms in the sample. Diamagnetic centers will (in the absence of a magnetic field) give rise to quadrupole doublets which are characterized by the quadrupole splitting (ΔEq) and the isomer shift (δ) (139, 187) (Figure 2-1). Identification of both parameters is often enough to identify the spin and oxidation state of an Fe species. For example HS ferrous (S = 2) sites with N/O ligands in octahedral geometry typically have parameters of ΔEq ~ 2.5 - 3.3 mm/s and δ ~ 1.2 - 1.3 mm/s. LS (S = 1/2) ferrous sites typically have ΔEq ~ 0.45 mm/s and δ ~ 1.2 - 1.3 mm/s (139, 187). Parameters found for typical Fe centers are listed in Table 2-1. Centers with half integer spins do not display quadrupole doublets. Instead, they are distinguished by paramagnetic hyperfine features. Paramagnetic features tend to be broad and shallow (Figure 2-1). This implies that paramagnetic species that are present at low concentrations (relative to diamagnetic species) will be difficult to detect (139).

The absorption of energy by each Fe species is directly proportional to the amount of that species in the sample. This means the relative concentrations of several types of Fe centers can be determined by calculating the area under each feature. Furthermore the only necessity for analyzing samples is that the concentration of ^{57}Fe needs to be high enough to allow analysis within an appropriate time frame. Since ^{57}Fe is present with only 2 % natural abundance, this presented a problem. In order to enrich our samples in ^{57}Fe, we incorporated 40 μM ^{57}Fe into our media during cell growth prior to the

Table 2-1. Parameters for typical Mössbauer features seen in our samples. A_{iso} is the ^{57}Fe magnetic hyperfine coupling constant in $A_{iso}S \bullet I$ for an $S = {}^5/_2$ spin Hamiltonian appropriate for high-spin Fe^{3+}. A negative value for the line width parameter Γ indicates a Voigt shape; Γ = - 0.40 mm/s indicates that a Lorentzian of 0.15 mm/s full width (fixed in WMOSS) has been convoluted into a Gaussian of full width 2σ = 0.40 mm/s. Use of Voigt shapes allows us to account for the presence of many similar species, such as those contained in the central doublet: $[Fe_4S_4]^{2+}$ clusters, and ferrous LS heme *a* and LS cytochrome *c*.

	δ (mm/s)	ΔE_Q (mm/s)	A_{iso} (T)	Γ (mm/s)
Central Doublet	0.45	1.15	-	- 0.35
HS Fe^{2+} Heme	0.85	2.15	-	- 0.35
Nonheme HS Fe^{2+}	1.30	3.00	-	- 0.40
Fe^{3+} Nanoparticles	0.51	0.63	-	- 0.52
Mono HS Fe^{3+}	0.45	0	- 22.4	0.40

production of any Mössbauer sample. Mössbauer spectra were obtained on the enriched samples and the general features of the Fe-ome were observed.

Mössbauer spectroscopy can quickly recognize and determine relative quantities of multiple Fe species (for samples enriched in ^{57}Fe). Not only is analysis of a complicated system like mitochondria possible, but the resulting spectra provides detailed information about the chemical environment and oxidation state of each type of Fe center present. Although spectra of mitochondrial samples exhibit several overlapping features, this level of resolution is unprecedented! Since Mössbauer can only distinguish between types of Fe species (such as $[Fe_2S_2]^{+}$, $[Fe_4S_4]^{2=}$ $[Fe_2S_2]^{2+}$, HS heme, etc., it is necessary to use other biophysical techniques to further characterize the Fe present.

Once the relative proportions of Fe-containing species have been determined by Mössbauer, it is possible to use other techniques to further investigate each unresolved feature. EPR is useful for probing paramagnetic species such as organic radicals and transition metals (i.e. Fe, Mn, and Cu). Unpaired electrons have an electronic spin (i.e.. S = ½) characterized by magnetic components ($m_s = \pm ½$). The difference in energy between these two states ($\pm g\beta H$) is ΔE, which varies proportionally to an applied magnetic field. The electron can move between the two states (m_s) when microwave radiation equal to the ΔE is applied in the presence of a magnetic field. As the electron changes states it absorbs microwave radiation. The first derivative of that

absorption of energy is depicted in the resulting spectrum (188). EPR spectral features can help determine the oxidation state, geometry and concentration of the species.

Isolated proteins have been investigated by EPR for several decades. Beinert *et al*. (45) first published the spectrum of cytochrome c oxidase in 1978. Fee *et al.* (51) reported the spectrum of the Reiske protein of the cytochrome bc1 complex in 1984. The parameters of all known Fe-containing proteins from yeast mitochondria are listed in Table 1-1. These parameters can be used to resolve individual contributions of proteins to spectra of intact mitochondria. It is possible to determine the concentrations of each protein in our samples using SpinCount (http://www.chem.cmu.edu/groups/hendrich/facilities/index.html) and our packing constant.

Although Mössbauer spectra show resolution between the feature due to HS heme components and other features, it is impossible to resolve low spin hemes from $[Fe_4S_4]^{2+}$ components. Furthermore, one cannot distinguish between the types of heme centers in samples. In order to investigate the heme content of our samples further we used electron absorption spectroscopy. The resulting spectra illustrate distinct α and β bands for heme *a*, heme *b* and heme *c* allowing the determination of the concentration of each component. Integrating the concentrations of each type heme with the known Fe-containing proteins (Table 1-1) allows the determination of concentrations of two proteins, cytochrome c oxidase and cytochrome c, who contain the bulk of heme *a* and

heme *c* respectively. The knowledge of the HS and LS heme components further allows the concentrations of several groups of proteins to also be determined. Integrating the information gained from these techniques provides a synergy that allows for a cumulative amount of information to be gained. A more in depth explanation of the integrated analysis will be included in Chapter III. In the following sections, each of the relevant methods used in generating the iron-ome of mitochondria will be described.

Growth of Saccharomyces cerevisiae

Strains W303 (generously provided by Roland Lill) and D237-10B (American Type Culture Collection) are both wild-type diploid yeast strains. All yeast experiments used one of these strains and are described by (139, 189). Frozen stocks were used to inoculate YPD (1 % w/v yeast extract, 2 % w/v peptone, 2 % w/v glucose, 1.7 % w/v agar) plates. When strain W303 was used, plates were also supplemented with 40 mg adenine. All chemicals were purchased from Sigma, Fisher Scientific or MP Biomedical.

Plates were allowed to grow at 30 °C for 2 - 3 days until single colonies were visible for selection. Plates were stored for a maximum of 2 months at 5 °C. Individual colonies were selected and used to inoculate 50 mL media. Cells were grown to an OD_{600} of ~ 1.2 at 30 °C with gentle shaking. The entire slurry was used to inoculate 1 L media. The inoculum was allowed to grown for

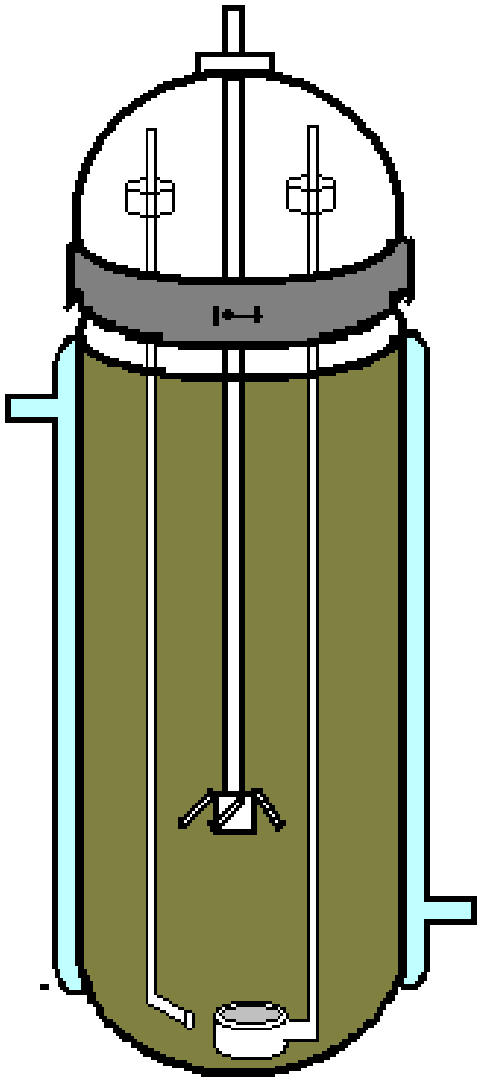

Figure 2-2. Bioreactor. One of two 25 L bioreactors available for growth of yeast cells.

12 - 36 hours until the OD_{600} was 1 - 2 before using the culture to inoculate 24 L media.

Our 25 L vessel (Figure 2-2) was custom built by ChemGlass. The 25 L chamber is surrounded by a water-jacketed region that controls the temperature during growth. The lid has four openings. The first contains a large rod with a teflon paddle that extends down the middle of the reactor and is attached to a motor that turns during growth. A second opening has a glass tube with a small pore fritz 60mm in diameter (ChemGlass). Oxygen is bubbled through this tube at 2 - 3 SCFH during growth. Oxygen is used rather than air to compensate for the small surface to volume ratio in the reactor. The third opening contains a long glass tube that is used to transfer sterile media into the reactor (and to remove the cell slurry after growth). The final opening is used to add the 1 L inoculum and other solutions (such as Fe^{57}, Cu and tryptophan). All cells were grown at 30 °C. All cultures were collected when the OD_{600} was 1 - 1.7 which afforded 200 - 300 g cell paste when grown on glucose media or 100 - 250 g cell paste when grown on glycerol media.

Media Recipes

All chemicals were purchased from Fisher Scientific, Sigma Aldrich or MP Biomedical. Growth medium was made just before use and autoclaved for 25 - 30 minutes at 121 °C. It was allowed to cool to room temperature prior to inoculation. When 24 L of media was required, components were split into four

6 L aliquots (in 9 L bottles) and autoclaved prior to combining them in the bioreactor. (For SSlac medium; salts, lactate, yeast extract and glucose all had separate bottles). A 5xSSlac stock could be made and stored for later dilution and use for small (volumes < 1 L) cultures. If the culture was to be used to produce Mössbauer samples, the media was supplemented with 40 µM ^{57}Fe (purchased from Cambridge Isotopes or Isoflex). The following recipes have been previously described (139, 189-190).

YPD

10 g/L	Yeast extract
20 g/L	Peptone
20 g/L	Dextrose

SSlac

3 g/L	Yeast extract
1 g/L	KH_2PO_4
1 g/L	NH_4Cl
0.5 g/L	glucose
0.5 g/L	NaCl
0.5 g/L	$CaCl_2$
0.6 g/L	$MgCl_2$

(47 mLs 60 % Na Lactate or 30 g/L) Na Lactate (pH 5.5)

Minimal

0.1 g/L	Leucine
0.04 g/L	Adenine
0.02 g/L	Histidine
0.02 g/L	Uracil
1.7 g/L	Yeast Nitrogen Base (YNB)
5 g/L	NH_4SO_4

Either 20 g/L glucose OR 30 mL Glycerol

Isolation of Mitochondria

The procedure for isolating mitochondria was modified from previously reported protocols (191-192) to allow for 25 L harvests as described in (139, 189). All chemicals were from Fisher Scientific, Sigma, or MP Biomedical. In order to collect enough mitochondria, the isolation was scaled up and slight modifications were made. Once cell walls were removed, spheroplasts were disrupted by homogenization with a Dounce homogenizer (Fisher Scientific or Kimbal). This process was initially difficult to regulate since the speed of the repeated lifting/lowering of the pestle varied depending on the strength of individuals. In order to standardize this process, a mechanical homogenizer was built (Texas A&M University Department of Chemistry Machine Shop) to house the glass homogenizer and pestle. The machine raises and lowers the pestle at

a regulated speed (one revolution every 3.5 seconds) When using the tight-fitting glass pestle, the number of strokes required for disruption remains the recommended 25 strokes (192). Additionally, in most experiments, buffers were supplemented with 1mM EGTA to remove adventitious Fe ions. Essentially the protocol is as follows.

1. Cells were collected at 5000 x g for 5 minutes at 5 °C in 1 L bottles (Kendro) in a Sorvall SLC-6000 rotor (this rotor is the only one used until step 10). The supernatant was decanted and cell paste was resuspended into Milli-Q (deionized and distilled) water and combined into one 1 L centrifuge bottle. From 24 L media 200 g of cells could be collected from YPD media, 100-200 g from SSlac media and 100 g from minimal media.
2. Cells were washed with water and centrifuged at 5000 x g for 5 minutes as 5 °C. The supernatant was decanted and the wet weight of the cell paste was determined. The bottle was capped and taken into an anaerobic box (MBraun) at 5 °C. All subsequent steps are carried out anaerobically (< 1 ppm O_2) with buffers that were degassed on a Schlenk line.
3. Cells were resuspended in 500 mLs (TD) buffer (100mM Tris pH 9.4, 1 mM EGTA, 10 mM dithiothreitol (DTT) that was added just prior to use).
4. Cells were incubated in the buffer at 30 °C with gentle shaking for 30 minutes. Cells were centrifuged at 5000 x g for 5 minutes at 5 °C.

5. The supernatant was decanted and cells were resuspended in 300 mL SP buffer (1.2 M sorbitol, 1 mM EGTA, 20 mM KH_2PO_4 pH 7.4). The slurry was centrifuged at 5000 x g for 5 minutes at 5 °C. This step was repeated.
6. Cells were resuspended with 300 - 400 mL SP buffer. A 1 mL aliquot was taken and set aside. Lyticase that had just been dissolved in 5-10 mL SP buffer was added to a concentration of 1500 activity units per gram cells. A second 1 mL aliquot was collected. The cells were incubated at 30 °C with gentle shaking until the OD_{600} of the aliquot containing lyticase was ~ 20 - 30 % that of the aliquot without lyticase (usually 1 - 1.5 hours).
7. The samples were kept at 5 °C for the rest of the isolation. Spheroplasts were centrifuged at 5000 x g for 5 minutes. The supernatant was decanted and the pellet was washed twice with SP Buffer and centrifuged again.
8. Spheroplasts were resuspended in 200 mL 2SH (1.2 M sorbitol, 1 mM EGTA, 40 mM HEPES pH 7.4). An equal volume of Milli-Q water containing 1 mM PMSF was added.

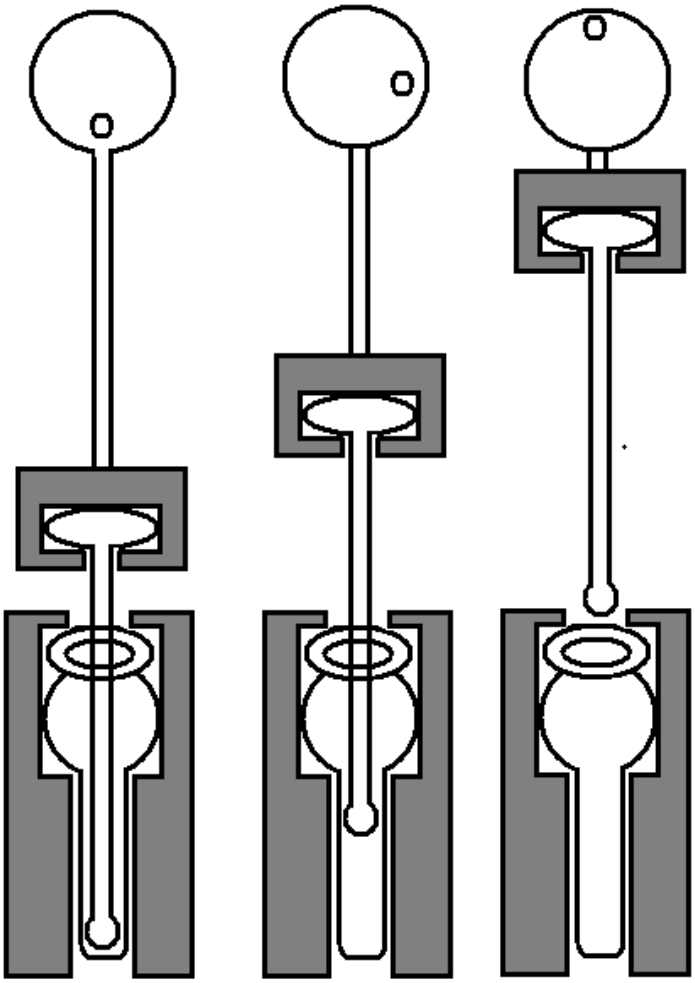

Figure 2-3. Homogenizer. The glass homogenizer available from FisherSci or Kontes was fit into a teflon block and held secure. The glass piston was attached to a second block which was moved at a fixed rate by a motor. Mitochondrial solutions were added in 40 mL aliquots to the apparatus and homogenized as described.

9. Samples were homogenized in a 40 mL Dounce homogenizer using a custom built machine (Figure 2-3). Samples were homogenized with 25 strokes of a tight fitting glass pestle (Fisher/Kontes) at a speed of one revolution per 3.5 seconds.
10. Samples were centrifuged at 3500 x g for 7 minutes. The supernatant was decanted into 250 mL bottles and centrifuged at 10,000 x g for 10 minutes in a Sorval SLA-1500 rotor.
11. The supernatant was decanted and the pellet was resuspended in 100 mL 1SH buffer (0.6 M sorbitol, 1 mM EGTA, 20 mM HEPES pH 7.4). The slurry was homogenized in a 15 mL glass homogenizer with a loose fitting piston using 3-5 strokes.
12. The resulting solution was centrifuged at 3500 x g for 7 minutes. The supernatant was decanted and centrifuged at 10,000 x g for 10 minutes.
13. The resulting pellet was resuspended into 10 - 15 mL 1SH buffer using a glass pipette. This solution contains crude mitochondria that must be further purified by a density gradient.
14. Histodenz (Sigma) or Nycodenz (Fisher Scientific) solutions were made in 1SH buffer. Gradients consisted of 2 layers (15 mLs each) 18.5 % (w/v) and 14.5 % (w/v). Nycodenz was weighed out and taken into the glove box in 50 mL tubes.

15. 1SH buffer was added to ~ 75 % required volume to make solutions and the solution was vortexed until all powder was dissolved. The volume of 1SH buffer was adjusted to the required amount.
16. 15 mL of 18.5 % Nycodenz was poured into 38 mL Thick-Wall Polycarbonate Centrifuge Tubes (Beckman). 15 mL of 14.5 % Nycodenz was gently overlaid with long tip glass pipettes. 2 - 3 mL mitochondrial solution was added to the top of the gradient.
17. Gradients were centrifuged for 50 - 60 minutes at 164,000 g (max RCF) in a Beckman L7 Ultracentrifuge.
18. Glass pipettes were used to collect the mitochondria from the interface. Mitochondria were diluted with 2 - 3 fold 1SH buffer and centrifuged at 10,000 g (average RCF) for 60 minutes.
19. The supernatant was decanted and the mitochondrial pellet was resuspended in 1 - 2 mL 1SH buffer. This solution is used for all further experiments.

Determining Sample Purity and Integrity with Electron Microscopy

The procedure is essentially as previously reported (139). All steps were done anaerobically at 5 ºC. A 0.1 - 0.5 mL solution of purified mitochondria was micro-centrifuged (Fisher Scientific) at 6,400 rpm for 5-10 min in an Eppendorf tube. The supernatant was decanted with glass pipettes and the pellet was resuspended in 1SH buffer containing 4.0 % (v/v) glutaraldehyde (Sigma). The

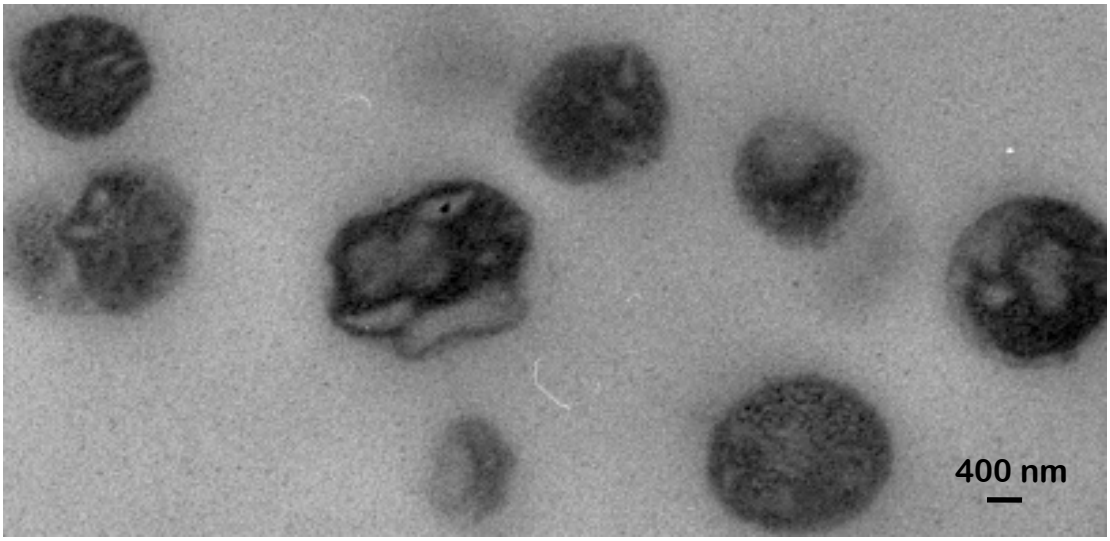

Figure 2-4. Electron micrographs. Mitochondrial samples were prepared as described. Electron micrographs of isolated mitochondria were essentially devoid of spheroplasts and membrane debris.

solution was allowed to incubate for 45 minutes. The slurry was micro-centrifuged for 5-10 minutes. Once the pellet had formed, glass pipettes were used to remove the supernatant. The pellet was rinsed twice with 1SH buffer. This was done by carefully resuspending the pellet in 1SH buffer and then micro-centrifuging the solution as above. Although most of the supernatant was removed, enough solution was left to cover the pellet to prevent dehydration. Samples were left in the MBraun box until right before taking them (on ice) to the Electron Microscopy Center at Texas A&M University.

Mitochondrial samples were routinely analyzed by Electron Microscopy to assess sample purity and membrane integrity. Images (139) of early preparations showed large size variations in mitochondria and the presence of some contamination from membranes and unbroken spheroplasts. As the protocol was optimized, the size distribution as well as the contamination of membranes, spheroplasts and other cellular components diminished somewhat (Figure 2-4).

Respiration Assays

The procedure was previously described (139) and was modified from (185). Prior to respiration assays, a portion of purified intact mitochondrial solutions were diluted to 5 mLs and sonicated on the Branson Sonifer 450 for 5-10 minutes at 20 % capacity. The protein concentration of these samples was determined by the Biuret method (193). Once the protein concentrations were

determined the remaining intact mitochondrial solution could be used for respiration assays.

A custom-built water-jacketed glass vessel was made to include a cap, which has a replaceable rubber septa for use in inserting specific reagents. The vessel was kept at 298 K during the analysis. 25 mL of respiration buffer (2 mM $MgCl_2$, 20mM phosphates pH 7.4, 250 mM sucrose and 10 mM KCl) was added to the vessel (185). A Clark oxygen electrode (YSI Bioanalytical Products) was used to calibrate the system at 100 % oxygen. The mitochondrial sample (with a total of 5 - 30 mg total mitochondrial protein) was injected and the system was allowed to incubate for a few minutes to establish a baseline. Once the system reached equilibrium, 1.5 mM NADH was injected and uncoupled respiration monitored. After several minutes 0.2 mM ADP was injected to the vessel separately to observed coupled respiration (194).

Once the oxygen readings stabilized (ideally near 0 %) the solution was discarded. The file was imported into Microsoft Excel and the rates of both coupled and uncoupled respiration were determined by a best fit line. The ratio was determined from these rates. Mitochondria isolated from respiring cells consumed oxygen at 0.2 µmol per mg protein per minute compared to 0.05 µmol per mg protein per minute for mitochondria collected from fermenting cells. This agrees with the reported values (139, 195-197). Coupling ratios were ~ 2-6 for all samples. These values are expected for samples with good membrane integrity and protein activity.

Determination of Packing Efficiency and Sample Pellet Composition

In order to determine the Fe-ome of mitochondria, it is necessary to determine the concentrations of many Fe-containing species in our samples. Many previous studies have reported concentrations of Fe species and/or proteins. However, most of these studies reported values in relative terms such as µM/mg protein. This type of information is incomplete because it does not indicate absolute concentrations. In order to determine these concentrations, we designed an experiment utilizing radio-labeled buffer (139, 189).

In order to obtain a high S/N ratio and to have samples with high mitochondrial enrichment, it is necessary to centrifuge samples to obtain mitochondrial pellets for analyses. However, it would be difficult to pack samples in a manner that allowed the exclusion of all buffer since the conditions that might allow the exclusion of all buffer would probably be damaging to mitochondrial membranes. Therefore we chose a centrifugation force and time (10,000 x g for 1 hour) that by Electron Microscopy had proven gentle on our samples as membrane remained intact after repeated steps at these conditions.

The volume of any packed sample must be comprised of the volume of purified mitochondria as well as any interstitial buffer. This relationship can be represented by

$$V_{pellet} = V_{mito} + V_{buffer} \quad [1]$$

where V_{mito} is the volume of mitochondria in the pellet and V_{buffer} is the volume of any interstitial buffer. Purified mitochondria were centrifuged at 10,000 x g for 1

Figure 2-5. Inserts for sample packing and treatment. A modified Lexan graduated cylinder insert was custom made for the SW32Ti Beckman Ultracentrifuge rotor. Lines around the tube allowed determination of the solution volume. B. Glass container could be sealed with rubber septa and flushed with oxygen for 20 - 30 minutes prior to incubation of mitochondria. Alternatively DDT could be added and brought into the MBraun box for dilution and treatment of mitochondria. C. Lexan tube designed to hold Mössbauer cups. Cups had small holes drilled in the sides which could be threaded with fishing line to provide small handles. Notches on opposite sides of the tube provided an area for the fishing line to fit. D. Teflon tubes designed to hold the 5 mm EPR tubes. Modified EPR tubes were fit with an aluminum adapter prior to putting into the instrument.

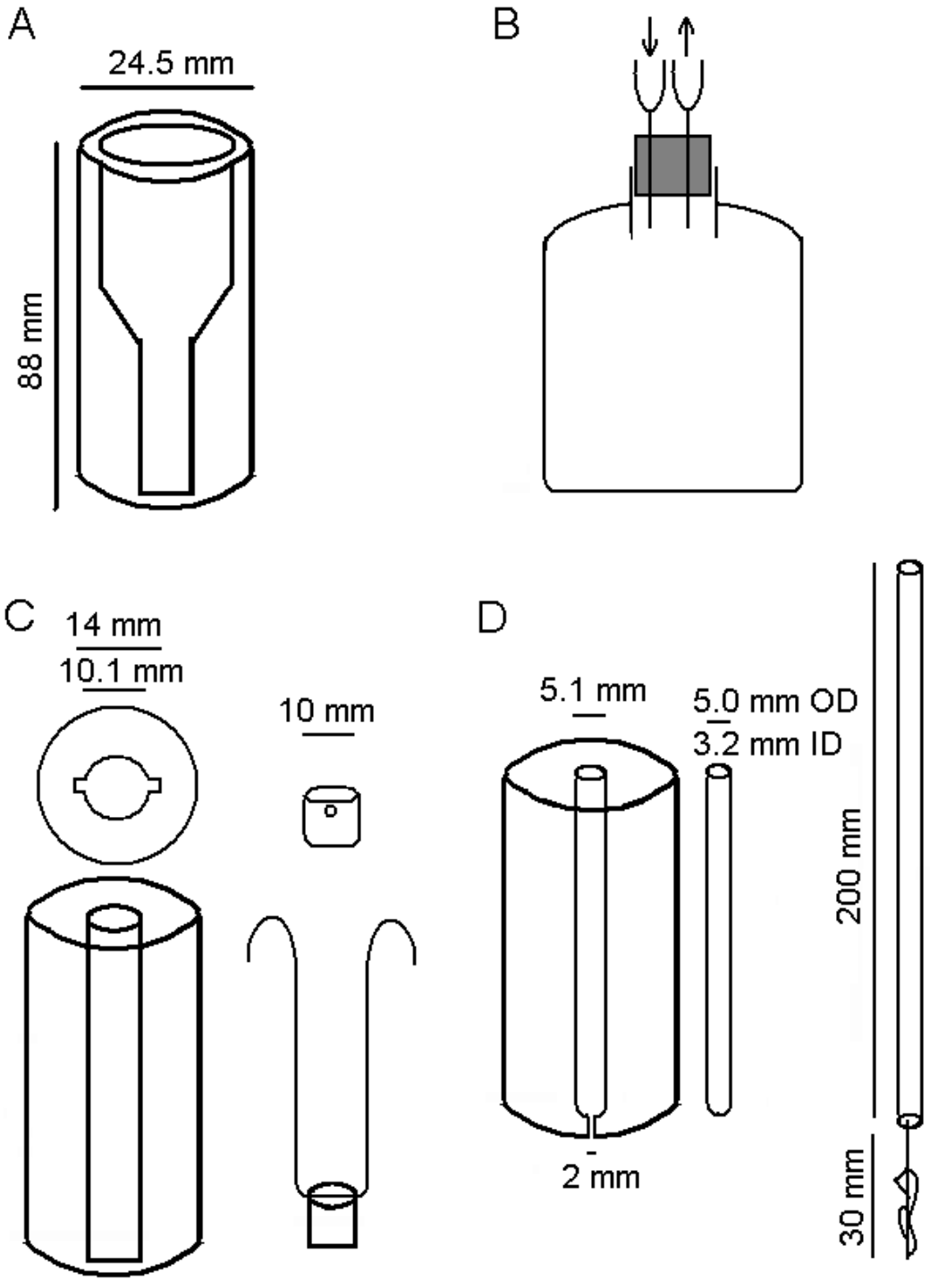

Figure 2-5. Continued.

Table 2-2. Determination of mitochondrial volume in packed samples. Samples 1-7 are of mitochondria grown on Na lactate media (respiring) while samples 8-12 were grown on YPD (fermenting) media.

	C^*_{stock} (cpm/ml)	V_{stock} (mL)	C^*_1 (cpm/mL)	V_{super1} (mL)	$V_{buffer1}$ (mL)	C^*_2 (cpm/mL)	V_{super2} (mL)	$V_{buffer2}$ (mL)	V_{pellet} (mL)	Ave % mito In V_{pellet}
1	24000	1.00	21000	1.00	0.14	2100	0.98	0.11	0.71	83
2	38000	1.00	36000	1.00	0.05	3200	0.98	0.10	0.40	82
3	49000	1.00	45000	0.99	0.11	8200	1.00	0.22	0.82	80
4	250000	1.00	240000	0.98	0.07	53000	1.00	0.28	0.52	66
5	59000	1.00	51000	1.01	0.14	7900	0.99	0.18	0.63	74
6	59000	1.00	45000	1.12	0.20	4100	0.99	0.10	0.92	84
7	59000	1.50	48000	1.49	0.37	14800	0.97	0.44	1.4	71
8	160000	0.6	860000	0.96	0.14	NA	NA	NA	0.82	83
9	110000	0.5	110000	0.45	0.058	NA	NA	NA	0.61	90
10	11000	0.4	10800	0.37	0.035	NA	NA	NA	0.41	91
11	11000	0.5	8800	0.45	0.17	NA	NA	NA	0.52	78
12	4400	0.5	4300	0.47	0.037	NA	NA	NA	0.41	91

hour in our special graduated cylinder inserts (Figure 2-5A) in the Beckman L7 Ultracentrifuge to obtain an initial pellet. The supernatant was removed with a glass pipette and residual buffer was removed from the walls of the inserts using paper towels. The pellet was resuspended in 1SH buffer which had a small amount of ^{14}C-labled sucrose (American Radiolabeled Chemicals, 625 mCi/mol) with counts per min (CPM) of radioactivity per mL given as C^*_{stock} in (Table 2-2). The purified mitochondria suspended in radiolabeled buffer were centrifuged as above. The volume of the resulting pellet could be measured by obtaining the height of the pellet in the inserts.

The supernatant was decanted and measured. The amount of the radionucleotide in the supernatant is proportional to the counts per minute (CPM) detected by a Beckman 5000SL scintillation counter. The radioactivity added to the mitochondrial pellet would then be diluted by the interstitial buffer such that

$$C^*_{stock} V_{stock} = C^*_{super1} (V_{super1} + V_{buffer1}) \quad [2]$$

where C^*_{super1} is the CPM/mL of the supernatant and V_{stock} is the volume of the initial radio-labeled buffer added. C^*_{super1} is the CPM/mL of the resulting supernatant, V_{super1} is the volume of the supernatant measured and V_{buffer} is the volume of the buffer that must remain in the sample. One can solve this equation for V_{buffer}.

An additional measurement can be done by repeating a wash with cold (non-radioactive) buffer. First, the sides of the vial were wiped with paper towel to ensure that no supernatant remained coated on the sides of the cylinder. The

pellet was resuspended with a known volume of cold 1SH buffer. The slurry was centrifuged as above. The supernatant was decanted and the volume of the pellet measured. The radiolabeled isotope remaining in interstitial buffer in the mitochondrial pellet would then be diluted with the added cold buffer.

$$C^*_{super1} V_{buffer2} = C^*_{super2} (V_{super2} + V_{buffer2}) \quad [3]$$

where C^*_{super1} is the CPM/mL of the interstitial buffer remaining from the last step, C^*_{super2} is the CPM/mL of the new supernatant and V_{super2} is the volume of cold buffer added. This process of washing the packed samples with a known volume of buffer and obtaining the relative amount of CPM in the resulting supernatant was repeated with an additional step such that two independent dilution factors could be calculated for the same sample.

Solving Equations 2 and 3 for V_{buffer} will give allow an average V_{buffer} (Table 2-2) which can then be used to determine the volume of mitochondria in the sample. The V_{mito} can be used to determine the packing efficiency by comparing the volume of the total pellet to the volume of mitochondria such that

$$V_{mito} / V_{pellet} \times 100 = \% \quad [4]$$

Repeating this packing protocol (RCF and time) and using this packing efficiency will allow the concentration of observed signals and features in our samples to be calculated for neat mitochondria in every sample. The packing constant for isolated mitochondria did not depend on carbon source. Mitochondria collected from cells grown on lactate media occupied 77 ± 7 % of a mitochondrial pellet while samples collected from cells grown on glucose media

occupy 85 ± 10 % of a mitochondrial pellet. We did not view this as a significant difference and we averaged the values to get a packing constant of 0.82. This value was used to correct calculated concentrations in samples to determine the absolute concentrations of metal and protein in neat mitochondria. These results will be discussed further in Chapter III.

Metal and Protein Analyses

Metal and protein concentrations were determined essentially as described (139, 189). Purified mitochondria were packed into EPR tubes for one hour at 10,000 x g. The supernatant was decanted with a glass pipette. The height of the resulting pellet was marked with for later volume determination. The sample was carefully transferred to a 15 mL centrifuge tube (Fisher) using a glass pipette in a manner that prevented the mitochondrial sample from traveling too far up the glass pipette and therefore adhering to the glass walls. 1SH buffer was added to the marked line in the EPR tube. The glass pipette was used to resuspend any residual mitochondria from the EPR tube into the buffer. This solution was removed and added to the first aliquot of mitochondria. Since the added buffer occupied the same volume as the mitochondrial sample, the dilution factor is 2. This combined with the packing constant can be used to determine absolute protein and metal concentrations.

The mitochondrial samples were either sonicated with a Branson Sonifer 450 for 5 - 10 minutes at 20 % capacity or treated with 1 – 2 % (w/v)

deoxycholate (Acros Organics) to disrupt membranes prior to metal or protein analysis. Failure to disrupt the membranes results in lower concentrations being determined.

For metal analysis three aliquots of the mitochondrial solution (ranging from 25 to 75 µL) were distributed into three 15 mL Falcon tubes. Each aliquot was treated with 100 µL of 15.8 M trace-metal-grade HNO_3 (Fischer Scientific). Each tube was securely wrapped with electrical tape and vortexed to mix the sample and acid prior to incubating overnight at 90 – 95 °C. The resulting solution was diluted with deionized and distilled H_2O to a final HNO_3 concentration of 0.2 M. Samples were run on an Inductively Coupled Plasma Mass Spectrophotometer PerkinElmer DRCII and calibrated with standards Environmental Standards ranging from 1 - 250 ppb metal.

Protein concentration was determined by the BCA (Pierce Scientific) method. BSA (Pierce or Sigma) was used to generate a standard curve. Dilutions and solutions are carefully described by (198) which is included with each kit purchased from Pierce Scientific. Measurements were made using the Hitachi U-3310 spectrometer with a head-on photomultiplier tube.

Treatment of Samples with Redox Agents

Mitochondria have been treated with redox agents previously (139, 189). Purified mitochondria were collected in the “as-isolated” state (without the addition of any redox agents). Samples prepared in the as-isolated state were

packed as described above without being reduced or oxidized. For oxidized samples, 40 mL glass vials were capped with rubber septa and a gas line of pure oxygen was inserted, a second needle was placed in the septa to provide an outflow (Figure 2-5B). The vial was flushed with oxygen for 20 - 30 minutes. The outlet needle was removed immediately prior to the inlet needle to preserve the high-oxygen concentration in the vial. The rubber septum was secured to the vial electrical tape. The entire vial was taken into the MBraun box. Mitochondrial pellets from the isolation protocol were resuspended in 0.5-1 mL 1SH buffer and a Hamilton Gastight 16 gauge syringe was used to insert the samples into the vial. Samples were incubated in oxygen for 30 - 40 minutes before being packed for analyses.

For reducing samples, packed mitochondria from the last step of the isolation protocol were resuspended into a 0.5 - 1 mL of 1ST buffer (0.6 M sorbitol, 1 mM EGTA, 20mM Tris, pH 8.5). Sodium dithionite (Fisher Scientific) was weighed out and anaerobically dissolved in 0.2 M NaOH. Samples were treated with 1.0 mM dithionite (final concentration) for 30 - 40 minutes. Reduced samples were packed at 10,000 x g for one hour and used for analysis.

Electron Paramagnetic Resonance

Sample preparation has been described by our lab previously (10, 14). Custom built Delrin inserts (Figure 2-5D) were made to fit centrifuge tubes for the SW-32Ti rotor for the Beckman L7 Ultracentrifuge. Custom made EPR

tubes (Figure 2-5D) were from Wilmad Labglass. Supracil tubes had dimensions 5.0 ± 0.05 mm OD, 3.2 ± 0.03 mm ID, 170 mm long. Each tube was cut in half and the bottom was rounded on the new tube—providing two ca 80 mm long tubes.

Samples were kept anaerobic until after being frozen. Purified mitochondria were pipetted into the Supracil EPR tubes which were placed in the inserts. Tubes were centrifuged at 10,000 x g for one hour. The supernatant was decanted. If the mitochondrial pellet did not occupy at least 2.5 cm height (or approximately 250 µL) more mitochondrial solution was added and the tube was centrifuged again. Once enough mitochondria were packed and the supernatant was decanted, the tube was capped with a rubber septa, brought out of the box and frozen slowly from the bottom of the tube upwards in liquid N_2.

Spectra were collected on a Bruker EMX X-band EPR with an Oxford Instruments ESR 910 crytostat. In order to collect spectra of samples, an adapter (Figure 2-5D) was necessary to extend the length of the modified tubes. The aluminum adapter has a length of approximately 200 mm and a thin gauge wire soldered to the bottom. The wire extends approximately 30 mm and folds back on itself with several bends and twists. Once inserted into the opening of the EPR tubes, these bends provide the force necessary to securely handle the sample for insertion and removal from the EPR.

Spectra were calibrated using a 1.0 mM Cu (II) EDTA standard run the same day as the samples. Spectra were imported into SpinCount (http://www.chem.cmu.edu/groups/hendrich/facilities/index.html) and assigned a Cu standard. Typical spectral features (which are discussed in detail in Chapter III) can be simulated with spectra (and the corresponding g values) of isolated species such as the organic radical, succinate dehydrogenase and the reiske protein. Concentrations were calculated using g values reported in Chapter III and adjusted manually for the best fit. Analysis of EPR spectra is discussed in greater detail in Chapter III.

Mössbauer Spectroscopy

All steps were done anaerobically. Custom made Lexan inserts (Figure 2-5C) were made for the SW-32Ti ultracentrifuge rotor. Mössbauer sample cups were made of Delrin and had dimensions shown in (Figure 2-5C). Small holes were drilled into the cups such that fishing line could be threaded through the holes and function as a handle for the sample cup. The cup was pushed to the bottom of the Lexan insert and the fishing line secured with tape to the outside of the insert. 5 - 8 mL of dilute purified mitochondria were packed into the apparatus at 10,000 x g for 1 - 2 hours. The fishing line was used to remove the sample cup from the insert. Any visible solution was decanted with a glass pipette. An aluminum block with a cavity just wider and shorter than the sample cup was cooled in liquid N_2 for ~ 30 minutes (usually during the late stages of

the centrifugation step). It was brought into the MBraun box. The sample cup was placed in the cavity until frozen before bringing the sample out of the box to store in liquid N_2.

All Mössbauer spectra were collected at 4.5 or 100 K on either a MS4 WRC spectrometer (SEE Co. Edina, MN) equipped with a CCR4K Closed Cycle He gas Refrigerator cryostat (Janis Instrument Co., Willmington, MA) or on a Super-Varitemp Dewar (Janis Instrument Co., Wilmington, Ma). Data were analyzed using the WMOSS software package (See Co. Edina, MN). All chemical shifts are reported relative to Fe metal (alpha Fe foil) at 298 K. Analysis of samples by Mössbauer spectroscopy is discussed in greater detail in Chapter III.

Electronic Absorption Spectroscopy

Samples were prepared essentially as described (189, 199). All samples were prepared under anaerobic conditions. Purified mitochondria were packed into EPR tubes for 1 hour at 10,000 x g as described above to obtain an accurate sample volume (by marking the height of the sample in the tube) and allowing the use of the packing constant. Samples were then resuspended in 2 - 3 fold volume buffer (also clearly marked on the EPR tube for accurate volume determination). Samples were quantitatively transferred to 2 mm path-length custom-made UV-Vis quartz cuvettes (NS Precision Inc). These cuvettes were adapted such that they could be sealed with rubber septa. Once mitochondrial

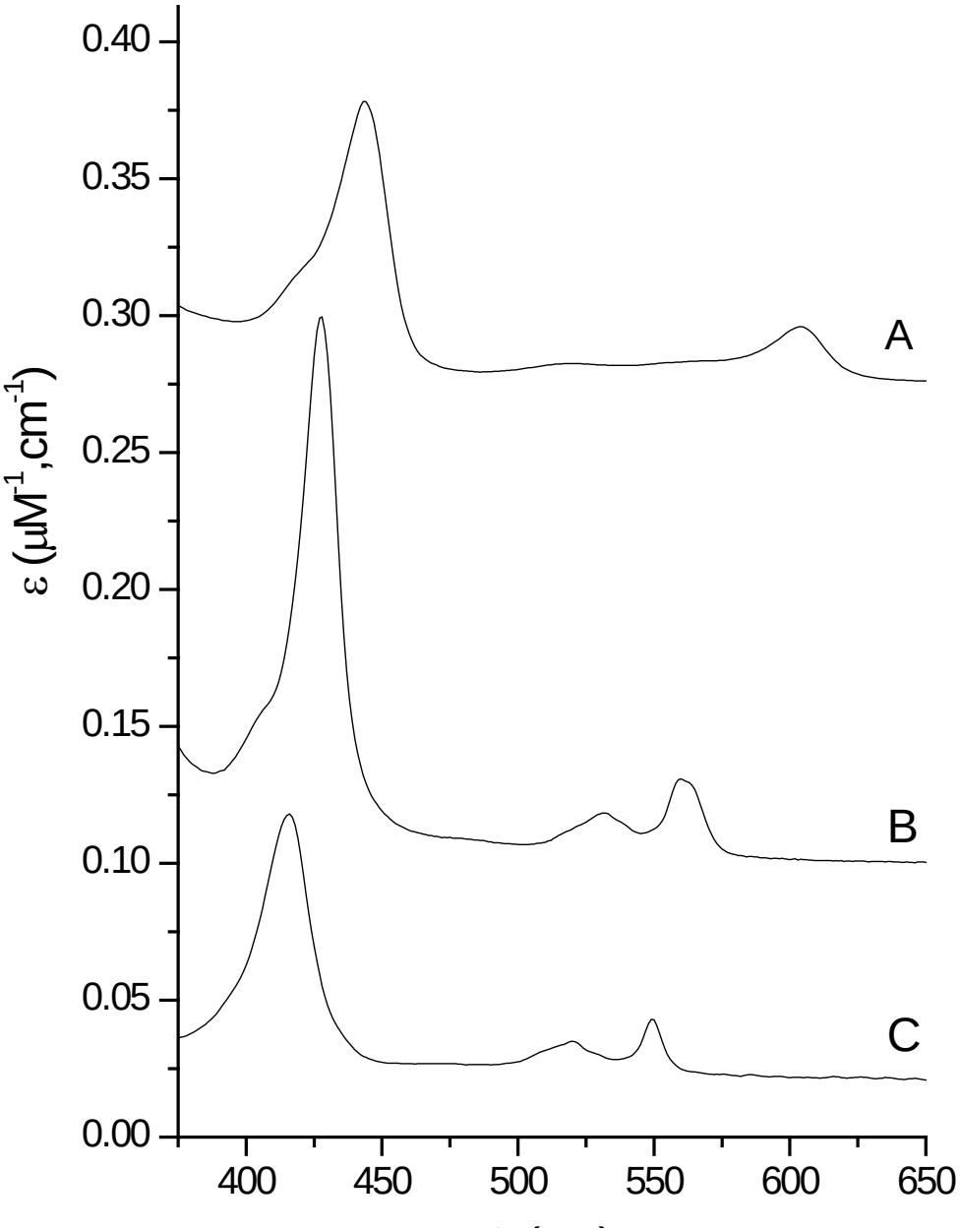

Figure 2-6. Electron absorption of isolated heme-containing proteins. Spectra are of A, cytochrome c oxidase (generously provided by Graham Palmer (200)); B, cytochrome b_5 (human); C, cytochrome c (bovine).

solutions were added to the cuvettes, they were sealed and remained anaerobic for the duration of the measurements. Spectra were collected on a Hitachi U-3310 with a head-on photomultiplier tube. The resulting spectrum was decomposed assuming

$$\text{Abs}(\lambda) = [\text{Heme } a]\varepsilon_a(\lambda) + [\text{Heme } b]\varepsilon_b(\lambda) + [\text{Heme } c]\varepsilon_c(\lambda) + \text{light scattering} \quad [5]$$

where [Heme x = a, b or c] is the concentration of each heme center and ε_x are the extinction coefficients. In order to determine the concentration of each heme, spectra were multiplied by the samples dilution factor, corrected for the path-length and divided by the packing constant. The resulting spectra were then imported into OriginPro and fit with individual contributions from heme *a*, *b* and *c*.

The spectra of cytochrome c oxidase (beef heart), human cytochrome b_5, and yeast cytochrome *c* were used to represent *a*, *b*, and *c* type hemes in the spectral decomposition. A spectrum of reduced cytochrome oxidase was obtained from (200). The spectral intensity was divided by two to account for the two heme centers (heme *a* and heme a_3). Purified cytochrome b5 and cytochrome c were purchased from Sigma. Each protein was dissolved in buffer, reduced with 1 mM dithionite and measured. Absorption intensities were divided by the concentration of the protein solution such that the extinction coefficient could be plotted vs. the wavelength (Figure 2-6). These individual protein curves were corrected so that the extinction coefficients were in μM^{-1} cm^{-1}. The resulting spectra were used to determine the relative contributions of each heme

center to the mitochondrial samples. Contributions were fitted manually, affording the composite spectrum shown in Chapter III.

Enrichment of Samples by Growth on ^{57}Fe

Preparation of samples for Mössbauer spectroscopy included addition of 40 μM ^{57}Fe to growth media. Samples were grown on either rich (YP*) or minimal media. Rich media contains approximately 40 μM Fe naturally. Therefore, rich media that was supplemented with ^{57}Fe contained ~ 50 % ^{57}Fe. Minimal media only has approximately 10 μM Fe naturally so the supplemented media contained ~ 80 % ^{57}Fe. The enrichment of our samples could also be determined during ICP-MS analysis. Since the concentrations of both ^{56}Fe and ^{57}Fe were determined (Table 2-3). Mitochondria grown on minimal media contained 40 ± 10 % ^{57}Fe (for respiring samples) or 81 ± 10 % ^{57}Fe (for fermenting samples). The enrichment dropped to 20 ± 4 % and 30 ± 5 % respectively when samples were grown on rich media. Interestingly there is not a direct relation between the percent ^{57}Fe in the media and the actual enrichment of our samples. However growth in minimal media did at least double the enrichment in our samples. This discovery led us to prepare most later (after the discovery of this fact) batches on minimal media. Analysis of our samples by Mössbauer is only sensitive to the ^{57}Fe concentration, therefore for the purposes of analysis, we assume that the distribution of ^{56}Fe and ^{57}Fe are identical.

Table 2-3. Enrichment of ^{57}Fe in typical samples. All samples were grown in media supplemented with 40 µM ^{57}Fe. Media was either minimal (M) or rich (YP). Rich media naturally contains approximately 40 µM Fe while minimal media has only ~ 10 µM Fe. Therefore the enrichment of the media was 50 % and 80 % (final concentration) respectively. The cultures were grown on either glycerol (R) or glucose (F). Concentrations of mitochondrial solutions (*) are reported where dilution factors were not calculated. All other concentrations were calculated for neat mitochondria. Estimated uncertainties are ± 20 % in every measurement.

Media	Carbon	^{56}Fe (µM)	^{57}Fe (µM)	enrichment
M	R	250	350	58
M	R	440	200	31
M	R	410	210	33
M	R	560	230	29
M	R	430	310	42
M	R	400	300	43
M	R	340	290	46
M	F	120	200	62*
M	F	190	820	81
M	F	26	250	90*
M	F	45	180	80*
M	F	180	600	77
M	F	19	480	96
M	F	110	550	83
M	F	260	1000	80
YP	R	520	150	22
YP	R	960	200	17
YP	R	110	18	14*
YP	F	490	240	32
YP	F	570	180	24
YP	F	620	290	31

CHAPTER III

THE Fe-OME OF MITOCHONDRIA ISOLATED FROM RESPIRING AND FERMENTING *Saccharomyces cerevisiae*[‡]

Introduction

Yeast cells can undergo two distinct modes of metabolism: respiration and fermentation. Fermentation is the process by which ethanol and carbon dioxide are produced from pyruvate. Cells grown on fermenting carbon sources are smaller and tend to have shorter cell cycles than when grown on respiring carbon sources (8, 22, 201). A small amount of energy is gained in this process as glycolysis produces 2 ATP molecules per glucose consumed (22). Fermentation is an anaerobic pathway since molecular oxygen is not required for glycolysis (202-205). Glycolysis occurs in the cytosol and therefore this type of metabolism does not utilize mitochondria or other cellular organelles (22, 205).

Unlike fermentation, respiration involves mitochondria extensively as most of the reactions of this metabolic pathway occur along the mitochondrial inner membrane and within the matrix. During respiration sugars are broken down or converted to intermediates of glycolysis or the citric acid cycle. By feeding into the citric acid cycle, the cell can utilize oxidative phosphorylation to produce more ATP per carbon. Thus, although respiration is slower, it is more efficient energetically (203).

[‡]Reprinted with permission from "Characterization of the iron in mitochondria isolated from respiring and fermenting yeast." by Morales, JG.; Holmes-Hampton, GP.; Miao, R.; Guo, Y.; Münck, E.; and PA Lindahl. *Proceedings of the National Academy of Science. Submitted* 2010. Proceedings of the National Academy of Sciences.

For yeast, glucose is a fermenting sugar because it actually represses the expression of genes involved in respiration (202, 206-209). However, if the cell culture is allowed to grow in the presence of glucose for a long duration, and enough glucose is consumed to alleviate the repression, both types of metabolism may occur simultaneously (205, 210-211). In addition, some carbon sources, such as galactose can be used for both respiration and fermentation and exhibit a mixture or intermediate type of metabolism (206, 208, 212). As cells shift their metabolism from fermentation to respiration, they are said to undergo a diauxic shift (190).

Related metabolic shifts occur in human metabolism. Human cells primarily produce energy through oxidative phosphorylation due to the efficiency of this process (213). A shift in metabolism occurs during different levels of exertion. Cells initially use cellular stores of ATP for energy. During anaerobic exercise this ATP is regenerated through glycolysis (213). This generally can only last for short durations. During aerobic exercise, cells have sufficient oxygen for the breakdown of sugar and fat for production of energy through oxidative phosphorylation (214).

A metabolic shift is also noted in oncology. Cancerous cells produce ATP via glycolysis followed by lactic acid fermentation (213, 215-216). Both of these processes occur in the cytosol even if oxygen is readily available (217). Healthy cells prefer pyruvate oxidation in mitochondria to lactic acid fermentation due to the higher efficiency of energy production. This fundamental change that occurs

in the metabolism of cancerous cells is known as the Warburg effect (213, 217). Because they are growing and dividing faster than normal, cancer cells have a low-oxygen environment, which favors glycolysis (213). Additionally mitochondria may be damaged in oncology, which would favor cytosolic pathways (213, 217). In order to gain insight to metabolic trends within our own cells, it is necessary to use model organisms where phenotypic and genotypic traits can be manipulated.

Respiring cells exhibit higher expression of proteins involved in oxidative phosphorylation and Fe metabolism than when grown on fermenting carbon sources (29, 205-206, 218-219). Derisi *et al.* (29) used microarrays to demonstrate how glucose concentrations in the media affect the expression of proteins. Media glucose concentrations above 2 % repress the expression of respiratory complexes, including cytochrome bc1 and cytochrome c oxidase. In contrast, many genes of unknown function are repressed as glucose concentrations decline (29). Gao *et al.* (206) found that 176 proteins were up-regulated during cellular growth on glucose while cellular growth on galactose up-regulated 231 proteins. Glucose-induced proteins were highly varied in function and included roles in membrane growth, protein degradation, amino acid biosynthesis and glucose metabolism (206). Galactose-induced genes were involved in galactose metabolism, protein synthesis, Fe metabolism and oxidative phosphorylation (206). The response of gene expression to changes in carbon source correlates to the metabolic needs of the cells. Respiring cells

utilize mitochondria and different metabolic pathways than fermenting cells, and it follows that expression of these pathways are activated by growth on respiring carbon sources (30, 205, 220).

As mentioned in Chapter II, mitochondria occupy a larger volume of the cell when grown on respiring carbon sources. Fermenting cells are known to produce fewer mitochondria. Furthermore, cells early in the exponential growth phase are largely devoid of mitochondria, while in later stages of fermentation, the organelle occupies 3 - 4 % of cell volume (221-223). Under respiration, mitochondria represent 10 – 12 % of cell volume (26). Also, the morphology of mitochondria in fermenting cells differs from that in respiring cells. Using fast high-resolution 3D microcopy of live cells, Egner *et al.* (224) found that mitochondria from both fermenting and respiring cells consist of a single large branched tubular network, but that fermenting mitochondria are thinner and possess fewer branch points.

This variation in cell volume occupied by mitochondria may seem partially intuitive since mitochondrial functions are utilized more during respiration. However, even cells not actively utilizing mitochondria may need to maintain some basal expression of mitochondrial respiratory proteins during fermentative growth in case they undergo a diauxic shift (22, 29, 205). The lack of involvement of mitochondria during fermentation raises the issue of what these organelles *do* during this growth mode.

In this study, we employed our integrative biophysical approach to assess the iron-ome of mitochondria isolated from yeast grown under fermenting, respirofermenting and respiring conditions. We report that respiration-related Fe-containing proteins and other $[Fe_4S_4]^{2+}$ cluster containing proteins dominate the iron-ome of mitochondria isolated from respiring and respirofermenting cells. Under fermenting conditions, the concentrations of these species decline while those of nonheme high-spin (NHHS) Fe^{2+} ions, mononuclear HS Fe^{3+} ions and Fe^{3+} nanoparticles increase. These NHHS Fe^{2+} ions may be feedstock for Fe/S cluster and heme biosynthesis.

Iron-ome of Respiring Mitochondria

Mitochondria were isolated from respiring yeast cells. The metal concentration of isolated respiring mitochondria was determined by ICP-MS (Table 3-1, Table 3-2). Mössbauer, EPR, and UV-Vis spectra of the same or equivalently prepared samples were obtained. The low-field Mössbauer spectrum of a respiring mitochondria sample (Figures 3-1 and 3-2) was dominated by the central doublet which extends between - 1 and + 1 mm/s Doppler velocities (percentages given in Table 3-1). This doublet has parameters ((isomer shift δ, quadrupole splitting ΔE_Q, and line width Γ) typical of S = 0 $[Fe_4S_4]^{2+}$ clusters and low-spin Fe^{2+} hemes; these two groups cannot be distinguished by Mössbauer spectroscopy. A minor contribution (< 10 %) of S = 0 $[Fe_2S_2]^{2+}$ and S = 2 $[Fe_3S_4]^{0}$ clusters to the central spectral region could not be

Table 3-1. Analytical properties of isolated mitochondria. Concentrations are for "neat" mitochondria (devoid of solvent) rather than mitochondrial suspensions or packed mitochondrial samples. Experimentally determined protein and metal concentrations of mitochondrial suspensions were multiplied by the dilution factor $(V_{mito} + V_{buffer}) / V_{mito}$ and dividing by 0.8 (packing efficiency, as measured previously (139, 189). Values listed are the average of individual determinations (Table 3-2). Relative uncertainties are standard deviations from batch-to-batch. There are additional uncertainties related to fitting (which we estimate to be 20 %). The number of samples evaluated is given in parentheses. Heme *a*, *b*, and *c* concentrations were determined by analysis of electronic absorption spectra. The percentages of Fe present as HS Fe^{3+} were determined solely from high-field Mössbauer spectra.

	Respiring	Respirofermenting	Fermenting
Protein (mg/mL)	170 ± 61 (5)	200 ± 60 (2)	110 ± 30 (11)
Fe (μM)	720 ± 210 (5)	840 ± 120 (2)	770 ± 320 (11)
Cu (μM)	210 ± 170 (5)	160 ± 80 (2)	50 ± 37 (11)
Mn (μM)	35 ± 20 (5)	12 ± 4 (2)	15 ± 12 (11)
Zn (μM)	290 ± 160 (5)	230 ± 150 (2)	290 ± 210 (11)
Central Doublet	60 ± 2 % (2)	50 % (1)	25 ± 4 % (5)
HS Fe^{2+} heme	7 ± 1 % (2)	4 % (1)	4 ± 1 % (5)
NHHS Fe^{2+} ions	2 ± 1 % (2)	3 % (1)	20 ± 5 % (5)
Mononuclear HS Fe^{3+}	0 % (2)	5 % (1)	15 ± 3 % (3)
S = ½ $[Fe_2S_2]^{1+}$	13 ± 2 % (2)	10 % (1)	~ 0 % (5)
$[Fe_2S_2]^{2+}$	< 5 % (2)	< 5 % (1)	~ 0 % (5)
Fe^{3+} nanoparticles	< 5 % (2)	< 5 % (1)	33 ± 7 % (5)
Central un-resolved material	20 %	25 %	5 % (5)
Heme *a* (μM)	51 ± 8 (4)	61 (1)	14 ± 1 (4)
Heme *b* (μM)	52 ± 8 (4)	55 (1)	27 ± 5 (4)
Heme *c* (μM)	120 ± 10 (4)	160 (1)	73 ± 15 (4)
g_{ave} = 1.94 (μM)	1 – 10 (3)	13 ± 4 (2)	1 - 3 (2)
g_{ave} = 1.90 (μM)	13 ± 3 (3)	29 ± 18 (2)	6 ± 2 (2)
g = 2.01 (μM)	0 – 1 (3)	1 - 2 (2)	0 (2)
g = 2.00 (μM)	0 – 2 (3)	0 – 6 (2)	0 – 1 (2)
g = 2.04 (μM)	1 – 3 (3)	3 ± 1 (2)	1 - 2 (2)
g = 4.3 (μM)	5 – 45 (3)	2 – 14 (2)	3 (1)
g = 5.8 (μM)	1 - 2 (3)	0 - 2 (2)	~ 0 (1)
g = 6.4, 5.3(μM)	1 - 4 (3)	0 - 5 (2)	1 (1)

Table 3-2. Protein and metal concentrations in isolated mitochondria. Mitochondria isolated from cells grown on glycerol, galactose, and glucose are designated R# (respiring), RF# (respiring/fermenting) and F# (fermenting), respectively. Samples F1 – F4 were from cells grown on YPD media while F5 – F11 were from cells grown on minimal media. Estimated uncertainties are ± 20 %.

Preparation	Protein (mg/mL)	Fe (µM)	Mn (µM)	Cu (µM)	Zn (µM)
R1	200	750	23	360	420
R2	180	600	46	63	320
R3	110	600	30	59	180
R4	120	670	42	110	82
R5	80	320	6.1	270	200
RF1	200	770	13	80	270
RF2	120	690	8	170	100
F1	74	640	30	36	540
F2	64	520	12	95	580
F3	86	650	11	92	220
F4	80	530	27	58	190
F5	120	850	7.2	46	180
F6	96	280	2.5	14	75
F7	74	620	6.3	28	220
F8	120	500	4.8	25	140
F9	99	560	3.9	22	140
F10	120	1300	1.6	41	280
F11	89	470	22	4.5	89
WCF1	55	440	16	34	570
WCF2	57	600	13	24	550
WCF3	55	430	9	22	540
WCR1	75	340	38	48	1300
WCR2	70	260	37	31	1100
WCR3	98	340	30	40	970

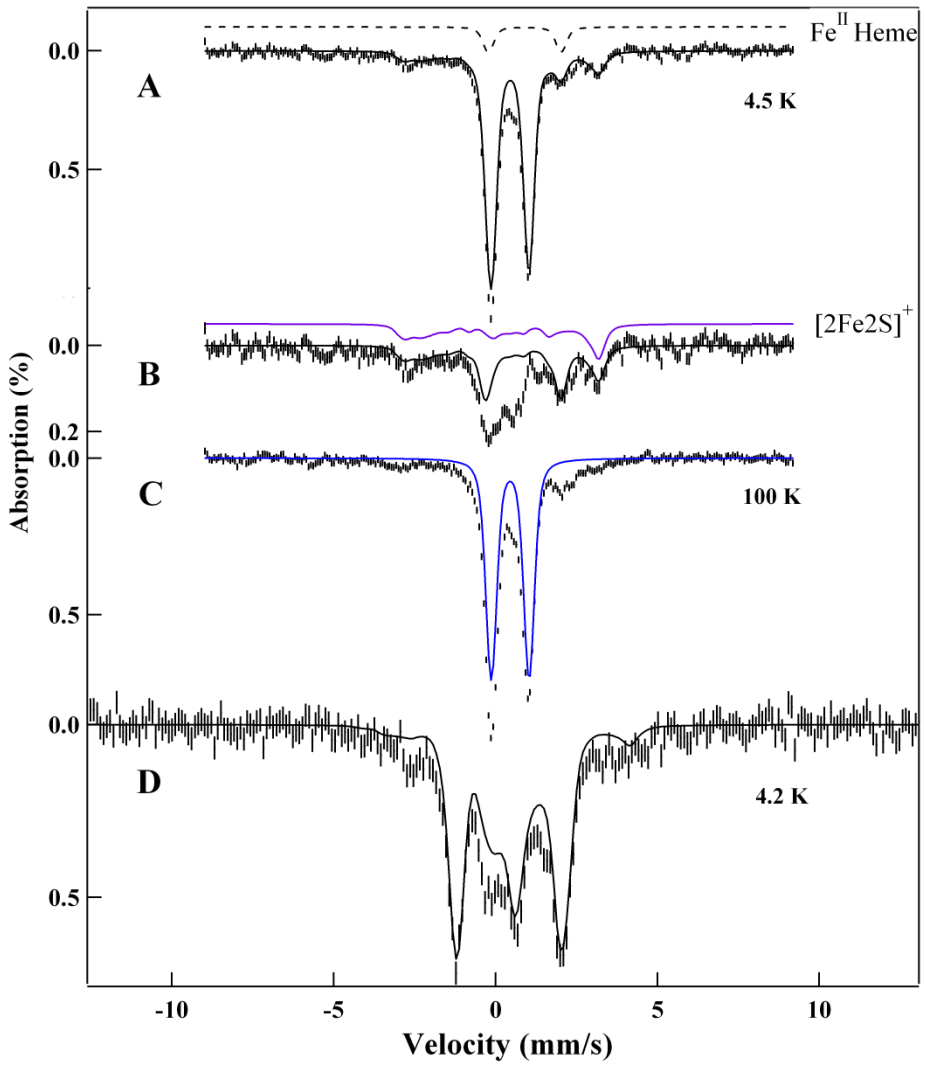

Figure 3-1. Mössbauer spectra of mitochondria isolated from respiring cells. A, 4.5 K, 0.05 T parallel applied magnetic field. The solid red line is a simulation using the parameters listed in Table 3-1 for the central doublet (60 % of the Fe), HS Fe^{2+} hemes (7 % of the Fe), nonheme HS Fe^{2+} (2 % of the Fe), and S = ½ $[Fe_2S_2]^{1+}$ clusters (14 % of Fe). B, same as A after subtracting the central doublet and HS Fe^{2+} heme contributions. The solid blue line is a simulation for S = ½ $[Fe_2S_2]^{1+}$ clusters, while the solid blue line is a composite simulation including this feature as well as that for HS Fe^{2+} hemes and nonheme HS Fe^{2+}. Most of the absorption that remains is the *central unresolved material*. C, same as A except at 100 K. D, same as A except with 8 T applied field. The red line is a simulation including 60 % of the central doublet and 14 % of S = ½ $[Fe_2S_2]^{1+}$ clusters.

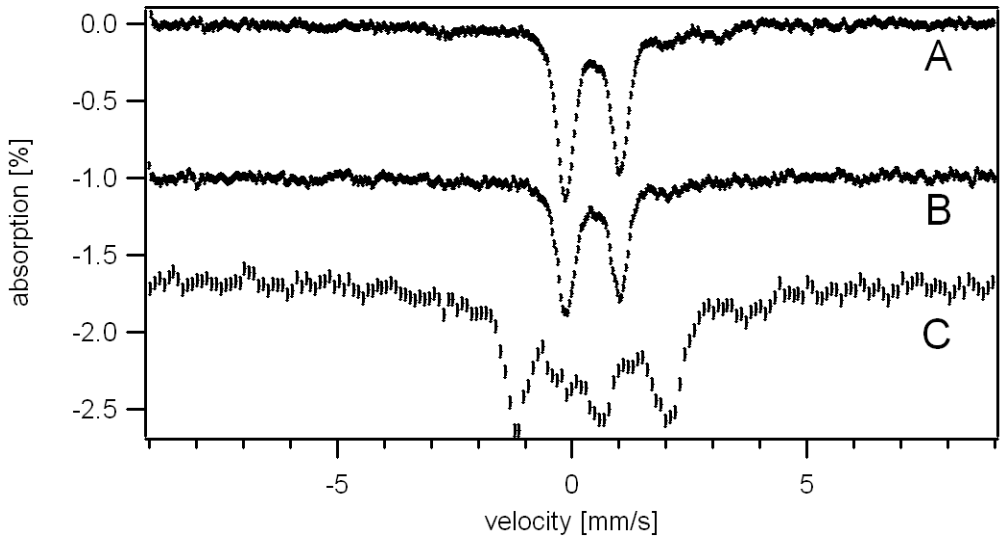

Figure 3-2. Mössbauer spectra of an additional respiring mitochondrial batch. Spectra were collected at 4.5 K, 0.04 T parallel field (A); 100 K 0.04 T parallel field (B); and (C) 4.2 K 8 T applied field. Fermenting samples reported in Table 3-1 but not displayed are shown in (225).

excluded but neither is there unequivocal evidence for such clusters in respiring mitochondria. Simulations that included ~ 5 % of total Fe in the form exhibited by S = 0 $[Fe_2S_2]^{2+}$ clusters improved low-field fits but not high-field fits.

Respiring mitochondria also exhibited a quadrupole doublet with parameters typical of high-spin Fe^{2+} heme centers (226). The high-energy line of this heme doublet is at 2.2 mm/s while the low-energy line is buried within the central doublet (Figures 2-1 and 3-1). Although difficult to distinguish from the baseline, the 4.5 K low-field spectrum had absorption due to magnetic Fe. This absorption is most clearly observed by subtracting the contributions of the central doublet and the HS heme doublet from the original spectrum. The solid red line overlaying the resulting spectrum (Figure 3-1B) simulates the contribution of a generic S = ½ $[Fe_2S_2]^{1+}$ cluster (we chose the parameters of the Reiske Fe/S protein (227)). Other paramagnetic centers (e.g. from $[Fe_4S_4]^{1+}$ clusters) might also contribute to this absorption but the spectral resolution is insufficient to distinguish the contributions of individual species. Rather, EPR spectroscopy was used to do this (see below). The Mössbauer simulation is useful, however, in revealing that much of the absorption at the velocity of the high-energy line of the nonheme HS Fe^{2+} doublet that is evident in fermenting mitochondria (see below) is actually due to magnetic Fe simulated here as S = ½ $[Fe_2S_2]^{1+}$ cluster. Only ~ 2 % of spectral intensity in the spectrum of respiring mitochondria appears to arise from nonheme high-spin (NHHS) Fe^{2+} ions.

After simulating all of these spectral features, and subtracting them from the data, some unresolved and absorption remains in the center of the spectrum (Figure 3-1). This so-called *central unresolved material* remains unassigned, but its apparent isomer shift suggests a magnetically interacting Fe^{3+} species.

Mitochondrial suspensions are turbid, leading to electronic absorption spectra with strong sloping baselines due to light scattering (Figures 3-3 and 3-4). Superimposed on this are Soret bands in the 400 nm region and α and β bands in the 500 – 620 nm region arising from both HS and LS Fe^{2+} hemes. UV-Vis spectra of respiring mitochondria were simulated by adding spectra of individual heme *a*, *b* and *c* containing proteins (Figure 3-3A dashed line). Resulting concentrations for each center (Table 3-1 and Table 3-3) reveal the dominance of heme *c*, followed by heme *b* and heme *a* in roughly equal amounts. The HS portion of these Fe^{2+} heme centers afforded the heme quadrupole doublet mentioned above, while the LS portion contributed to the central doublet. Most heme *a* groups observed by UV-Vis are found in cytochrome c oxidase; the portion observed reflects reduced Fe^{2+} states of the *a* and a_3 sites.

EPR spectra of respiring mitochondria revealed additional details regarding the magnetic Fe observed by Mössbauer. The low-field spectrum (Figure 3-5D) was dominated by signals at g = 6.4, 5.9, and 5.3. These signals are assigned to the partially oxidized heme [a_3:Cu_b] center of cytochrome c oxidase (64), in which the a_3 heme is Fe^{3+} and the Cu_b site is Cu^{1+}. The signal

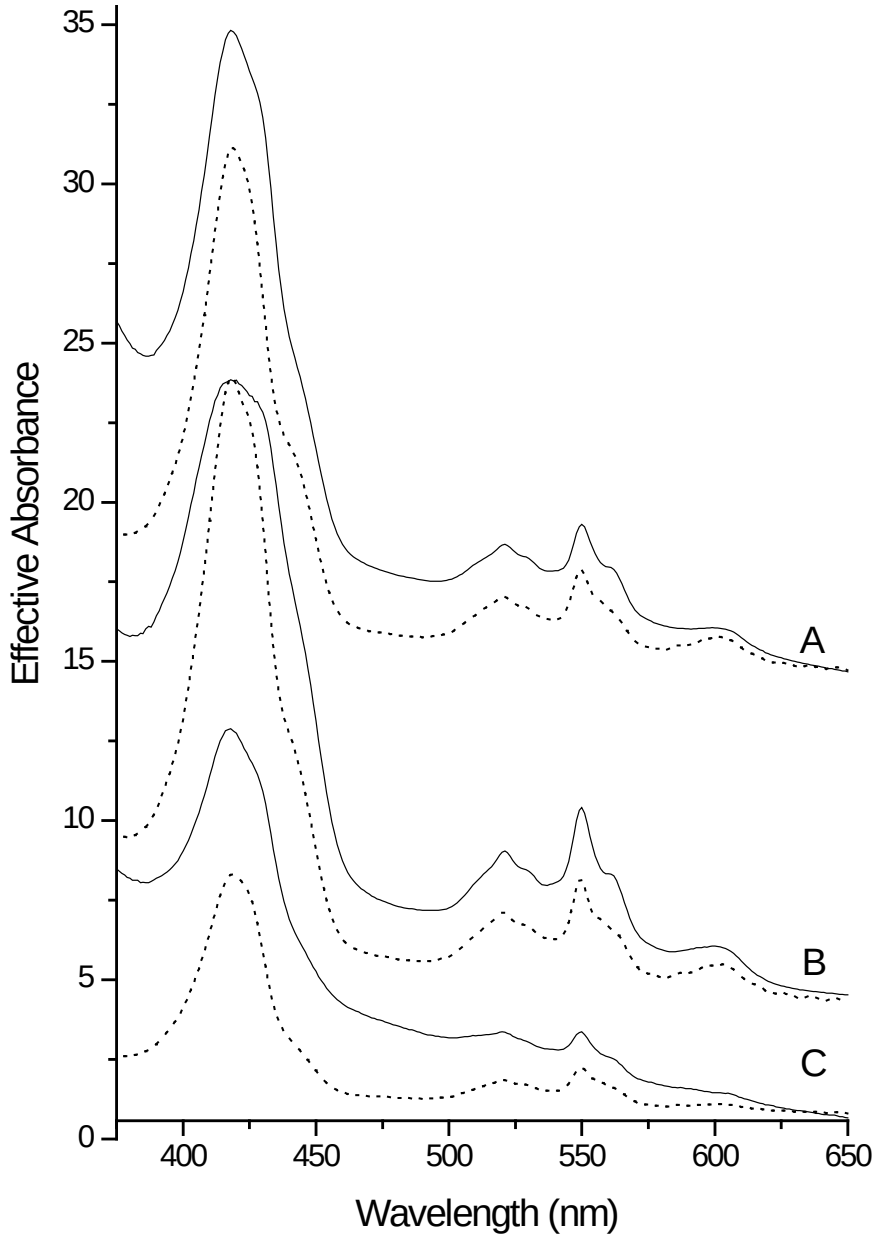

Figure 3-3. Electronic absorption spectra of mitochondria in buffer suspension. A, respiring (R1); B, respirofermenting (RF2); C, fermenting (F3). Effective absorbances of neat mitochondria normalized to a 10 mm path-length cuvette are plotted. These values were obtained by multiplying raw absorbance by 2 (the dilution factor relative to packed mitochondria) and by 5 (path-length factor due to the use of a 2 mm path-length cuvette) and dividing by 0.82 (the packing factor). Dashed lines are composites of spectra from individual heme *a*, *b*, and *c* containing proteins, using parameters given in Table 3-3 (average values are given in Table 3-1).

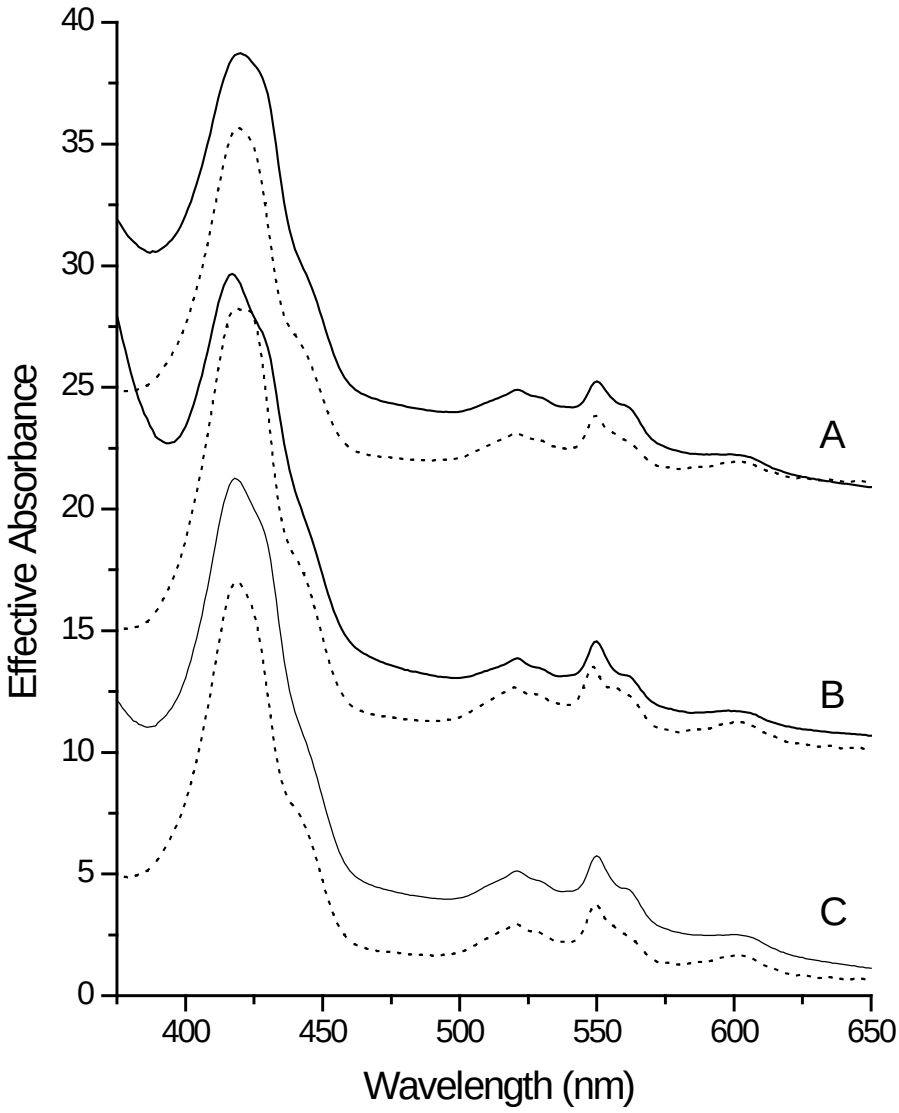

Figure 3-4. Electronic absorption spectra of different batches of respiring mitochondria. A, batch R3 (protein concentration, 45 mg/mL); B, R4 (44 mg/mL); and C, R2 (74 mg/mL). Dotted lines are composite spectra using the [Heme *a*], [Heme *b*], and [Heme *c*] concentrations given in Table 3-3.

Table 3-3. Concentrations of individual heme components determined for mitochondrial samples. Values are in μM and are for neat mitochondria. Estimated uncertainties are ± 20 % for each entry.

Sample	[Heme *a*]	[Heme *b*]	[Heme *c*]
R1	45	43	110
R2	55	44	130
R3	60	60	130
R4	44	44	120
F1	15	30	85
F2	15	33	85
F3	13	22	61
F4	12	23	61

at g = 6 has axial symmetry while that at g = 6.3 and 5.4 has rhombic symmetry; spin concentrations are given in Table 3-1.

The g = 2 region of the EPR spectrum of as-isolated respiring mitochondria (Figures 3-5A and 3-6) was dominated by signals with g_{ave} = 1.94, g_{ave} = 1.90 and a nearly isotropic signal with g_{ave} = 2.01 (perhaps combined with another signal at g = 2.00). The dashed spectrum in Figure 3-5A is the sum of simulations of these signals, assuming the spin concentrations listed in Table 3-1. The similarity of the observed g-values to signals of isolated mitochondrial proteins suggests that the g_{ave} = 1.94 and 1.90 signals arise, respectively, from the $[Fe_2S_2]^{1+}$ clusters in succinate dehydrogenase (44-45) and the Reiske protein of cytochrome *bc₁* (51). The g_{ave} = 2.01 signal is typical of S = ½ $[Fe_3S_4]^{1+}$ clusters, arising perhaps from the oxidized inactivated form of aconitase or homoaconitase, or from the $[Fe_3S_4]^{1+}$ cluster in succinate dehydrogenase. The overlapping signal at g = 2.00 is probably an organic-based radical. A signal with g_{ave} = 2.04 may be due to the electron transfer flavoprotein-ubiquinone oxidoreductase (ETF-QO) (228). Minor features with resonances between g = 2.2 – 2.1 are reproducibly observed but remain unassigned. The species affording these EPR signals should collectively correspond to some or all of the ~ 13 % of the Fe of respiring mitochondria associated with magnetic Mössbauer features (Figure 3-1B). To evaluate this, we summed the spin concentrations for the g = 2 region signals, weighted by the number of irons that are likely to be associated with each species, and then

Figure 3-5. EPR spectra of mitochondria isolated from respiring (A), respirofermenting (B), and fermenting (C) cells. Spectra are of batches R2, RF1 and F11 respectively. Spectra A and C were collected at 10 K and 0.05 mW, spectrum B was collected at 10K and 0.2 mW. Dashed lines are simulations assuming parameters given in Table 3-1. Lowfield spectra of respiring (D), respirofermenting (E) and fermenting (F) mitochondria are also shown. Spectra were collected at 10K and 20 mW.

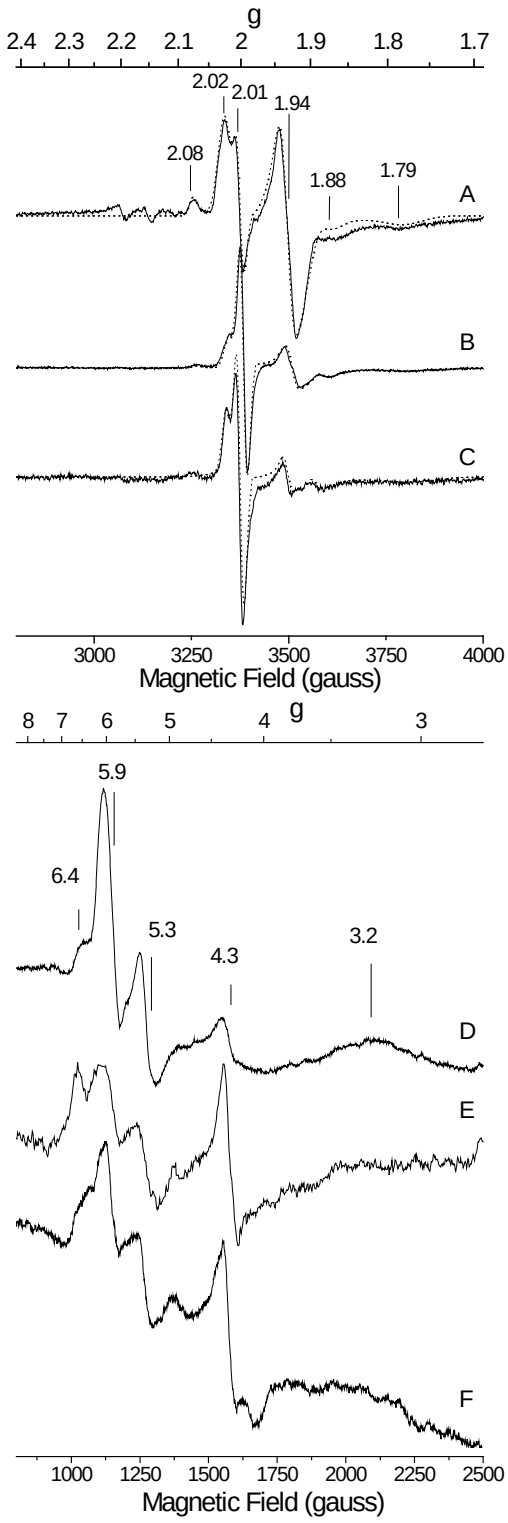

Figure 3-5. Continued.

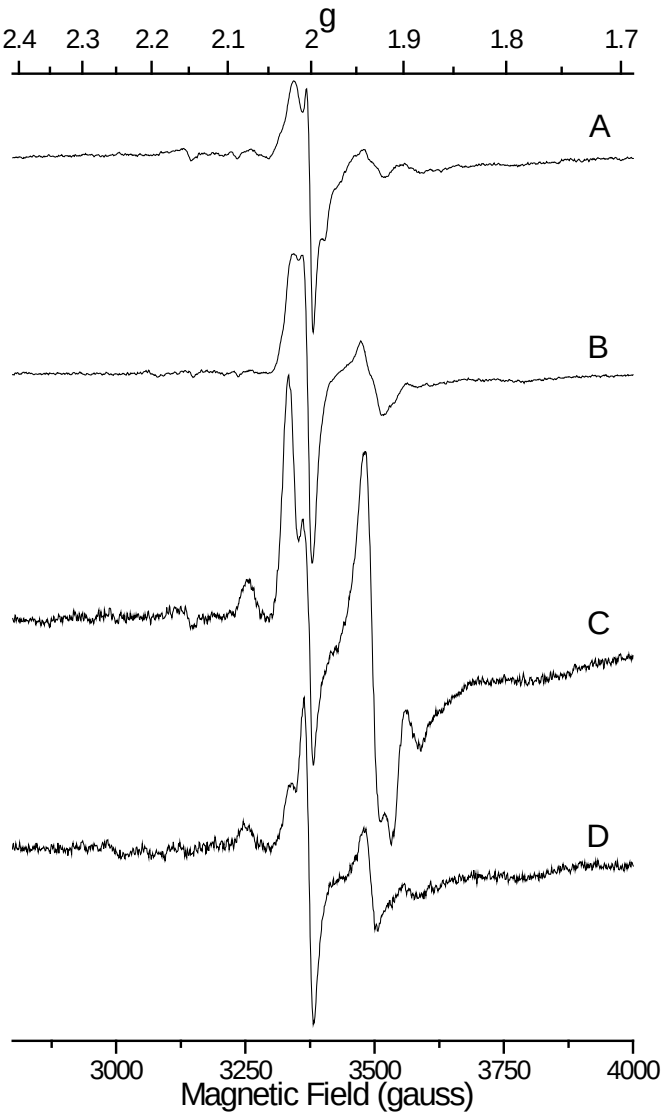

Figure 3-6. 10 K EPR spectra of batches not shown in Figure 3-5 but used in the construction of Table 3-1. Spectra A, B, C and D are of samples R5, R1, RF2 and F11, respectively. Spectra A, B and D were collected at 0.05 mW microwave power while spectrum C was collected at 0.2 mW. For ease of viewing, spectra A and C were multiplied by 1.5 while D was multiplied by 15.

divided by the concentration of Fe in the sample. This calculation indicated that EPR-active species should account for ~ 7 % of mitochondrial Fe, about half of that observed by Mössbauer to be magnetic. The uncertainties associated with both estimates are large; EPR spin intensities are difficult to determine accurately, and distinguishing the small amount of magnetic Fe from baseline in these weak Mössbauer spectra is difficult.

These results are generally similar to those reported in a preliminary study of mitochondria isolated from yeast grown on glucose/lactate media (139). However, there are some differences that we describe in the *Discussion* section of Chapter IV.

Iron-ome of Respirofermenting Mitochondria

Protein and metal concentrations of mitochondria isolated from cells grown under respirofermenting conditions (Table 3-1) were similar to those of respiring mitochondria, except that the Mn concentration was 2-fold lower. Mössbauer spectra (Figure 3-7) were also similar. Simulations of individual components are indicated above the spectrum. Compared to respiring mitochondria, the proportion of Fe present as the central doublet, HS Fe^{2+} hemes, and magnetic Fe in respirofermenting mitochondria declined slightly, while the percentages due to NHHS Fe^{2+} ions and the central unresolved material increased slightly. The presence of this latter species is most evident from the mis-match of the spectrum and simulation (Figure 3-7A) which does

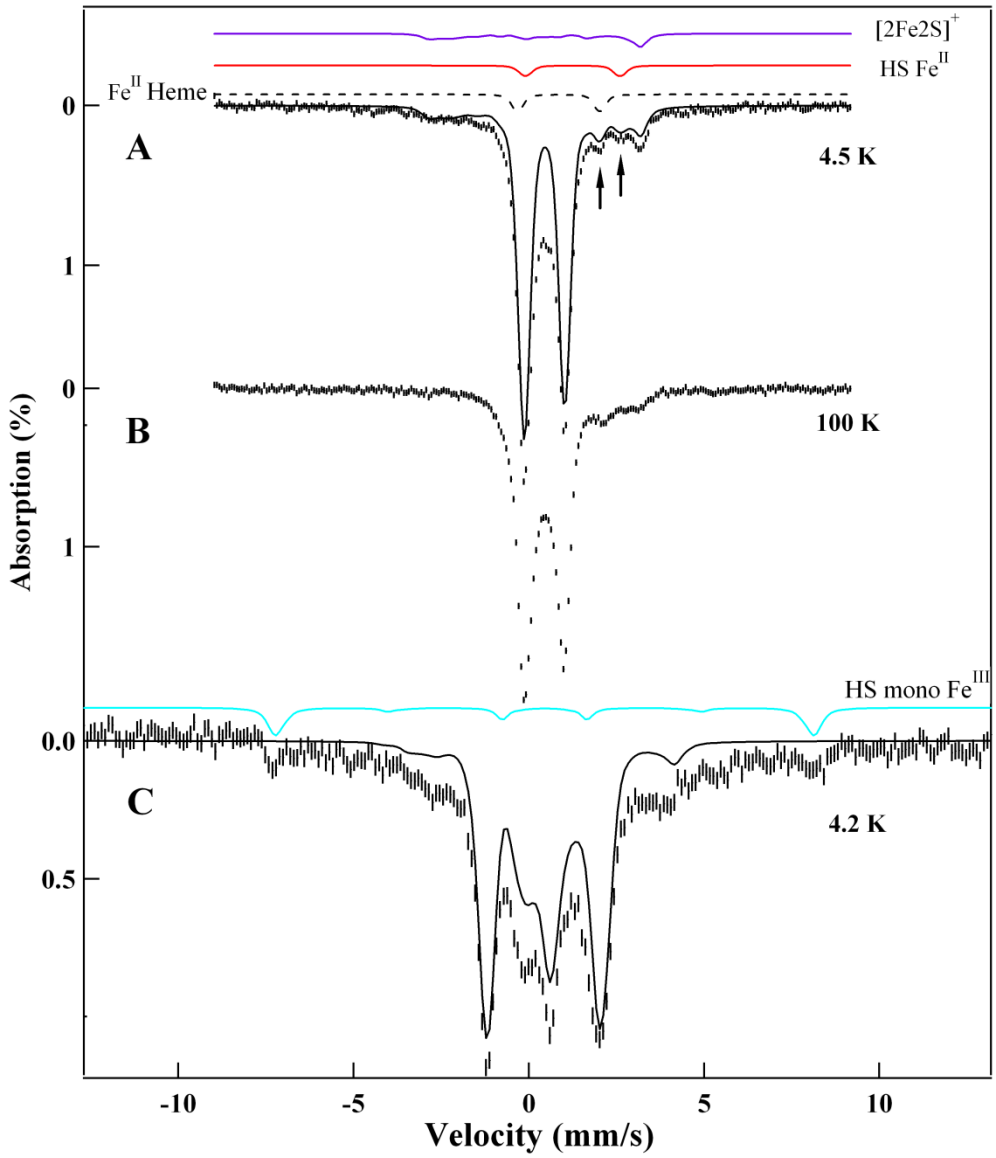

Figure 3-7. Mössbauer spectra of respirofermenting mitochondria. A, the spectrum measured at 4.5 K, 0.05 T parallel applied magnetic field. The red line is a simulation using parameters and percentages listed in Table 1 for the central doublet, HS Fe^{2+} hemes, nonheme HS Fe^{2+}, and S = ½ $[Fe_2S_2]^{1+}$ clusters. The lines above the spectrum are the simulations for S = ½ $[Fe_2S_2]^{1+}$ clusters, the nonheme HS Fe^{2+} and the HS Fe^{2+} hemes. B, same as A except at 100 K. C, same as A except with 8 T applied field. The blackline is a simulation including 50 % of the central doublet and 10 % of S = ½ $[Fe_2S_2]^{1+}$ clusters. The blue line above is a simulation for HS mononuclear Fe^{3+} species assuming 5 % of the total Fe.

not include this species at ~ 0 mm/s Doppler velocity. The high-field spectrum (Figure 3-7B) revealed the presence of mononuclear HS Fe^{3+} ions (simulated by the blue line). The red line in Figure 3-4B is a simulation of the diamagnetic Fe associated with the central doublet at low-field.

The UV-Vis spectrum of respirofermenting mitochondria (Figure 3-3B) revealed heme *a*, *b* and *c* concentrations (Table 3-1) that were similar to those obtained for respiring mitochondria. EPR spectra (Figure 3-5B and 3-5E and Figure 3-6) exhibited the same group of signals that were observed in respiring mitochondria. Spin concentrations (Table 3-1) were significantly higher for the g_{ave} = 1.94 and 1.90 signals, while that for the g_{ave} = 2.04 and 2.01 signals were similar to that observed with respiring mitochondria. The observed collective spin concentrations for g = 2 region signals correspond to ~ 17 % magnetic Fe, somewhat greater than the ~ 10 % magnetic Fe observed by Mössbauer spectroscopy. We suspect that this discrepancy is due to uncertainties in EPR spin quantification and/or in identifying the baseline in the Mössbauer spectrum.

Iron-ome of Fermenting Mitochondria

Protein and Fe concentrations for fermenting mitochondria (Table 3-1) were again similar to those obtained for respiring and respirofermenting mitochondria; the protein concentration might be reduced somewhat, but the variability among batches was too high to correlate these changes to metabolic mode. The Mn concentration was similar to that of respirofermenting

mitochondria and substantially lower than in respiring mitochondria. The Cu concentration of fermenting mitochondria was nearly 4-fold lower relative to that in respiring or respirofermenting mitochondria.

Mössbauer spectra of fermenting mitochondria (Figures 3-8, 3-9 and Table 3-1) differed substantially from those of respiring or respirofermenting mitochondria in that there was a substantial decline in the intensity of the central doublet and the heme doublet, and an increase in the proportion of NHHS Fe^{2+} ions. We included EGTA in all isolations to remove any adventitiously bound Fe. Despite these efforts, the nonheme, non-Fe^{2+}(EGTA) HS Fe^{2+} doublet was observed in all of the ~ 30 independently-prepared batches of EGTA-washed fermenting mitochondria that we have examined.

The blue line in Figure 3-9A is a simulation assuming isomer shift, quadrupole splitting and effective line width parameters of $\delta \approx 1.25$ mm/s, $\Delta E_Q \approx 3.35$ mm/s, and $\Gamma = - 0.65$ mm/s, respectively (in WMOSS, a negative line width indicates a Voigt profile with a Lorentzian of 0.15 mm/s full width convoluted into a Gaussian with $\Gamma = 0.65$ mm/s). These values are typical of mononuclear $\{Fe^{2+}(O)_m(N)_n\}$ complexes for which $5 \leq (m + n) \leq 6$ and $m \geq 4$ (229). HS Fe^{2+} hemes have distinctly different parameters (δ ranging from 0.92 - 0.95 mm/s and ΔE_Q ranging from 2.02 to 2.20 mm/sec (230-231)). The low-energy absorption line of the NHHS Fe^{2+} doublet is hidden within the central doublet (see below) while the high-energy line, which contains half of the doublet's intensity, is generally resolved. In Figure 3-9A, the spectral area of the doublet represents

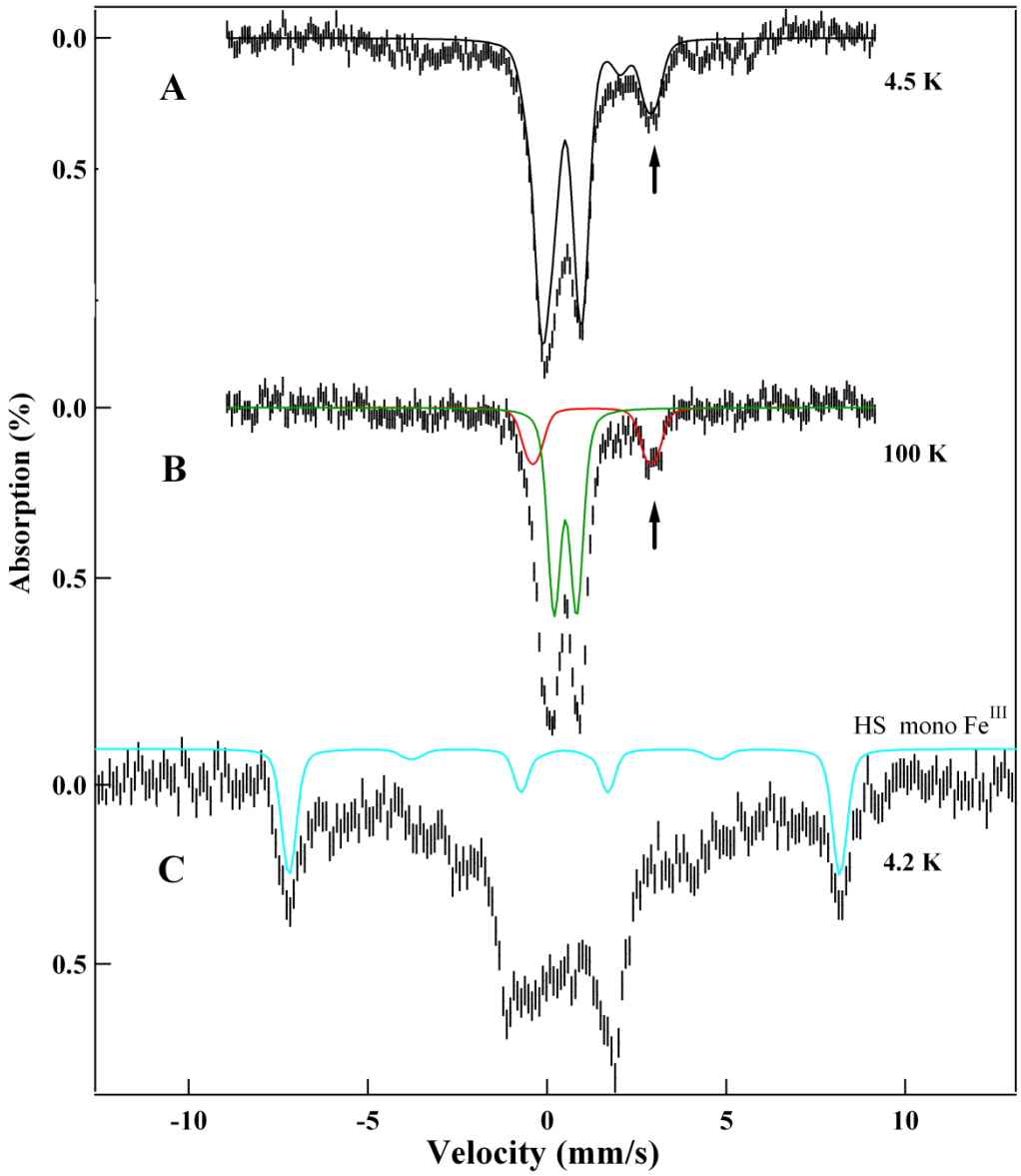

Figure 3-8. Mössbauer spectra of fermenting mitochondria (F9). A, 4.5 K, 0.05 T parallel applied magnetic field. The red line is a simulation of the central doublet (25 % of the Fe), HS Fe^{2+} hemes (5 % of the Fe), nonheme HS Fe^{2+} (16 % of the Fe), and the ferric nanoparticles (20 % of the Fe). B, same as A except at 100 K. The red line is a simulation including the central doublet (25 % of the Fe), HS Fe^{2+} hemes (5% of the Fe), nonheme HS Fe^{2+} (16 % of the Fe), and Fe^{3+} nanoparticles (30 % of the Fe) at essentially the percentages given in Table 3-1. C, same as A except with 8 T applied field. The red line is a simulation for HS mononuclear Fe^{3+} species assuming 20 % of total Fe.

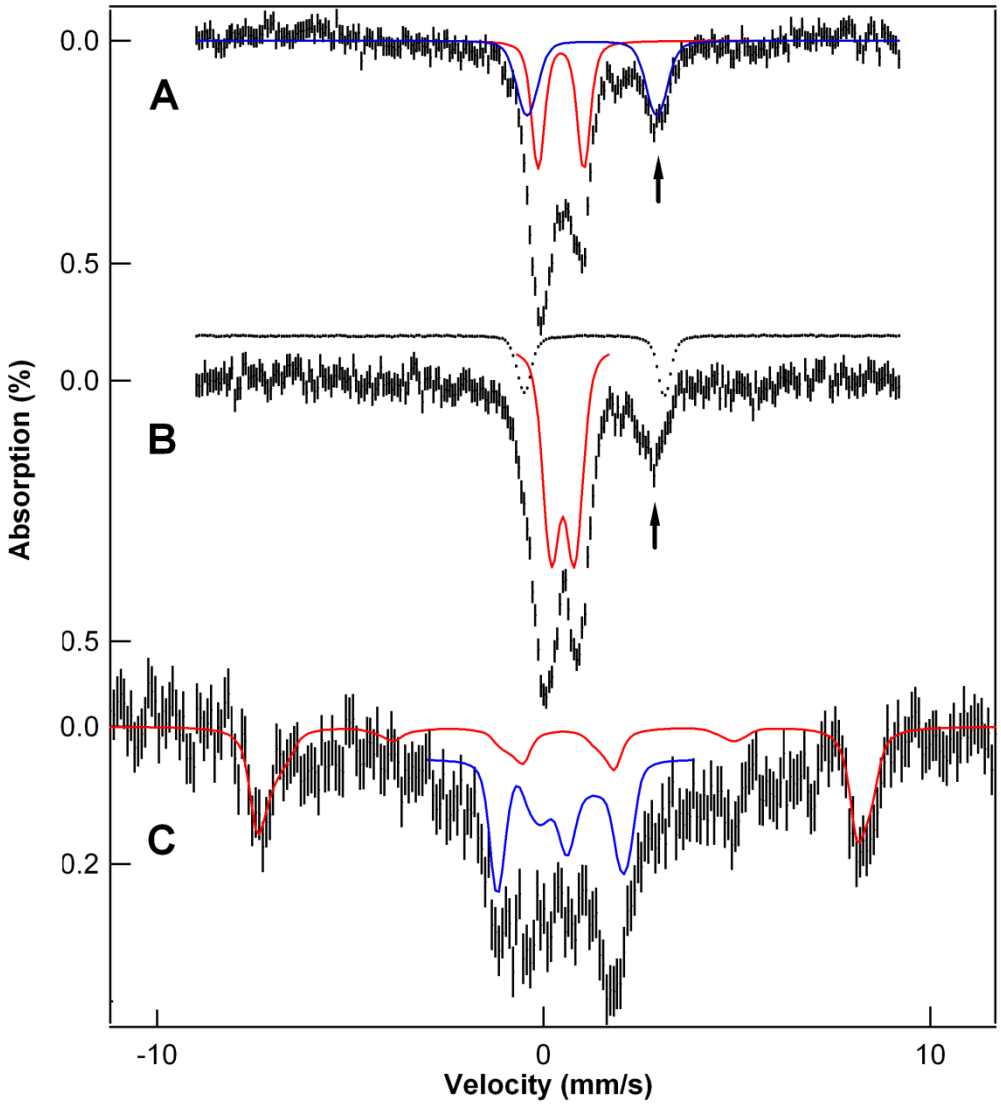

Figure 3-9. Mössbauer spectra of EGTA-washed fermenting mitochondria. (Sample F12) recorded at 4.5 K and 0.05 T (A), 100 K and 0.05 T (B), and 4.2 K and 8 T (C). Solid lines simulate the contributions of NHHS Fe^{2+} species (blue line in A, ~20 % of total Fe), the central doublet (red line in A and blue line in C, ~ 20%), Fe^{3+} nanoparticles (red line in B, ~ 40%), and mononuclear HS Fe^{3+} species (red line in C, ~ 20 %). Shown offset above B is the experimental spectrum of Fe^{2+}(EGTA) (black hash marks). The black arrows in Figures 1-3 point to the high energy absorption line of the NHHS Fe^{2+} species.

20 % of the Fe in the sample, corresponding to ~ 150 μM Fe^{2+}. The large width of the absorption lines suggests the presence of multiple species. This experiment shows that the NHHS Fe^{2+} ions in our sample are protected from EGTA chelation despite extensive washing of mitochondria with EGTA-containing buffers.

Mössbauer spectra of fermenting mitochondria also contain the central doublet representing ~ 20 % of the total Fe in the sample with δ ~ 0.45 mm/s and ΔE_Q ~ 1.15 mm/s. In strong applied fields the spectra of these species can readily be simulated (Figure 3-9C, blue line) because the effective field at the nucleus arises solely from the applied field. In contrast, HS Fe^{2+} ions exhibit paramagnetic hyperfine structure spread over a wide velocity range, making it difficult to characterize such species in our 8.0 T spectra.

EGTA-washed fermenting mitochondria also exhibited spectral features from magnetically isolated high-spin ($S = {}^5/_2$) mononuclear Fe^{3+} species with E/D ~ ${}^1/_3$; D and E are the zero-field splitting and rhombicity parameters, respectively. In weak applied fields (0.05 T here), magnetically isolated Fe^{3+} yield intricate Mössbauer patterns exhibiting paramagnetic hyperfine structure. With the low ^{57}Fe concentrations in these samples, such features cannot be analyzed well or even distinguished from baseline (which distorts the quantification of other species). Fortunately in 8 T applied fields, the outmost features of HS Fe^{3+} components are well resolved (Figure 3-9C), allowing simulation (red line) and

an accurate estimate of concentration (here 20 % of spectral intensity, corresponding to ~ 150 μM ^{57}Fe).

In 0.05 T applied fields, and at 4.5 K (Figure 3-9A) and 100 K (Figure 3-9B), EGTA-washed fermenting mitochondria also yielded a quadrupole doublet with $\Delta E_Q \approx 0.63$ mm/s and $\delta \approx 0.52$ mm/s; in Figure 3-9B, the red line is a simulation using these parameters. Similar doublets were present in spectra of mitochondria isolated from Yfh1p-, Yah1p-, and Atm1p-depleted cells (142, 148, 232); they arise from Fe^{3+} phosphate nanoparticles exhibiting superparamagnetism.

In strong applied fields, these nanoparticles yield broad unresolved features (see Figure 2D of (232)). Quantification is most accurate at temperatures well above the so-called blocking temperature, T_B; for $T >> T_B$, spectra consist of a quadrupole doublet (in the present samples, $T_B < 4.2$ K). The 100 K spectrum (Figure 3-9B) shows that ~ 40 % of the Fe of the sample belongs to Fe^{3+} nanoparticles.

In summary, the Fe in EGTA-washed fermenting WT mitochondria is distributed into four main groups. Approximately 20 % of the Fe is NHHS Fe^{2+}, ~ 20 % is a combination of $[Fe_4S_4]^{2+}$ and LS Fe^{2+} hemes (e. g. cytochrome c), ~ 40 % Fe^{3+} resides in nanoparticles, and ~ 20 % is non-interacting mononuclear high-spin Fe^{3+}. These organelles also contain small amounts of other Fe-containing species (29). All of these Fe-containing species were present despite

extensive exposure of the mitochondria to a strong Fe^{2+} chelator, suggesting that they are located within the organelle and protected from chelation.

The UV-Vis spectrum of fermenting mitochondria (Figures 3-4C, Figure 3-10 and Table 3-1) exhibited lower quantified intensities of heme centers. The concentrations of heme *b* and *c* were ~ half of those in respiring and respirofermenting mitochondria, and the heme *a* contribution was diminished substantially. This is consistent with the observed decline in intensity of the high-spin heme doublet in Mössbauer spectra of fermenting mitochondria. The EPR spectra of fermenting mitochondria (Figures 3-5C, 3-5F and 3-6) were qualitatively similar to those of respiring and respirofermenting mitochondria, but again spin concentrations were reduced (Table 3-1). The intensity of the g = 6 features, assigned to the partially oxidized a_3 site of cytochrome c oxidase, was also diminished. Summing the spin concentrations of the signals in the g = 2 region suggests that ~ 3 % of Mössbauer spectral intensity should be magnetic, which is within the uncertainty of that observed by Mössbauer.

Discussion

The major objective of this study was to characterize the iron-ome of mitochondria isolated from respiring, respirofermenting, and fermenting yeast cells using a biophysical approach. We can now integrate the results from the various techniques with the known composition of some proteins in mitochondria,

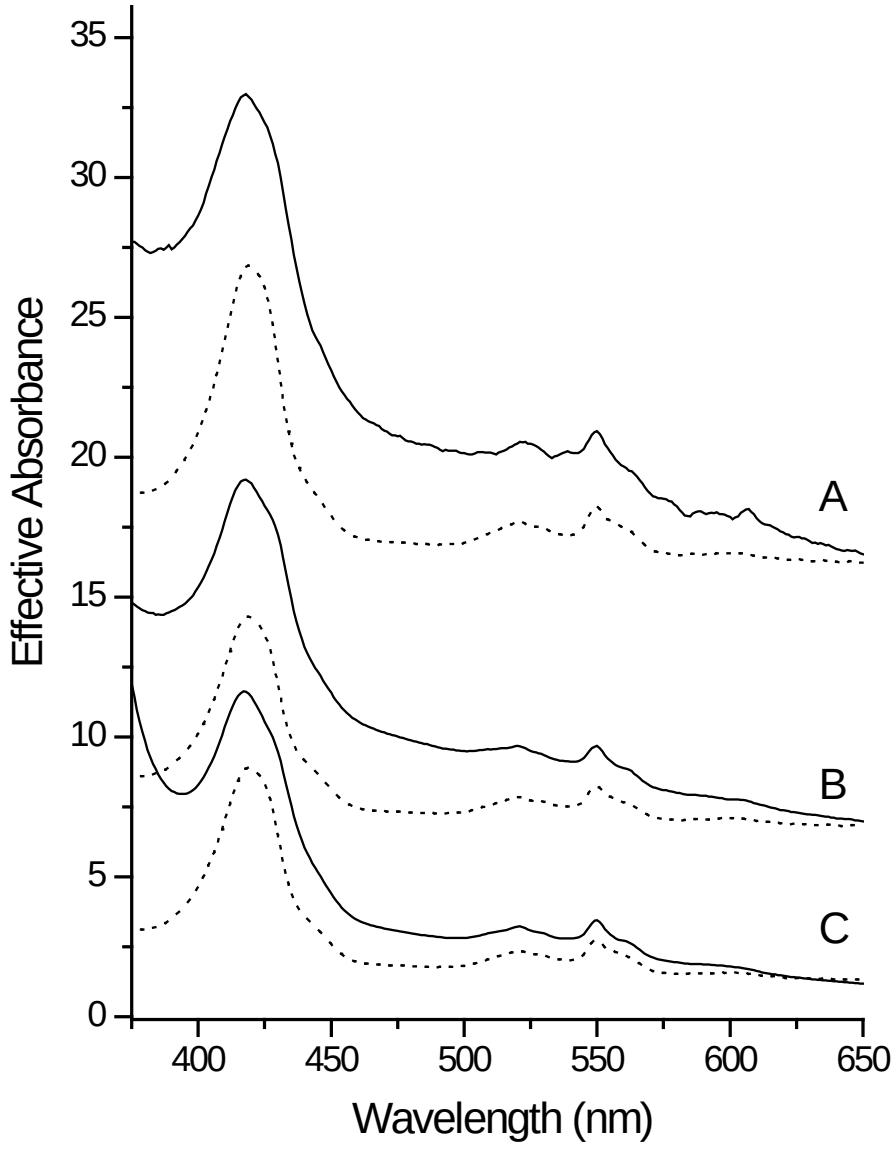

Figure 3-10. Electron absorption of fermenting mitochondria. A, F4 (33 mg/mL); B, F1 (30 mg/mL) and C, F2 (27 mg/mL). Dotted lines are composite spectra using the concentrations given in Table 3-2.

beginning with the respiring state. Our data allow an estimate of the concentration of cytochrome c oxidase in the organelle. There are few other heme *a* containing proteins in mitochondria, such that the heme *a* concentration essentially reflects twice the cytochrome c oxidase concentration in the organelle. Mitochondrial heme monoxygenase (Cox15p) may have sub-stoichiometric amounts of heme *a* bound (97), but we will assume that this amount is insignificant. The total Fe^{2+} heme *a* concentration in respiring mitochondria (Table 3-1) suggests a cytochrome *c* oxidase concentration of ~ 25 µM. The absence of EPR signals at g ~ 3 indicates the lack of LS Fe^{3+} hemes in as-isolated respiring mitochondria. EPR spectra did exhibit two signals from HS Fe^{3+} hemes (probably from the partially oxidized {Fe(III)a_3:Cu_b(I)} state of cytochrome c oxidase), and so the collective concentration of these signals were added to the UV-Vis-based estimate. This affords a cytochrome *c* oxidase concentration of ~ 30 µM in "neat" mitochondria (see Table 3-2 for a complete compilation).

Since cytochrome c oxidase contains 3 molar equivalents of Cu, ~ 90 µM Cu out of 210 µM total Cu in respiring mitochondria should be contained in this enzyme. The remainder might be present as the Cu pool as suggested by Winge and coworkers (134), although the percentage of Cu that we calculate for this pool (~ 60 %) is less than they determined (~ 90 %). The absence of Cu^{2+} EPR signals in our preparations is consistent with their proposal of a Cu^{1+} oxidation state for this pool.

The HS Fe^{2+} heme doublet in Mössbauer spectra of respiring mitochondria should include contributions from heme a_3 and HS heme *b* containing proteins (we are unaware of any HS heme *c* – containing proteins). After subtracting the heme a_3 contribution, the concentration of HS heme *b* species in respiring mitochondria is calculated to be ~ 20 µM. We are aware of three HS heme *b* proteins, including Ccp1p, Cta1p and Yhb1p. Subtracting the HS heme *b* concentration from the total heme *b* concentration suggests that the concentration of LS heme *b* species in mitochondria is ~ 30 µM. The LS heme *b* proteins in the mitochondria include succinate dehydrogenase (Sdh), cytochrome bc_1 (2 heme *b*), Cox15p, and Cyb2p, and perhaps others. This can be described by the relationship

$$30\mu M = [\text{succinate dehydrogenase}] + 2[\text{cytochrome } bc_1] + [\text{Cox15p}] + [\text{Cyb2p}] + \ldots \quad [6]$$

The g_{ave} = 1.94 and 1.90 EPR spin concentrations suggest succinate dehydrogenase and cytochrome bc_1 concentrations of ~ 5 µM and ~ 10 µM respectively, which implies, by this relationship, that most of the LS heme *b* centers in mitochondria arise from these two respiratory complexes.

The known heme *c* containing proteins in mitochondria include two isoforms of cytochrome *c* and cytochrome c_1. Taking ~ 10 µM for the cytochrome bc_1 concentration suggests ~ 110 µM concentration for both

cytochrome *c* isoforms. Thus, the heme *a* and *c* contents of respiring mitochondria are dominated by cytochrome *c* oxidase and cytochrome *c*, respectively. The heme *b* content is rather evenly distributed between HS and LS, with LS forms dominated by succinate dehydrogenase and cytochrome bc_1.

Quoted concentrations were calculated with respect to the entire mitochondrial volume. Since species are located in particular regions of the mitochondria, their regional concentrations will be higher, sometimes dramatically so. For example, cytochrome *c* oxidase is located in the inner membrane (61), which occupies only 20 % of the total mitochondrial volume (233). This suggests a regional concentration of ~ 150 μM! All other concentrations reported here are with respect to overall mitochondrial volumes, but this effect of compartmentalization on concentration could become important in future studies.

Succinate dehydrogenase contains 10 molar equivalents of Fe (1 heme *b*, 1 [Fe_2S_2] cluster, 1 [Fe_3S_4] cluster and 1 [Fe_4S_4] cluster), so a concentration of ~ 5 μM for this respiratory complex implies a ~ 50 μM Fe contribution overall. Similarly, cytochrome bc_1 contains 5 molar equivalents of Fe (1 heme c_1, 2 heme *b*, and 1 [Fe_2S_2] cluster), also implying a ~ 50 μM overall Fe contribution. Including a 60 μM Fe contribution for cytochrome *c* oxidase and 110 μM for cytochrome *c* reveals that respiration-related complexes constitute ~ 40 % of the iron-ome in respiring yeast mitochondria.

The central doublet of the Mössbauer spectra of respiring mitochondria includes contributions from $[Fe_4S_4]^{2+}$ clusters and LS Fe^{2+} heme centers. Table 3-1 and the relationships mentioned above suggest ~ 30 µM (LS heme *a*) + ~ 30 µM (LS heme *b*) + ~ 120 µM (LS heme *c*) = 180 µM LS Fe^{2+} hemes. Subtracting this from the central doublet leaves ~ 35 % of mitochondrial Fe as S = 0 $[Fe_4S_4]^{2+}$ clusters. This corresponds to ~ 250 µM Fe and ~ 60 µM of cluster. Subtracting an additional 5 µM contribution due to the succinate dehydrogenase $[Fe_4S_4]^{2+}$ cluster leaves ~ 55 µM for such clusters in other mitochondria proteins. Some mitochondrial proteins contain only $[Fe_4S_4]$ clusters (e.g. Aco1p, Lys4p, Ilv3p) while others contain both $[Fe_4S_4]$ clusters and $[Fe_2S_2]$ clusters (e.g. Bio2p and Lip5p). We have attempted to fit simulations of S = 0 $[Fe_2S_2]^{2+}$ clusters into the Mössbauer spectra of respiring mitochondria but we have no unambiguous evidence for their presence. We conclude that < 5 % of the Fe is in this form. This suggests that the majority of the non-succinate dehydrogenase-containing $[Fe_4S_4]^{2+}$ clusters in respiring mitochondria arise from proteins that contain only $[Fe_4S_4]^{2+}$ clusters (i.e. 55 µM ≈ [Aco1p] + [Lys4p] + [Ilv3p] + ...).

Respirofermenting and fermenting mitochondria were analyzed similarly; results are shown in Tables 3-1 and 3-4. In general, the total Fe concentration in mitochondria was similar regardless of metabolic mode. Also, the overall distribution of Fe in respirofermenting mitochondria was similar to that in respiring mitochondria. In contrast, the Fe distribution in fermenting mitochondria was significantly different. This suggests that the *repression of*

respiration by glucose, rather than the occurrence of fermentation *per se*, is responsible for the major shifts observed in the iron distribution. Thus, we will simplify our analysis by averaging the Fe distributions observed for respiring and respirofermenting mitochondria, and then comparing the averaged distribution to that obtained under fermentation.

Viewed in the respiration → fermentation direction, cytochrome c oxidase ↓ (declined) 4×, succinate dehydrogenase ↓ 3.8×, cytochrome bc1 ↓ 2.5×, and cytochrome c ↓ 2×. LS hemes generally ↓ 2× and $[Fe_4S_4]^{2+}$ containing proteins ↓ 3.5×. On average, these species declined ~ 3-fold. The Cu(1) pool decreased ↓ 3×. The decline in the size of the Cu^{1+} pool contrasts with a previous report (134) that the concentration of this pool was independent of the metabolic growth mode. In terms of Fe pools, the nonheme HS Fe^{2+} pool, the mononuclear HS Fe^{3+} pool and the Fe^{3+} nanoparticles went from nearly undetectable in respiring mitochondria to representing nearly 70 % of the Fe in the fermenting organelle. These are dramatic changes that reflect major differences in the way that Fe is handled in the organelle depending on metabolic mode.

These results can be compared to proteomic studies that also indicate a substantial shift in the yeast mitochondria proteome due to the diauxic shift (161). Ohlmeier *et al.* (219) found that the concentration of 17 proteins were significantly lower in fermenting *vs*. respiring cells. Most of these were involved in respiration or the TCA cycle, including the Fe-containing enzymes cytochrome

Table 3-4. Concentrations of dominating Fe and Cu containing species in yeast mitochondria. Concentrations are reported in μM and are for neat mitochondria.

	Respiring	Respirofermenting	Fermenting
Cytochrome c oxidase	30	35	8
Succinate dehydrogenase	5	10	2
Cytochrome bc_1	10	20	6
Cytochrome c	100	140	60
Other HS heme b (Ccp1, Cta1, Yhb1…)	20	minor	minor
LS hemes combined	180 (30a +30b + 120c)	230 (35a + 55b +140c)	100 (7a + 12b + 83c)
$[Fe_4S_4]^{2+}$ only (Aco1p, Lys4p, Ilv3…)	55	36	13
$\{[Fe_4S_4]^{2+} + [Fe_2S_2]^{+}\}$ (Bio2, Lip5…)	minor	minor	minor
$[Fe_2S_2]^{2+}$ only (Yah1…)	minor	minor	minor
Cu(I) Pool	120	60	30

c oxidase (Cox4p, ↓ 3.7×), cytochrome bc_1 (Qcr7p, ↓1.3×), lactate dehydrogenase (Cyb2p, ↓ 68.6×) and succinate dehydrogenase (Sdh1p, ↓ 7.0×, Sdh2p, ↓ 9.8×, Sdh4p, ↓ 4.6×). Dihydroxyacid dehydratase (Ilv3p, ↑ 2.3×), the sole Fe-containing protein mentioned whose concentration increased under fermenting conditions, is involved in amino acid biosynthesis.

The mitochondrial transcriptome changes more dramatically with growth mode (29). When glucose repression is relieved (such that respiration is allowed), the Cyc1 (cytochrome c, isoform 1) transcript ↑ 6× (34). Mn-superoxide dismutase (MnSod2p) activity and the mRNA level for this protein also increased so as to bolster the cell's defenses against formation of reactive oxygen species during respiration (234). Consistent with this, we observed a 3-fold increase in the Mn concentration of respiring mitochondria relative to respirofermenting and fermenting conditions. MnSod2p is the major Mn-containing protein in yeast mitochondria, suggesting that the increased Mn concentration might reflect an increased level of MnSod2p. However, we have not observed an EPR signal from this protein, suggesting that most of the Mn in our samples arises from other species. In some batches of mitochondria, we have observed aqueous Mn^{2+} EPR signals, but the intensity of these signals is not apparently correlated to Mn concentration.

The observed changes in Fe distribution are highly complex, but they can be interpreted simply given the known roles of mitochondria in respiring vs. fermenting cells. In respiring cells, these organelles are critical for energy (ATP)

production, which requires the biosynthesis of Fe/S clusters and heme centers, as well as their installation into apo-respiratory complexes. Under fermentation conditions, energy production is associated with glycolysis, where no such centers are involved. Thus, *the production of Fe/S clusters and heme centers is probably reduced in fermenting mitochondria because the metabolic need for these centers is reduced.* Our results suggest a 3-fold reduction in production of these centers. However, the presence of these centers at reduced levels might allow fermenting cells to be poised to convert rapidly into respiration mode. If no respiratory complexes were present under fermenting condition, the cell might not be able to change metabolism abruptly with a change of environmental conditions (e.g. in the absence of glucose).

The Fe feedstock for mitochondrial Fe/S cluster and heme biosynthesis is imported into the organelle as Fe^{2+} complexes. Neither the structure nor composition of the imported complex(es) are known but they are probably of low molecular weight as they must pass through protein transporters (Mrs3p and Mrs4p) in the inner membrane (127, 235). *We propose that the nonheme HS Fe^{2+} ions present in fermenting mitochondria are these imported ions and that they serve in this capacity.* The model of Figure 3-11 assumes this role and can rationalize the observed changes in the level of this pool. During respiration, the size of the Fe^{2+} pool is small since the biosynthesis rates of Fe/S clusters and hemes are elevated. During fermentation, the pool increases because the rate of Fe/S cluster and heme biosynthesis is reduced. Consistent with the nearly

invariant Fe concentrations in respiring and fermenting mitochondria, the overall rate of Fe^{2+} import appears to be unaffected by changes in metabolic growth mode; i.e. *the cell does not regulate the rate of Fe^{2+} import into mitochondria according to metabolic growth mode.* The Fe^{2+} import rate is thought to be controlled by the transcriptional regulator Aft2p (236). We find this lack of regulation intriguing but somewhat non-intuitive, given how precisely other aspects of cellular function are regulated.

Whether the other pools of Fe in fermenting mitochondria, including Fe^{3+} nanoparticles, mononuclear HS Fe^{3+} ions, and perhaps the central unresolved material, are related to the NHHS Fe^{2+} pool remains uncertain. These pools may exist in a dynamic equilibrium with each other, which implies that they are imported by the same IM transporter(s). Alternatively, these pools may be independent of the Fe^{2+} pool and of each other, and imported by different IM transporters. Also uncertain is the cellular *function* of these other pools. They certainly appear to store Fe in fermenting mitochondria that can be used when the cell respires. However, whether this can be construed as a cellular *strategy* for storing Fe in mitochondria (analogous to mitoferrin in human mitochondria (237) or more like a “malfunction” resulting from the lack of a coordinating ligand, or a shift of pH or oxidation status in fermenting mitochondria is unknown. We favor the latter possibility, as we suspect that the Fe^{2+} ions composing these pools are not protein bound and thus not under the direct genetic control of the cell. Nevertheless, they may impact cellular function, e.g. by generating reactive

oxygen species during their formation. Further studies are required to evaluate these possibilities.

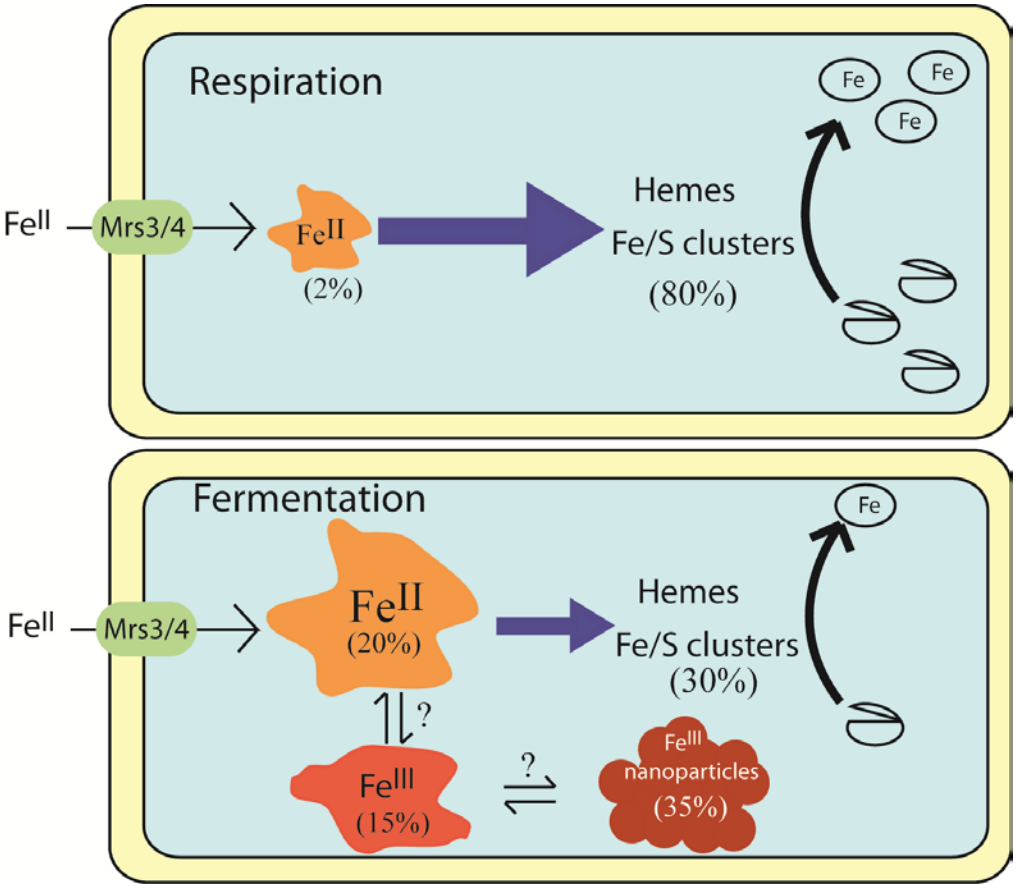

Figure 3-11. Model describing the shift in iron-ome with metabolic growth mode. Under respiration conditions, the size of the nonheme HS Fe^{2+} pool is small because the rate of Fe/S cluster and heme biosynthesis is elevated. When cells ferment, the rate of Fe/S cluster and heme biosynthesis declines, leading to an increase in the size of the Fe^{2+} pool. The rate of Fe^{2+} import from the cytosol is not significantly affected by the change in metabolism. A portion of the pool Fe^{2+} ions may become oxidized and a subset of these mononuclear HS Fe^{3+} ions may precipitate as Fe^{3+} nanoparticles (not shown).

CHAPTER IV

FURTHER BIOPHYSICAL CHARACTERIZATION OF MITOCHONDRIA: DISCOVERY OF A Mn EPR SIGNAL AND THE EFFECT OF REDOX TREATMENT

Introduction

This chapter includes results that provide some insight into the iron and manganese metabolism in cells and mitochondria, but have not been organized into a publication. These aspects are included here to suggest future studies. Early mitochondrial samples were prepared using isolation protocols established by other labs (139, 191-192). As discussed in Chapter II, we have made several modifications to those procedures. These modifications were made over the course of several years as experimental results implicated necessary changes. Some of the experiments included in this chapter used procedures at intermittent stages of refinement.

The Presence of a Mn^{2+} EPR Signal

Mitochondria were isolated under anaerobic conditions and packed for EPR analysis. The g = 2 region of EPR spectra of isolated mitochondria is sometimes (but not always) dominated by a signal (Figure 4-1) with a six-line hyperfine pattern (magnetic hyperfine coupling constant, a = 90 G) typical of an I = $^5/_2$ Mn^{2+} species with E/D

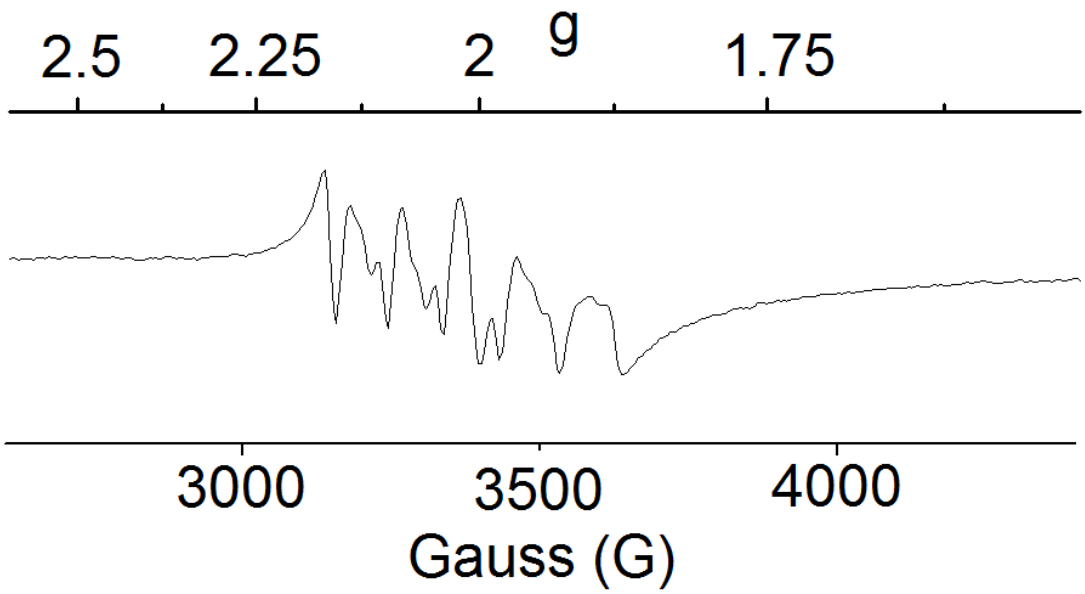

Figure 4-1. An EPR feature due to Mn^{2+} sometimes dominates spectra of mitochondria. Mitochondria were isolated from cells grown on glucose. Spectrum was collected at microwave power 0.2 mW, 10 K, microwave frequency 9.44 GHz, and modulation amplitude 10 G.

~ 0. Spin concentrations determined ~ 20 μM Mn^{2+} contributed to this feature. Spin concentrations of ~ 5 μM Mn cannot be reliably detected by our instrument (139). A feature at g = 1.94 (most likely due to succinate dehydrogenase) is also evident but is obscured by overlap with the Mn^{2+} signal (139). It is unclear whether the Mn is adventitiously bound, whether it is inside a contaminating organelle or whether it is inside the mitochondria.

In order to remove any adventitiously bound Mn^{2+} (as well other metals), mitochondria were isolated in the presence of 1 mM EGTA. Addition of a chelator to isolation buffers resulted in the removal of the Mn signal from ~ half of our preps. It is unclear why the Mn signal appears or does not appear in all preps and we wanted to explore what factors might be contributing to this variability.

Correlation Between EPR and Mn Concentrations

Since the Mn signal is not always removed by the addition of a chelator, perhaps its presence correlates to variations in our samples. For example, the Mn EPR feature would not be detected in mitochondrial samples with Mn concentrations below the detection limit (< 10 μM) of the EPR. Additionally it was unclear whether all mitochondrial Mn contributes to the EPR feature. It would be beneficial to know the proportion of mitochondrial Mn in the EPR active state.

Mitochondria were isolated and packed for analysis essentially as described in Chapter II. Since the [Mn] of neat mitochondria depends on metabolism, samples were collected from cells grown on either glycerol or glucose. ICP-MS analysis reveals that the Mn EPR feature does not correlate to deviations in mitochondrial Mn concentrations (Table 4-1). Neat mitochondria collected from cells grown on glycerol contain 35 ± 20 μM Mn. The fermenting mitochondria in Table 4-1 have 25 ± 15 μM Mn. The average [Mn] in fermenting samples reported in Table 4-1 is slightly higher than reported in Chapter III, but these samples were isolated from cells grown on rich media which has been shown to contribute to higher mitochondrial metal concentrations (134). Interestingly, mitochondrial Mn concentrations show less variation than the intensity of the Mn signal.

Of the 23 samples included in Table 4-1, 9 exhibited the Mn EPR feature. Spin concentrations of the feature ranged from 0 to 30 μM. Samples not exhibiting the feature are assumed to have 0 μM Mn contributing to the signal. When the feature was present, spin concentrations ranged from 15 to 30 μM. Interestingly spin concentrations do not depend on the carbon source used for cell growth (Table 4-1). Detected signals from mitochondrial samples collected from cells grown on either glycerol or glucose have spin concentrations of ~ 25 ± 4 μM.

Table 4-1. Comparison of samples isolated for Mn EPR studies. Each row indicates an individual prep. Samples were grown on glycerol or glucose. Samples were grown on either rich (YP) or minimal (min) media. Respiring samples were often grown on minimal media enhanced with 5 % rich media. Rich and minimal media contain approximately 40 µM and 10 µM Fe respectively. The final concentration of Fe (the Fe the media contains plus any supplementary Fe) in the media during growth is reported. Spectra of samples exhibiting the Mn EPR signal were integrated to determine spin concentrations of Mn contributing to the feature. Spin concentrations of the Mn EPR signal may be overestimated since spectral integration will include concentrations of any other signals hidden by the Mn feature.

Carbon Source	Media Type	Oxygen (SCFH)	Media Fe (µM) Final	Mn Signal (µM)	Mito Mn (µM)
Glucose	YP	0.4 - 0.6	40	-	35
Glucose	YP	2 - 3	40	-	11
Glucose	YP	2 – 3	40	15	16
Glucose	YP	4 - 5	40	26	27
Glucose	YP	8 – 12	40	-	11
Glucose	YP	0.4 - 0.6	80	19	31
Glucose	YP	2 - 3	80	30	34
Glucose	YP	4 - 5	80	22	17
Glucose	YP	8 – 12	80	26	41
Glucose	YP	4 – 5	250	-	7.5
Glucose	YP	4 – 5	1000	-	-
Glucose	YP	2 – 3	40	-	-
Glucose	Min	2 – 3	40	-	16
Glucose	YP	2 – 3	80	-	-
Glucose	YP	2 – 3	80	-	-
Glycerol	5 % YP	2 – 3	40	24	30
Glycerol	5 % YP	2 – 3	40	-	23
Glycerol	5 % YP	2 – 3	80	-	6.1
Glycerol	5 % YP	2 – 3	80	30	42
Glycerol	5 % YP	2 - 3	80	-	-
Glycerol	5 % YP	2 - 3	80	22	46
Gal	5 % YP	2 – 3	80	-	13
Gal	5 % YP	2 - 3	80	-	8

Since the mitochondrial Mn concentrations were invariant regardless of whether the EPR feature was detected, it must be the proportion of EPR active Mn that is changing. The proportion of Mn contributing to the EPR feature ranges from 0 – 100 %. In respiring samples exhibiting the Mn EPR signal, the percentage of mitochondrial Mn contributing to the feature was 72 ± 10 %. Fermenting samples with a detectable feature have 91 ± 22 % mitochondrial Mn contributing to the feature.

The proportion of samples exhibiting the Mn EPR feature did not depend on carbon source. The Mn EPR signal was detected in 3 of the 6 samples isolated from respiring cells. It was also detected in 6 of the 15 fermenting samples. Furthermore, the spin concentrations of the Mn signal did not depend on metabolic mode. Although the proportion of mitochondrial Mn contributing to the feature may be slightly higher in fermenting samples, this cannot be said with certainty due to the large errors associated with determining spin concentrations. Therefore, it appears the Mn feature does not correlate to changes in metabolism.

The presence of the Mn EPR feature does not correlate to changes in mitochondrial Mn concentrations. Table 4-1 lists 14 samples that do not show the Mn EPR feature. All of these samples had sufficiently high mitochondrial Mn to have potentially contributed to a detectable Mn EPR signal. The fact that no signal is detected suggests that Mn is either in the EPR-silent Mn^{3+} state or that the Mn^{2+} ions are spin-coupled. Furthermore, since mitochondrial Mn

concentrations are stable regardless of whether a Mn EPR signal is detected, the same concentration of Mn is always present in samples but only sometimes in the EPR active state. This raises the question *what causes the changes in mitochondrial Mn to allow the Mn EPR feature to be detected in some samples?* This question drove us to develop several more experiments to further examine mitochondrial Mn.

Response of Mn EPR to Redox Treatment

We wanted to determine whether the species giving rise to the Mn signal was redox active. Mitochondria were isolated as described in Chapter II. Prior to packing, the sample was split into three aliquots. One was packed into an EPR tube in the as-isolated state (without treatment with a redox agent). One was treated with 100 % molecular oxygen for 30 minutes. The third aliquot was treated with 1 mM dithionite (pH 8.5) for 30 minutes prior to packing samples. Since we could not predict when we would detect the Mn EPR signal (and since we were also interested in the redox activity of Fe in our samples) this treatment was done routinely. Five of the samples in Table 4-1 exhibiting the Mn signal had been prepared for redox studies.

If the Mn feature was detected in one aliquot of a mitochondrial sample, it was present in aliquots representing all three redox states (Figure 4-2). Oxidized samples had large g = 2.01 signals (1 – 5 μM Fe) that overlap the Mn signal (Figure 4-2).

Spin concentrations for the signal did not depend on redox treatment. The spin concentrations for Figure 4-2 were 26 µM (as-isolated), 23 µM (oxidized) and 25 µM (reduced). For all samples treated with redox agents the spin concentration of the Mn signal remained constant (which we define as varying by less than 15 %) within the individual prep's aliquots. Therefore if the as-isolated sample exhibited a Mn feature with a spin concentration of 30 µM, the oxidized and reduced aliquots of the same sample would be within 15 % of 30 µM. This indicates that the Mn^{2+} EPR species is not responsive to treatment with redox agents. Therefore the Mn^{2+} is probably not redox active or it is redox active but is buffered in some way.

Correlation of Mn EPR and Media Oxygen

The sporadic appearance of the Mn EPR signal causes us to examine the effect of several variables in our growth and isolation protocol. One of these variables was the gas used during cell growth. Pure oxygen (and not air) is typically bubbled through the bioreactor during cell growth. Oxygen is used to compensate for the low surface to volume ratio of our bioreactor. Since the Mn EPR signal is due to Mn^{2+}, perhaps the oxygen flow rate during cell growth could explain the appearance of the Mn feature. Oxygen could also explain the occasional appearance of the g = 4.3 signal (Fe^{3+}) that accompanies the Mn feature. Additionally, samples with oxygen bubbling at over 30 SCFH have been reported to sometimes exhibit the Mn signal (139).

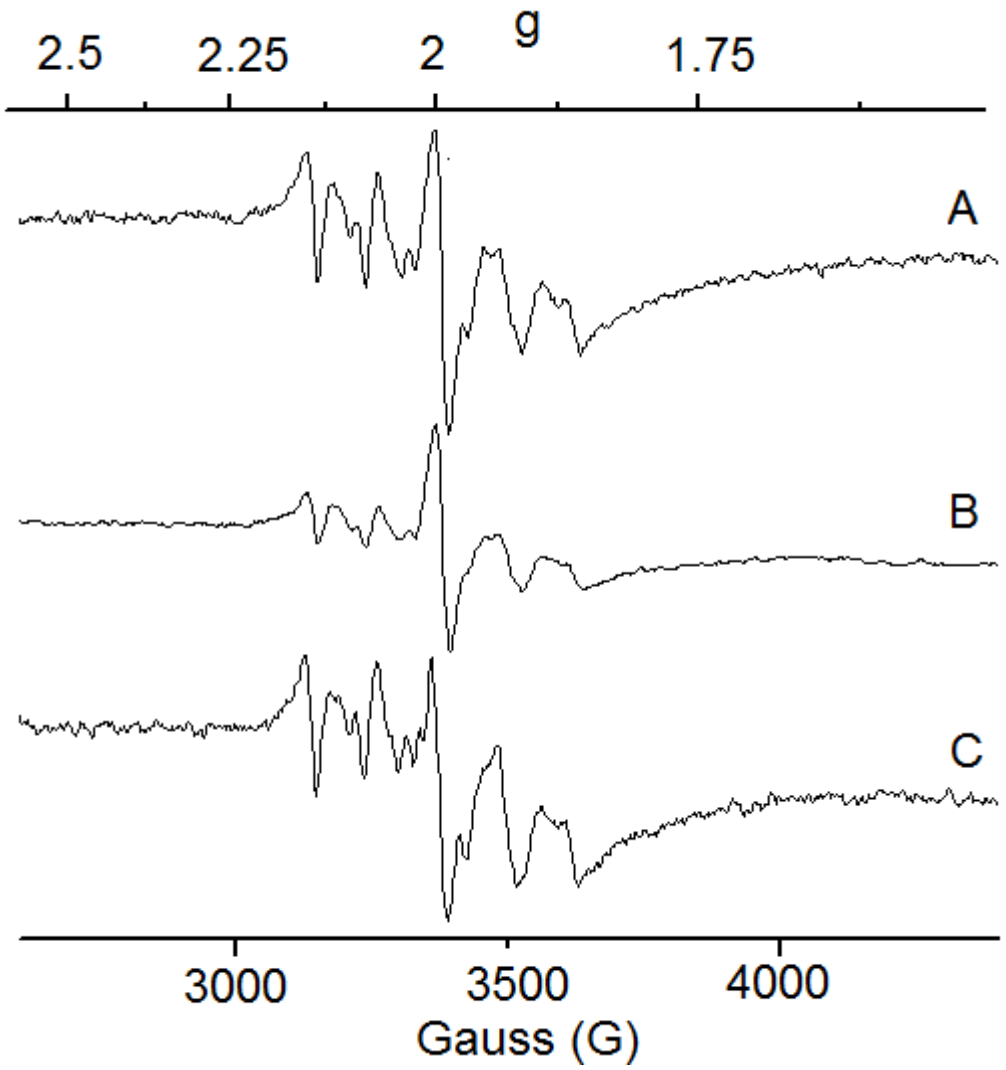

Figure 4-2. Redox treatment did not affect Mn signal. Spectra were collected at 30 db and 10 K. Samples were collected from cells grown in YPD media. Spectra were of a single prep. Isolated mitochondria were split into three aliquots, packed and frozen after (A) no treatment, (B) exposure to pure O_2 (C) treatment with 1 mM dithionite. Due to the presence of a large g = 2 signal (due to an organic radical) in the oxidized spectrum, the intensity of spectrum B was divided by 3 to graph all spectra on the same axis. Spin concentrations for the Mn EPR signal differed by 5-10 % for Spectra A-C.

In order to determine whether the rate of oxygen bubbled through media during cell growth correlated to the appearance of the Mn EPR feature, oxygen flow rates were varied from batch to batch (Table 4-1, Figure 4-3). Mitochondria were isolated from cells grown on rich media containing glucose. Typical preps were grown using 2 SCFH (standard cubic feet per hour). Flow rates ranging from 0.5 to 10 SCFH were investigated. Since we sometimes add 40 μM ^{57}Fe to media for preparation of Mössbauer samples, oxygen flow rates were varied in the presence and absence of supplemental Fe.

Figure 4-3 show the results of preps grown without Fe added to the media and oxygen flow rates of 0.5, 2, 5, and 10 SCFH. Samples that were grown without additional Fe added to media exhibited the Mn EPR feature in two preps. One of these was grown using an oxygen flow rate of 5 SCFH. The other prep exhibiting the feature was one of the two preps prepared using an oxygen flow rate of 2 SCFH. Interestingly the Mn feature was not detected using the high 10 SCFH flow rate. Since the Mn signal could not be detected in either samples grown in the presence of the high or the low oxygen flow rates, there appears to be no correlation between oxygen in the media and the appearance of the Mn EPR signal.

Samples prepared with supplemental media Fe had a slightly different result (Table 4-1). For these samples, the Mn feature was present in the samples grown with 0.5, 5, and 10 SCFH (Table 4-1). The Mn EPR signal was also found in one of the three preps grown using 2 SCFH oxygen. The

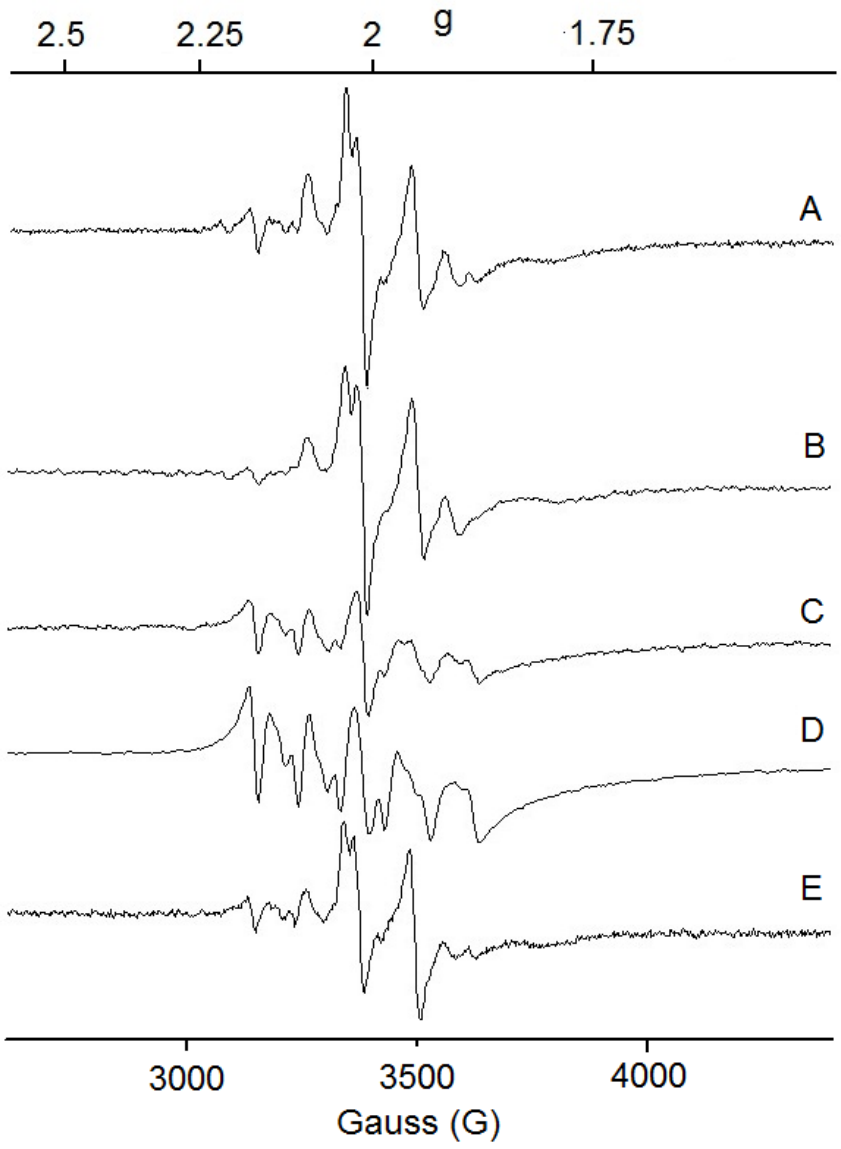

Figure 4-3. Media oxygen and Mn EPR. Samples were prepared under equivalent conditions except that the rate of O_2 bubbling through the media during cell growth was varied. Spectra were collected at 30 db and 10 K. Mitochondria were collected from cells grown with oxygen bubbled at a rate of (A) 0.5, (B-C) 2, (D) 5 and (E) 10 SCFH.

fact that the Mn feature was detected at both low and high oxygen flow rates confirms that there is no correlation between media oxygen and the Mn EPR feature. However, the presence of the Mn feature in more of the samples prepared in the presence of supplemental Fe raised the question of whether the Mn EPR feature was related to media Fe concentrations.

Effect of Isolating Samples at Different OD_{600}

Yeast go through several stages of growth—each with specific characteristics. Once an innoculum is added to media there is a lag phase (OD_{600} 0.02 - 0.10)—where yeast grow slowly. This is followed by an exponential growth phase (OD_{600} 0.1 - 2.0) (8, 190). During this phase, cells grow and divide at established rates. This is the ideal phase to collect cells for mitochondrial isolation because cell walls are easily disrupted and mitochondrial yields are higher (190, 192). The last stage of growth is the stationary phase (OD_{600} >2.0). Cells grow very slowly and store nutrients for use during divisions (190, 192). In order to optimize the yield of cells and mitochondria, most protocols call for cells to be collected during the last part of the exponential phase—right before they enter stationary growth. When we first began this project, we collected cells in a broad range of OD_{600} (1-2). Perhaps cells from some of our preps began to enter stationary phase earlier than anticipated. Perhaps the Mn signal intensity could be correlated to the OD at harvest.

The optical density (OD_{600}) for cell collection was altered to determine whether there was a correlation between OD_{600} and the Mn signal. Mitochondria were isolated in the same way except for the OD_{600}. Mitochondria were isolated from cells at an OD_{600} much higher (> 3) and much lower (~ 0.5) than our established protocol (1.0 – 1.2). The Mn signal was not seen in either the high OD or the low OD prep (Table 4-1). It seems unlikely that the cell density correlates to the appearance of the Mn EPR signal.

Correlation Between Media Fe and Mn EPR

Results from several of the above experiments indicated a potential relationship between mitochondrial Fe and Mn. The Mn EPR feature is often accompanied by a large g = 4.3 signal typical of a nonheme Fe^{3+} with an E/D = 0.27 – 0.33 (Figure 4-4). This feature was removed from some preps by treatment with a chelator. Other samples (including some discussed in Chapter III) isolated in the presence of a chelator still exhibit the g = 4.3 with spin concentrations above 40 μM (Figure 4-5 and Table 3-1). This suggests that the Fe contributing to this feature is protected from chelation and is most likely inside the mitochondria. However, it is unclear why this feature is only present in some of our samples. Another indication for a relationship between mitochondrial Fe and Mn is seen in the experiment where cells were grown in media with different flow rates of oxygen. In this experiment, the Mn feature was present in two of the five samples grown without supplementing Fe in the media.

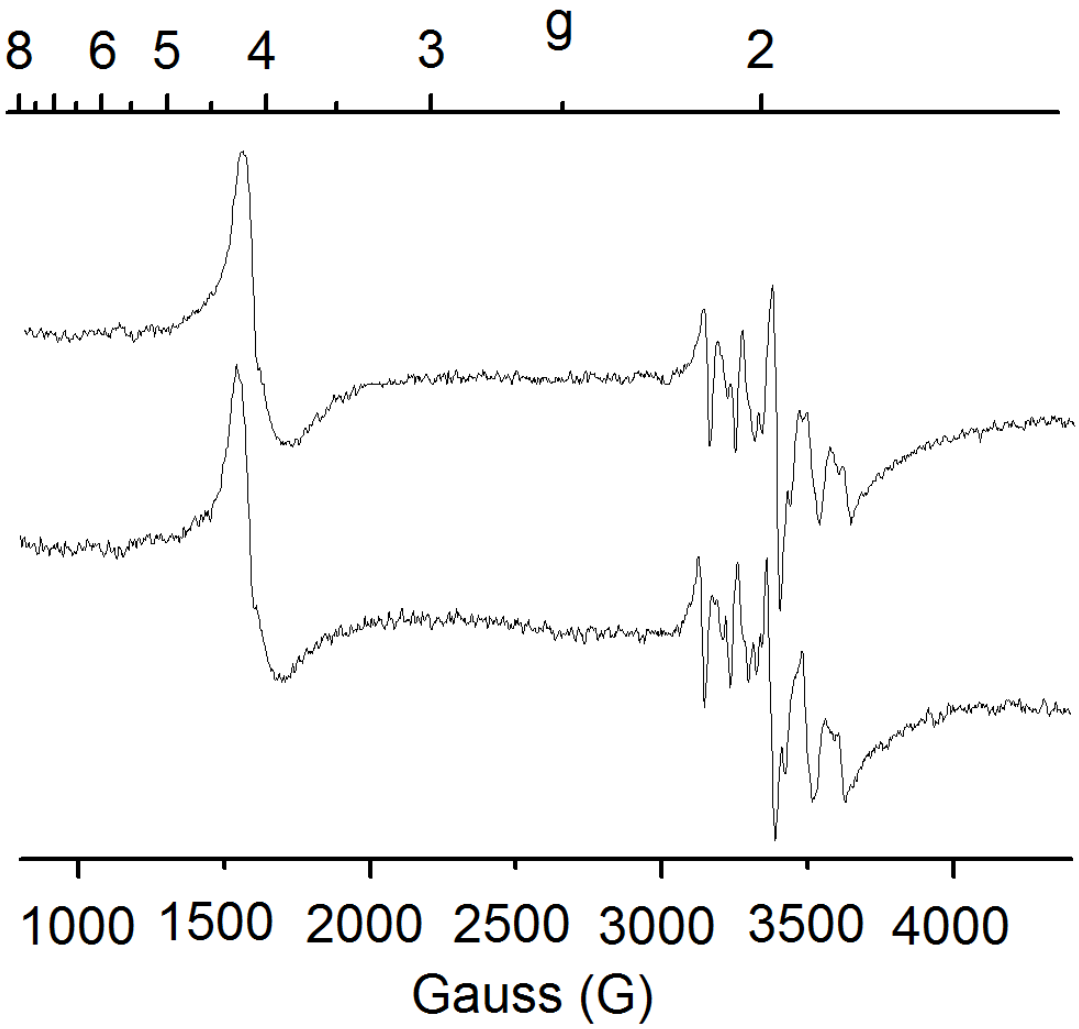

Figure 4-4. Mitochondria isolated with a chelator often exhibit a Mn^{2+} and a g = 4.3 EPR signals. Two individual preps where mitochondria were isolated from fermenting cells in the presence of a chelator. Spectra were collected at microwave power 0.2 mW, microwave frequency 9.45 GHz, 10 K and modulation amplitude 10 G.

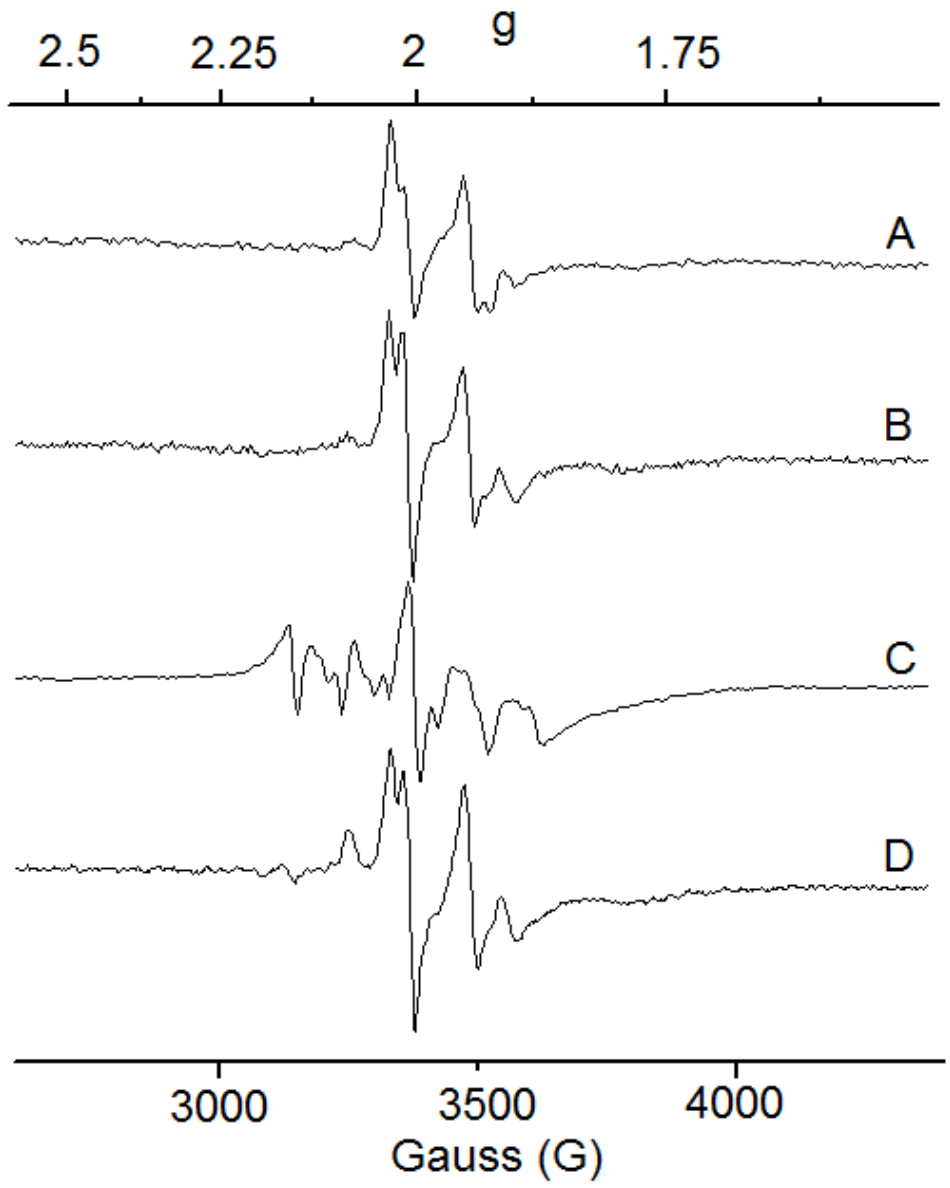

Figure 4-5. The Mn EPR signal did not depend on media Fe concentrations. Spectra were collected at microwave frequency 0.2 mW, microwave frequency 9.44 GHz and 10K. Cells were grown in the presence of (A) 1.0 mM, (B) 0.25 mM, (C) 40 µM and (D-G) 0 added ^{57}Fe. Rich media already contains approximately 35 µM Fe which means total Fe concentrations were higher by this amount.

In contrast, 4 of the six preparations in which 40 µM Fe was added to the media exhibited the signal. It appeared there may be a correlation between high media concentrations and the presence of the Mn EPR signal. Furthermore, studies by other labs suggest that supplementing media with metals such as Fe or Cu affect the mitochondrial concentrations of those components (134). However, results (Chapter III) by our lab have not been able to confirm that adding supplemental Fe to media during cell growth affects the mitochondrial [Fe]. However, we had not investigated whether adding supplemental Fe could result in the appearance of the Mn EPR feature.

In order to test whether media [Fe] and the Mn feature were connected, we grew cells on media with different concentrations of [Fe]. The total media [Fe] depends on both the initial [Fe] in the media as well as any added supplements. There are two types of media used in our lab: minimal and rich. Rich media has approximately ~ 35 µM Fe naturally while minimal media contains only ~ 10 µM Fe. Therefore the addition of 40 µM Fe to rich growth medium results in the final concentration of ~ 80 µM. The resulting EPR spectra of isolated mitochondria were then collected and analyzed.

We analyzed the effect of media Fe concentrations for cells grown in rich glucose media. Samples were grown with equivalent conditions (oxygen flow rate, media supplements, OD_{600} for cell collection, etc.) except that the Fe added to the media was varied. Cells were grown in the presence of 40 µM, 80 µM, 250 µM, or 1.0 mM media Fe (final concentration). The Mn signal was present

in 2 of the 8 samples prepared from cells grown in 40 µM Fe. It was also present in 6 of the 8 samples isolated from cells grown in 80 µM Fe. However no Mn EPR signal was depicted in samples collected from cells grown in media containing 250 µM or 1.0 mM. Thus, there does not appear to be a correlation between media [Fe] and the Mn EPR signal.

In summary, we have been unable to establish the factor responsible for the Mn EPR signal. We tested multiple parameters of cell growth and mitochondrial isolation to determine what factor might contribute to the appearance of a Mn EPR feature. Growth parameters investigated include the carbon source and media type. Carbon source did not have an effect as the Mn signal has been seen in samples isolated from glucose (Table 4-1), lactate (139) and glycerol media (Table 4-1). Samples isolated from both rich and minimal media have exhibited the signals. Although we are not certain what is causing the Mn EPR signal, we do know the presence of this signal is not correlated to media [Fe], the rate of oxygen bubbling during growth, OD_{600} when cells are isolated, metabolic mode or media type. The Mn may be from a contaminating species that is present in some of our preparations. One possibility is that the Mn is inside other organelles (such as vacuoles or ER) that co-localize with mitochondria.

Assessment of Redox Properties of Mitochondria

We have reported on the Fe-ome of respiring mitochondria previously (139). As mentioned above, we constantly used experimental results as indicators of how to adjust our isolation protocol. Here we will mention some of our early results and how they were used to evaluate our protocol and develop new procedures. Early studies in our lab indicated that treatment of purified organelles with redox agents had a significant impact on the mitochondrial Fe-ome.

Mössbauer spectra of mitochondria isolated from cells grown on lactate media and treated with redox agents showed a tremendous difference in spectral features. Oxidized samples exhibited only ~ 50 % of the magnetic material present in as-isolated samples. Treatment of mitochondria with 1 mM dithionite resulted in a 2 - 3 fold increase in the NHHS Fe^{2+}. In addition, nearly 50 % of the Fe/S clusters in our samples could be reduced with dithionite (139). Since dithionite is negatively charged, it should not be able to enter the IM and should not reduce samples with intact membranes. The changes induced by treatment of dithionite were disconcerting. Are mitochondria unable to control their redox state?

We were unsure as to whether those early results were indicative of the long sample preparation times (resulting in damaged membranes and Fe centers) or whether intact mitochondria are responsive to redox treatment. We repeated several of the experiments presented in Hudder *et al*. (139) to address

this issue. In order to understand the Fe-ome, it would be helpful to evaluate whether intact mitochondria have an ability to resist internal redox changes upon exposure to a redox agent.

Disruption of Mitochondrial Membranes

Traffic through the inner mitochondrial membrane is highly regulated. The negatively charged dithionite ion should not be able to cross the IM and only mitochondria with damaged membranes would be subject to reduction. We wanted to determine whether the response to redox treatment was a result of compromised membranes. Therefore, we needed to treat samples with redox agents while membranes are intact and after their complete disruption. Mitochondrial membranes can be disrupted by either sonication or the addition of a detergent. Disruption of membranes by sonication is difficult. Sonication for a short time may not disrupt all the membranes while long periods can damage proteins and remove metal ions from enzyme active sites. However, the addition of detergents is fairly straightforward. Addition of 1 % deoxycholate, is sufficient to disrupt mitochondrial membranes.

Since sonication can potentially damage enzyme active sites and thus give a skewed Fe distribution, we wanted to begin using a more gentle method of membrane disruption. However, it was first necessary to establish whether a detergent like deoxycholate would cause a similar situation. Mitochondria were isolated from cells grown on glucose media as described in Chapter II. Purified

mitochondria were split into two aliquots. They were packed for analysis after treatment with either nothing or 1 % deoxycholate. Samples were then evaluated by both EPR (Figure 4-6) and Mössbauer spectroscopy (Figure 4-7).

The EPR spectrum of the untreated sample had spin concentrations of features similar to those discussed in Chapter III. Features had the following spin concentrations g_{ave} = 1.94 ~ 2.5 µM, g_{ave} = 1.90 ~ 5.0 µM, g_{ave} = 2.00 ~ 1.0 µM and g_{ave} = 2.04 ~ 1.5 µM. These spin concentrations did not change in the sample treated with deoxycholate. There were two differences in the treated spectrum. First, it appeared that there was an increased resolution between the g = 2.01 and g = 2.02. However, this could not be confirmed by simulation. The same line-width was used in each simulation. The treated spectrum also had a broad feature around g = 1.7. This feature may be an artifact and was not simulated.

The Mössbauer spectrum of the untreated sample in Figure 4-7 had an Fe distribution similar to that discussed in Chapter III. The treated sample did not change except for a nominal increase (~ 4 %) in the NHHS Fe^{2+}, the significance of this remains unclear. These results indicate that deoxycholate did not have a significant effect on the Fe distribution of our samples. Therefore membranes could be disrupted with deoxycholate prior to treatment with redox agents.

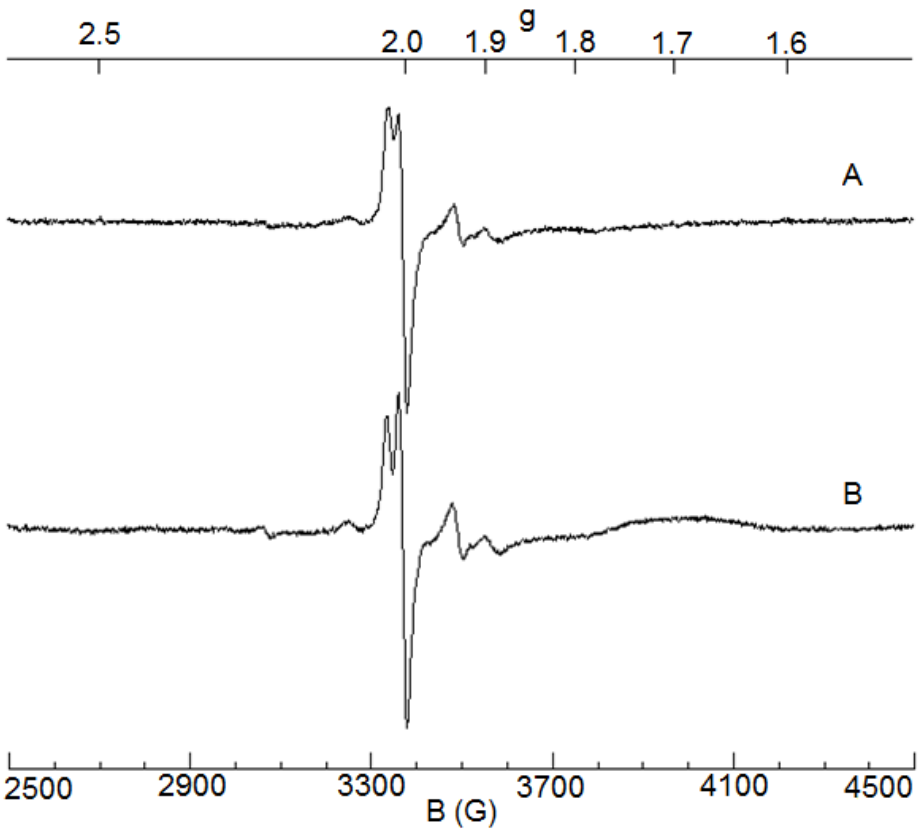

Figure 4-6. Deoxycholate did not affect EPR spectra. Spectra of mitochondria isolated from cells grown on minimal glucose media. Spectra were collected at microwave power 0.2 mW, microwave frequency 9,43 GHz and 10 K. Samples were packed in EPR tubes with either (A) no treatment or (B) treatment with 1 % (w/v) deoxycholate.

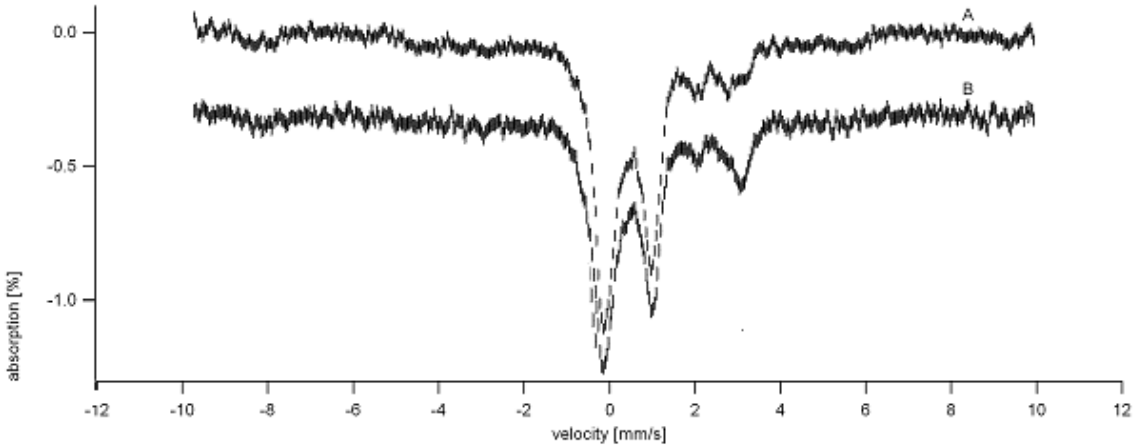

Figure 4-7. Deoxycholate did not alter Fe distribution. Spectra were collected at 4.5 K and 0.05 T. Mitochondria were isolated from cells grown on minimal media containing glucose. Samples were packed for analysis with (B) or without (A) treatment with 1 % deoxycholate. There may have been a slight increase (~ 4 %) in the NHHS Fe^{2+} but the significance of this is uncertain.

Mössbauer Analysis of Mitochondria Treated with Reductant

As discussed above, when we started this project, we saw substantial changes in spectra upon treating samples with a reductant. Since dithionite should not be able to cross the mitochondrial inner membrane, the significant differences seen with its treatment indicated one of two things. Either the bulk of the Fe in our samples was adventitiously bound outside of the mitochondria and therefore accessible to reduction, or the mitochondrial membranes had been compromised, allowing dithionite to flow freely throughout the samples and reduce mitochondrial Fe complexes.

In another experiment, mitochondria were isolated as described from cells grown on respiring media. The sample was split into two aliquots. One was treated with 1 mM dithionite for 30 – 45 minutes prior to packing. The other was treated with 1 % deoxycholate prior to dithionite treatment. Mössbauer spectra were obtained and are shown in Figure 4-8. The sample treated with dithionite in the absence of deoxycholate had an Fe distribution discussed in Chapter III. Treatment with deoxycholate prior to incubation with dithionite resulted in an increase in the NHHS Fe^{2+} and a decrease in the amount of HS Fe^{2+} heme. This may indicate that the dithionite is only able to reduce the sample once membranes have been disrupted. However, the changes induced with dithionite treatment in the presence of deoxycholate are smaller than anticipated. This may indicate that mitochondria are already resting in a reduced state when isolated under anaerobic conditions.

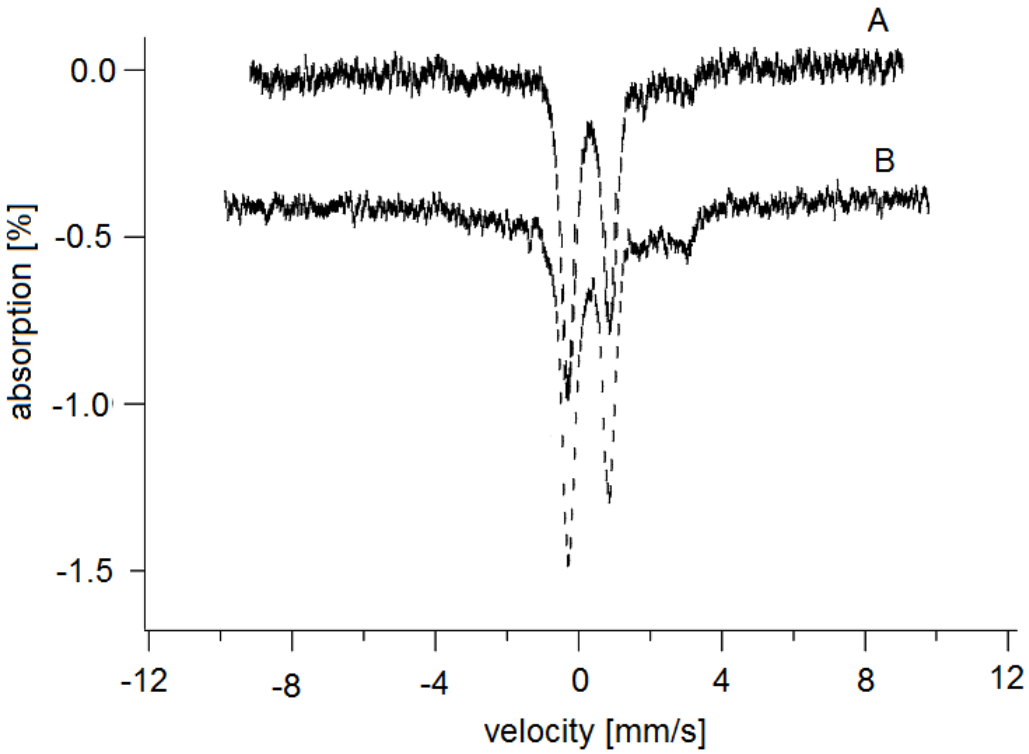

Figure 4-8. Mitochondria reduced in the presence and absence of deoxycholate. Spectra were collected at 4.5 K and 0.05 T. Mitochondria were isolated from respiring cells. Sample was split into two aliquots. Spectrum A was treated with 1 mM dithionite for 30 minutes prior to packing. Spectrum B was matched except that prior to incubation with dithionite, the sample was treated with 1 % deoxycholate to disrupt membranes.

There are reductants that can freely pass through the inner mitochondrial membrane. Malate and glutamate are trafficked by transporters through the inner membrane. They can therefore serve as reductants to samples with intact membranes. We wanted to treat isolated mitochondria with these compounds to see if they could reduce our samples.

Mitochondria isolated from respiring cells were split into two aliquots. One was treated with 5 mM malate, 5 mM glutamate as described (238) prior to packing. The other was packed without treatment. Mössbauer spectra were obtained and are shown in Figure 4-9 and Figure 4-10. The low field Mössbauer spectra are shown in Figure 4-9. The as-isolated spectrum (black) is also shown in Figure 3-1. Simulations for the as-isolated sample (discussed in greater detail in Chapter III) include assumptions that there is 63 % central doublet, 7 % HS Fe^{2+} heme, 13 % Rieske protein, 2 % NHHS Fe^{2+} and < 10 % $[Fe_2S_2]^{2+}$. Figure 4-9 shows both the as-isolated and reduced spectra can overlap. For ease of viewing, the reduced spectrum was graphed without the corresponding error bars. The reduced spectrum showed essentially no change in Fe distribution and the same simulation could be fit to both spectra. Similar results were seen in mitochondria isolated from fermenting cells(225).

The high field Mössbauer spectra of the as-isolated and reduced samples are shown in Figure 4-10. The as-isolated spectrum (black) which is also depicted in Figure 3-1 is shown in Figure 4-10. It is overlaid with a simulation (blue) assuming 65 % $[Fe_4S_4]^{2+}$ and 13 % Reiske protein. In addition, it is shown

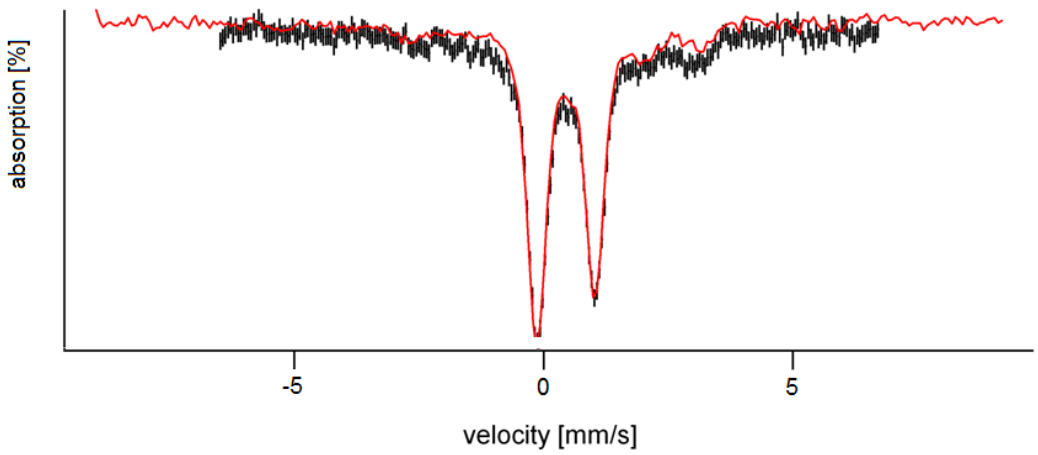

Figure 4-9. Low field Mössbauer spectra of as-isolated and reduced mitochondria. Spectra were collected from 4.5 K and 0.05 T. Mitochondria were isolated from respiring cells. Sample was split into two aliquots-one was packed for analysis without treatment (black), the other was treated with 5 mM malate and 5 mM glutamate (red) to reduce the sample. The as-isolated sample is also shown in Figure 3-1. Analysis of the as-isolated spectrum is discussed in detail in Chapter III but includes a simulation assuming 63 % central doublet, 7 % HS Fe^{2+} heme, 4 % NHHS Fe^{2+}, 13 % Rieske protein and < 10 % $[Fe_2S_2]^{2+}$. The reduced aliquot was fit with the same simulation.

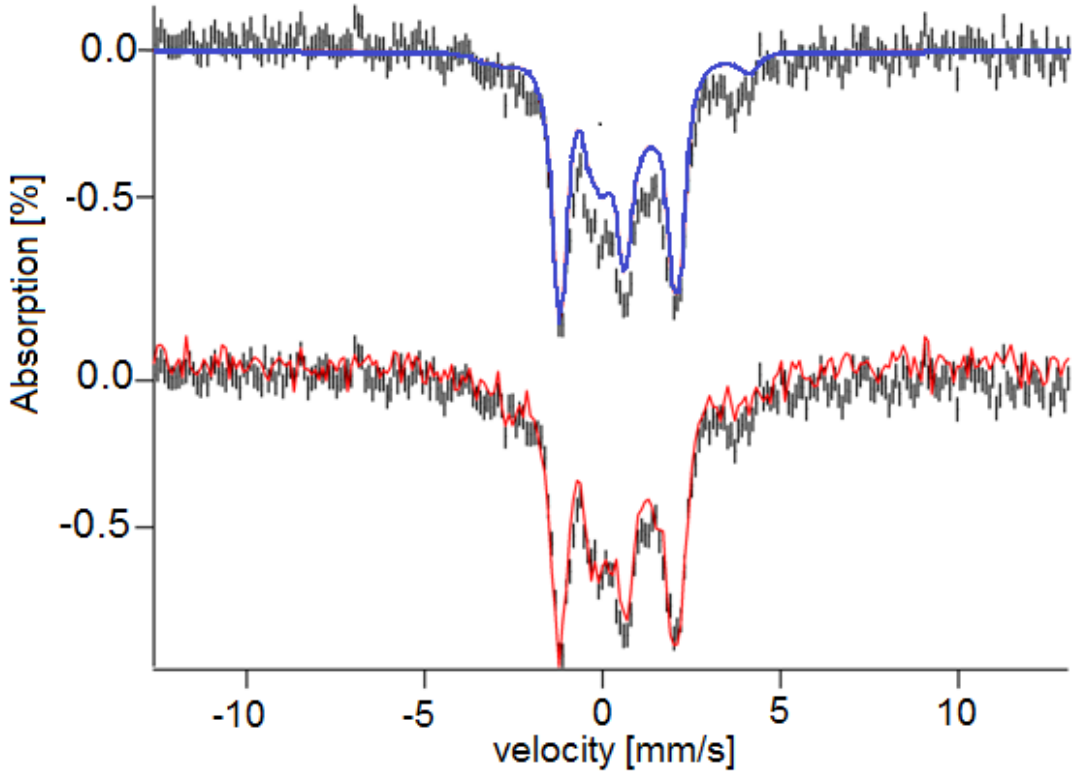

Figure 4-10. High field Mössbauer spectra of mitochondria. Spectra were collected at 4.2 K and 8 T. Mitochondria were isolated from cells grown on glycerol media. Isolated mitochondria were split into two aliquots. One aliquot was packed in the as-isolated state (black spectrum). The blue simulation assumes 65 % $[Fe_4S_4]^{2+}$ cluster (with δ = 0.46 mm/s and ΔEq = 1.15 mm/s) and 13 % reduced Rieske protein. The second aliquot was treated with 5 mM malate and 5 mM glutamate prior to packing (red spectrum). The as-isolated and reduced spectra are overlaid to show there is essentially no difference between the as-isolated and reduced spectra. For ease of visualization, the reduced spectrum is plotted without error bars.

with the reduced spectrum (red) superimposed. There is essentially no difference between the reduced and as-isolated spectra. This further indicates that anaerobically isolated mitochondrial samples are in a reduced state.

EPR Analysis of Mitochondria Treated with Reductant

Mössbauer spectra indicated that the percentage of magnetic Fe was unchanged by treatment with a reductant. However, this information is not complete. The concentrations of several paramagnetic species could be changing even though the percent of Fe contributing to the paramagnetic Mössbauer feature is constant. Therefore, mitochondria isolated from cells grown on respiring (Figure 4-11) and fermenting (Figure 4-12 and Figure 4-13) media were treated with reductant and evaluated by EPR.

Interestingly, the spin concentration of the g_{ave} = 1.90 signal in both fermenting and respiring samples was unchanged by treatment with reductant. The g_{ave} = 1.94 concentration increased 20 % from 7.5 ± 2 to 10 ± 2 μM in respiring samples while the fermenting concentrations remained unchanged at 2.2 μM. The main difference found in the g = 2 region of the EPR spectra of reduced samples is the significant diminishing of the g_{ave} = 2.00 from the organic radical. This signal can be diminished by treatment with dithionite, even in the absence of a detergent. The low field region of the EPR spectra further exhibited the reducing power of dithionite. Here spin concentrations of heme centers which totaled ~ 5 μM in the as-isolated samples were diminished to ~ 0

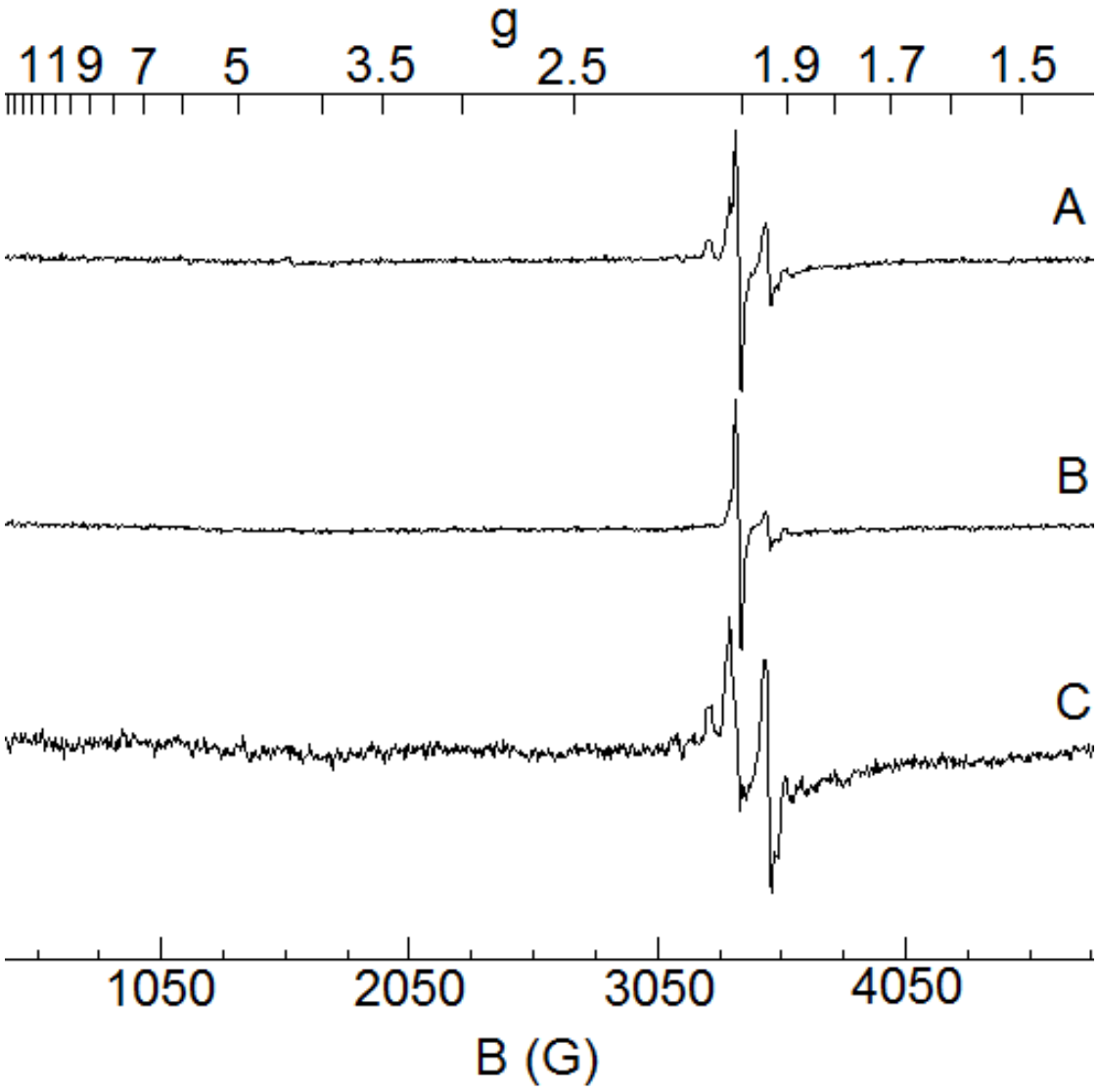

Figure 4-11. Respiring mitochondria treated with redox agents. Mitochondria were isolated from respiring cells and split into three aliquots. Samples were packed and frozen after treatment with (A) nothing, (B) 100 % molecular oxygen or (C) 1 mM dithionite for 30 minutes. Spectra were collected at microwave power 0.2 mW, microwave frequency 9.44 GHz and 10 K. Spectra were normalized for differences in spectral parameters, but then the intensity of B was divided by 2 and intensity of C was multiplied by 2.5 to graph all three spectra on same axis.

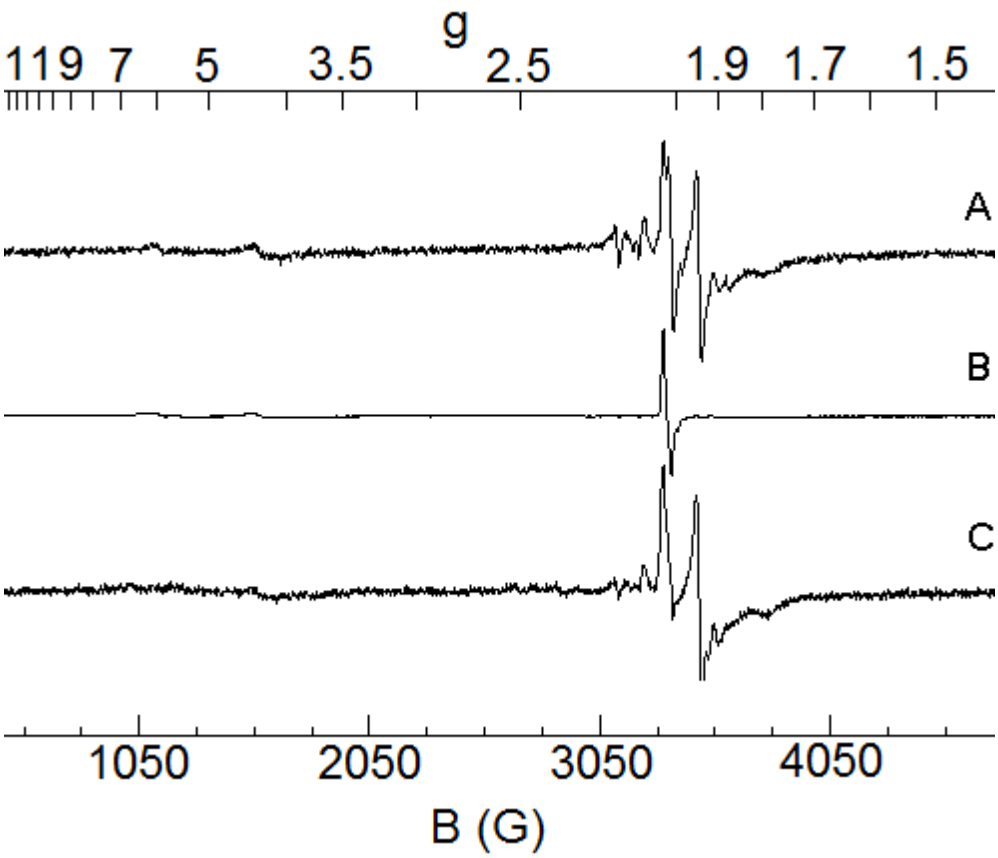

Figure 4-12. EPR spectra of fermenting mitochondria treated with redox agents. Mitochondria were isolated from fermenting cells and split into three aliquots. Samples were packed after treatment with (A) nothing, (B) 100 % molecular oxygen or (C) 1 mM dithionite for 30 minutes. Spectra were collected at microwave power 0.2 mW, microwave frequency 9.44 GHz and 10 K. Spectra were normalized and the intensity of spectrum B was divided by 4 to graph all three spectra on the same axis.

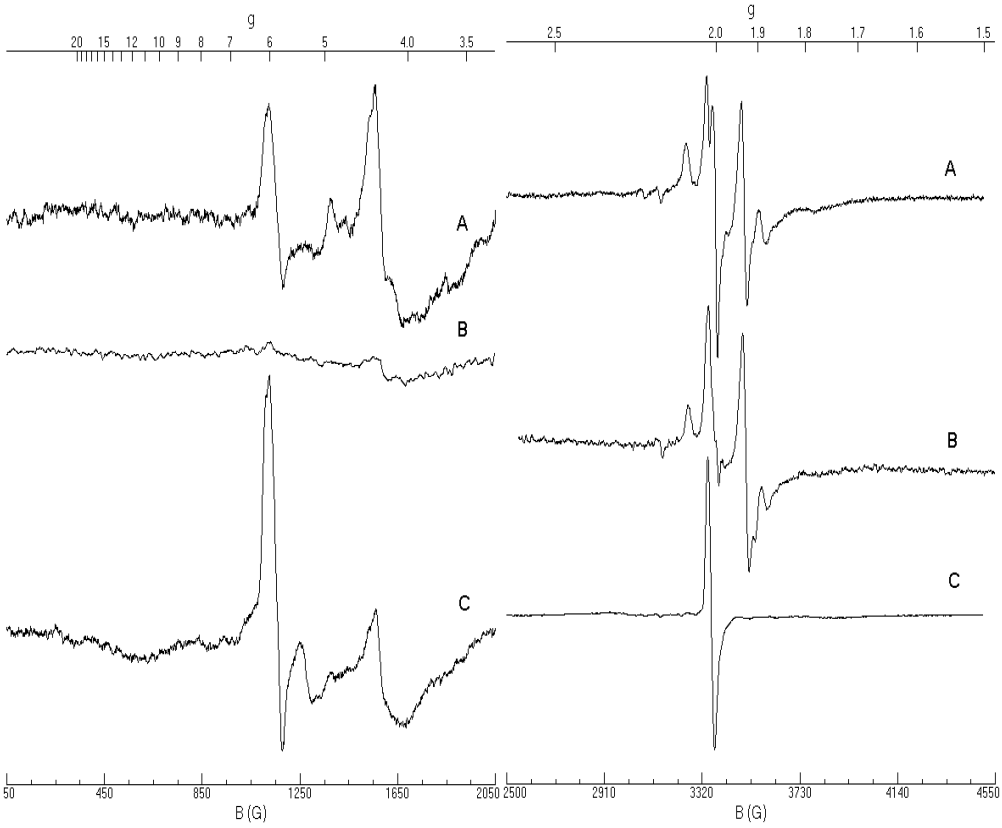

Figure 4-13. EPR spectra of fermenting samples showing dithionite reduction of hemes. Spectra are of isolated mitochondria collected from fermenting cells. Samples were either treated with (A) nothing, (B) 1 mM dithionite (pH 8.5) for 30 minutes or (C) 100 % molecular oxygen for 30 minutes. Spectra were all collected at 10 K and microwave frequency 9.43. The low field spectra were collected at microwave power 20 mW. The g = 2 region was collected at microwave power 0.2 mW.

In the reduced sample. This change, although appears significant, (Figure 4-13) only encompasses ~ 2 % of the total heme concentration in our samples calculated by electron absorption.

Thus treatment with dithionite had only a minor effect on the g = 2 region of EPR spectra with concentrations of the g_{ave} = 1.90 and g_{ave} = 1.94 only changing by standard errors in our experiments. In contrast, the changes in the low field EPR spectra reveal that ferric HS hemes are much more susceptible to treatment with dithionite. The oxidized hemes are most likely arising from cytochrome c oxidase. This enzyme is housed in the IM, with Cu_A, in redox equilibrium with the IMS and may be in redox equilibrium with dithionite or oxygen. In contrast other heme-containing species may be redox equilibrium with the matrix and inaccessible to redox treatment by exogenous redox agents.

Electron Absorption of Mitochondria Treated with Reductant

In order to confirm the changes in distribution of Fe seen by EPR, mitochondria were evaluated by Electron Absorption Spectroscopy in the as-isolated state and after treatment with 1 mM dithionite.

Figure 4-14 shows mitochondrial samples treated with 1 mM dithionite in the presence of 1 % deoxycholate. The reduced and as-isolated spectra could be overlaid and were simulated with identical heme concentrations. Thus heme centers were essentially unaffected by treatment with reductant. This corresponds to the changes seen by EPR where the minor ferric heme

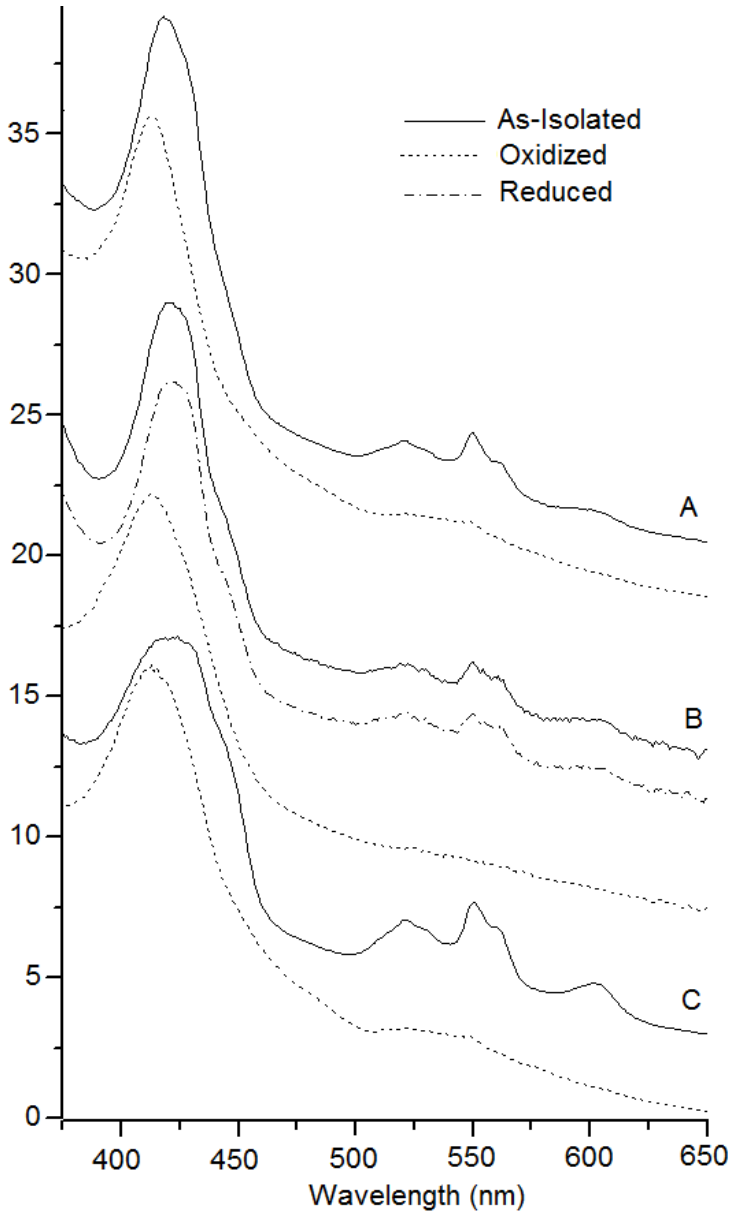

Figure 4-14. Electron absorption spectroscopy of mitochondrial samples treated with redox agents. Three individual preparations are shown. Electron absorption spectra were collected of the as-isolated state. Samples were then treated with oxygen for 30 - 45 minutes. An electron absorption spectra was collected of the oxidized state. After oxidation, one sample (B) was treated with 1 mM dithionite. The reduced spectrum could be overlaid with the original as-isolated spectrum (collected prior to redox treatment), indicating heme oxidation is reversible.

contributions (~ 5 μM) are reduced by dithionite. This further confirms that mitochondrial heme centers rest in the reduced state.

Mössbauer Analysis of Mitochondria Treated with Oxygen

In order to understand the Fe-ome of isolated mitochondria, it is necessary to evaluate how Fe-containing species change upon treatment with oxygen. A Mössbauer spectrum of respiring mitochondria treated with oxygen (Figure 4-15) showed an increase in the NHHS Fe^{2+} (~ 20 %). This increase is surprising since O_2 is an oxidant. This feature could be due to residual Fe:EGTA in the sample or damaged Fe centers. It seems counter-intuitive that an oxidant should increase the amount of reduced NHHS Fe^{2+}. Perhaps an endogenous reductant is present.

Since it was unclear whether molecular oxygen was able to oxidize the Fe in intact samples, a separate sample was treated with 1 % deoxycholate to disrupt membranes prior to treatment with oxygen. This sample (Figure 4-15B) showed a feature that begins at ~ - 4 mm/s with parameters corresponding to LS ferric heme (239), possibly from oxidized cytochrome c. Simulation of this feature is difficult since it is buried in the baseline. However, we can tentatively assign 5 - 10 % of the Fe to this feature which corresponds to 30 – 70 μM Fe. This is much lower than the only a fraction of the cytochrome c in our samples was oxidized with treatment with molecular oxygen.

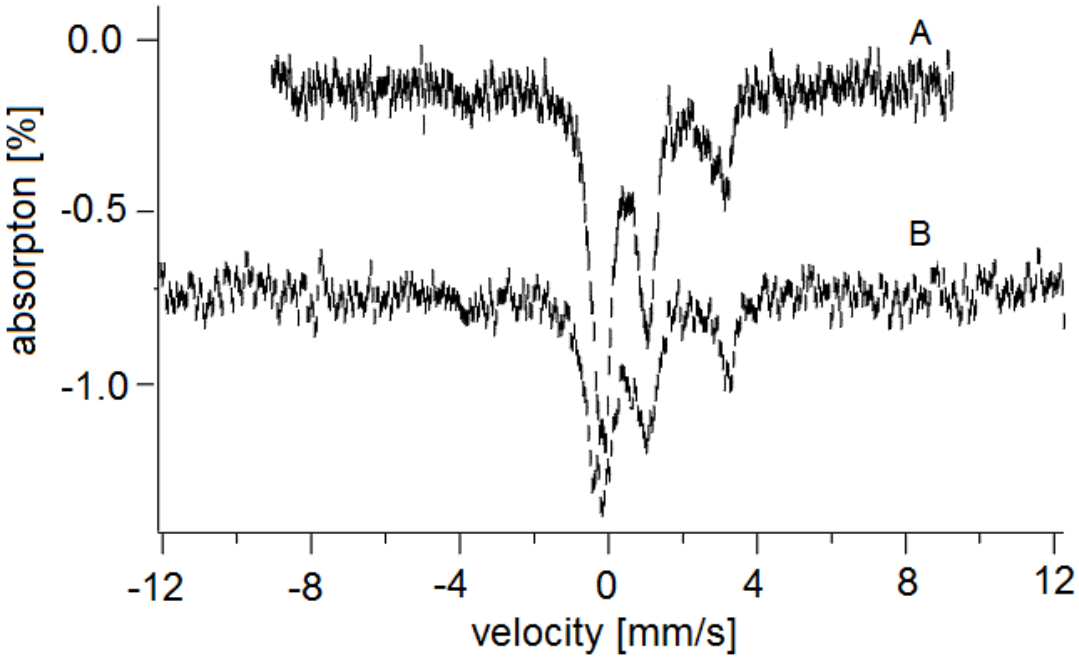

Figure 4-15. Mössbauer spectra of mitochondria treated with oxygen. Spectra were collected at 4.5 K and 0.05 T. Sample was isolated from respiring cells and split into two aliquots. The aliquots were treated with molecular oxygen for ~ 30 minutes in the presence (B) and absence (A) of 1 % deoxycholate.

EPR Analysis of Mitochondria Treated with Oxygen

EPR spectra of some oxygen-treated mitochondrial samples exhibit a g = 3.1 feature from ferric hemes (Figure 4-16). Simulation of spectra indicates this feature has a spin concentration ranging of ~ 5 µM. We have seen this feature in 3 individual oxidized spectra. This concentration implies that either heme centers are protected from oxidation or the samples were not being completely oxidized.

The g = 2 region of the oxidized EPR spectra were often dominated by an organic radical that overlaid the g_{ave} = 1.90 and g_{ave}=1.94 signals. The concentration of the g_{ave} = 2.0 signal increased from 1 - 3 µM in as-isolated samples to 2 - 5 µM in oxidized samples. The g_{ave} = 1.90 and g_{ave} = 1.94 signals may be present, but are obscured by the dominant radical feature. Simulation of this feature gave a spin concentration of ~ 7 µM. This is within the expected uncertainty of that determined for the as-isolated sample. Since the radical (perhaps from CoQH·) dominates the EPR spectra for all of the fermenting samples we have, it is impossible to determine the spin concentration of the g_{ave} = 1.94 in these samples.

The low field region of oxidized samples (Figure 4-13 and Figure 4-16) indicate that hemes are the most responsive to oxidation. In both situations the spin concentrations of the hemes increased substantially when reduced samples were treated with oxygen. In Figure 4-13, the spin concentrations collectively rose from ~ 5 µM to ~ 12 µM.

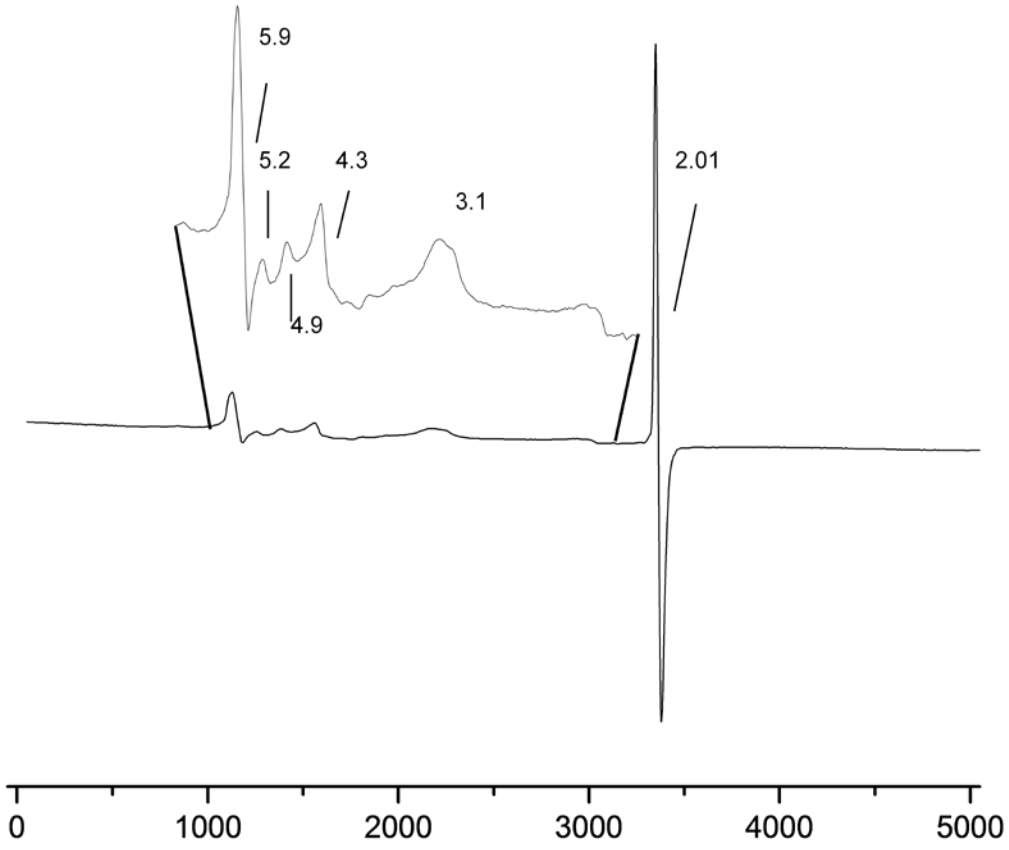

Figure 4-16. EPR spectrum of an oxidized sample showing a LS ferric heme feature. Sample was isolated from fermenting mitochondria and treated with oxygen as described above. Spectrum was collected at 10 K, microwave frequency 9.43 GHz and microwave power 20 mW.

Electron Absorption Spectroscopy of Mitochondria Treated with Oxygen

UV-Vis spectra of oxidized samples isolated from respiring samples are included in Figure 4-14 and Figure 4-17. In Figure 4-14, isolated mitochondria were incubated in a septum vial with pure oxygen bubbled through for 30 minutes. Samples were immediately analyzed by Electron Absorption Spectroscopy. Molecular oxygen completely oxidized α and β bands of all three hemes.

We wanted to determine whether heme oxidation was time dependent. A freshly purified mitochondrial sample was isolated as described and evaluated by electron absorption. The sample contained heme *a, b* and c in 45, 50 and 110 μM. The sample was treated with pure molecular oxygen for 30 minutes before a second spectrum was collected. As expected, the α and β bands were completely diminished (Figure 4-17B). The sample was incubated in air and without O_2 bubbling for 10 minutes, then another spectrum was collected. The spectrum (Figure 4-17C) exhibited the original heme features at as-isolated concentrations. This process was repeated 5 more times (Figure 4-17D-E). The sample was treated with molecular oxygen, evaluated by UV-Vis, allowed to sit and was re-evaluated by UV-Vis. In each instance, the spectrum collected immediately after O_2 exposure had completely oxidized heme centers while the spectrum collected several minutes later had reduced heme signals with the same concentrations as of the as-isolated state. This implies that there are

Figure 4-17. Kinetic studies of oxidation. Mitochondria were isolated from respiring mitochondria and evaluated by Electron Absorption Spectroscopy (A). Pure oxygen was then bubbled through the sample for ~ 30 minutes and evaluated (B). After an additional 10 minutes had passed, with the sample sitting in air, without O_2 bubbling, the sample was analyzed again (C). Reduced heme content was recovered. This process was repeated several times. D represents the spectra that had been oxidized 5 times for a total of ~ 2.5 hours. Spectra E was taken ~ 10 minutes later with the sample sitting in air. Before samples are frozen for EPR analysis, they were evaluated by electron absorption (F). The sample was treated with oxygen (H) and immediately frozen. This sample was the oxidized EPR spectrum in Figure 4-16. The sample was thawed aerobically and evaluated (G).

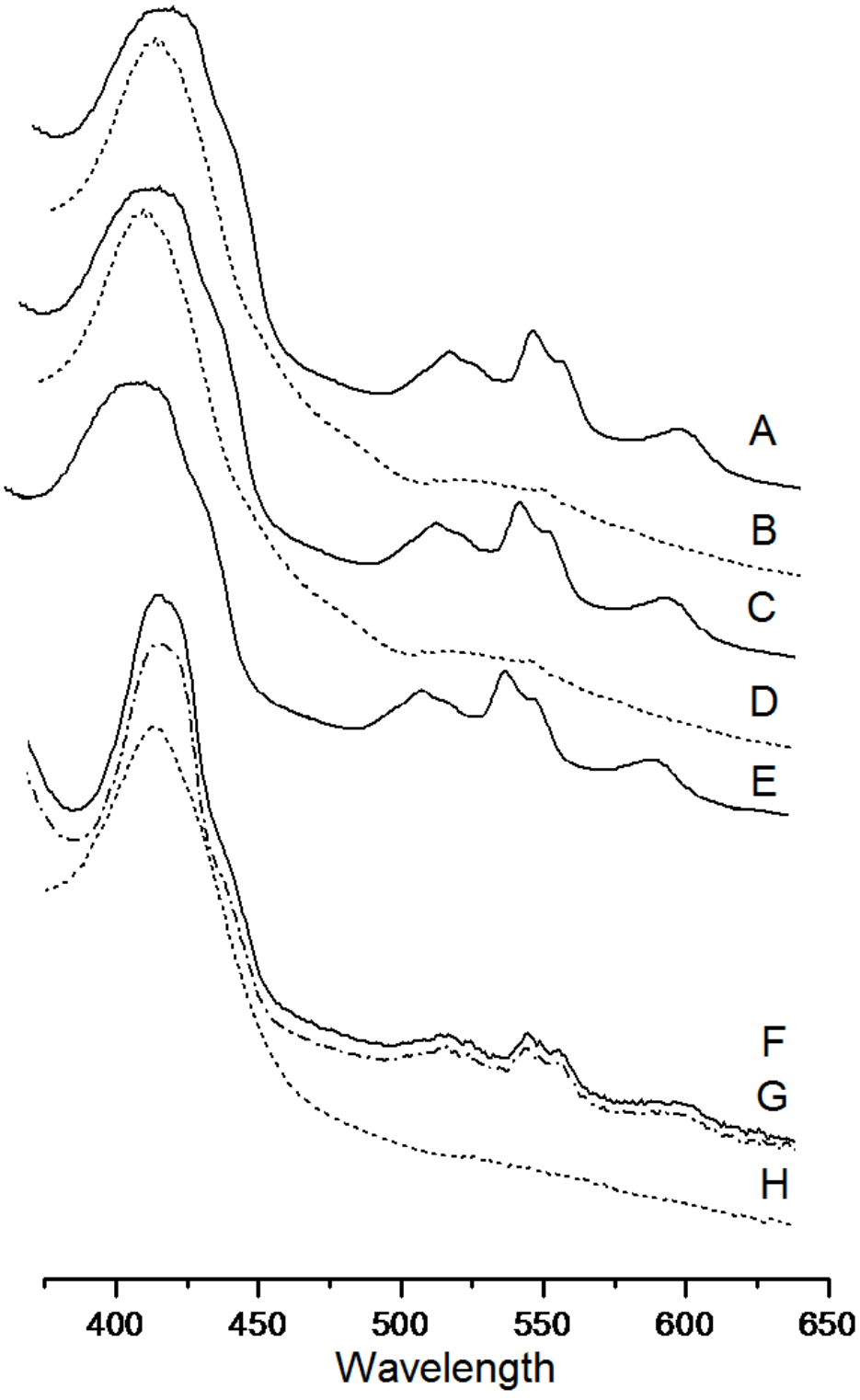

Figure 4-17. Continued.

endogenous reductants present in mitochondrial samples. Furthermore, it suggests that mitochondria return to a specific redox state.

We wanted to confirm whether this phenomenon was present in all of our samples. Although several EPR samples were analyzed by Electron Absorption Spectroscopy prior to storage for EPR analysis (Figure 4-17F-G), an oxidized EPR sample (from Figure 4-16) was thawed and analyzed for heme content (Figure 4-17H). Heme concentrations were 35, 40 and 100 μM for heme *a, b* and *c* respectively. The heme content had almost completely recovered to the as-isolated concentrations. This recovery of reduced heme centers explains why results of EPR, Mössbauer and electron absorption spectra do not correlate. Depending on how quickly the sample was frozen after treatment with oxygen, there would be a different amount of oxidized heme centers in the sample.

Taken together, mitochondrial heme centers are able to be oxidized. However, this oxidation is temporary with reduced heme centers recovering within several minutes. Mitochondria appear to have a default redox state to which they return after oxidation. This buffering capacity is probably maintained by endogenous reductants in the organelle.

Spectral Changes After Sample Storage

Isolating mitochondria and preparing samples quickly is commonly assumed to minimize sample degradation. Similarly, storing samples in liquid N_2 is generally thought to prevent them from changing redox state over time.

Prepared samples are often stored in liquid N_2 until run by EPR. Since samples stored in liquid N_2 are thought to be safe from changes in redox state and degradation, this variation in storage times was not initially an issue of concern for us.

The sample shown in Figure 4-18A was originally packed and stored in a Mössbauer cup. Figure 4-19A shows a spectrum collected two weeks after mitochondria were isolated. Once Mössbauer spectra were obtained, the sample was crushed and packed into an EPR tube as described (189). Spectrum A was obtained only hours after preparing the EPR sample.

For both Figures 4-18 and 4-19, spectrum B was collected on the same sample after a period of time during which it was stored in liquid N_2. For Figure 4-18B the sample was stored almost two weeks between runs, while for Figure 4-19B the spectra were run within 6 days of one another. In each instance the shape of the spectra has changed. The g_{ave} = 1.94 and g_{ave} = 1.90 signal intensities did not change, and were simulated as 8.5 ± 3 and 14 ± 3 μM respectively. However, both signals were overlapped by the appearance of a Mn signal which had not been present in the original spectrum.

These spectra raised two questions. First, what was causing the appearance of Mn EPR signal in stored samples—could samples be damaged during storage? Secondly, why was signal intensity decreased after storage and why could it be recovered? To address these questions, samples were thawed

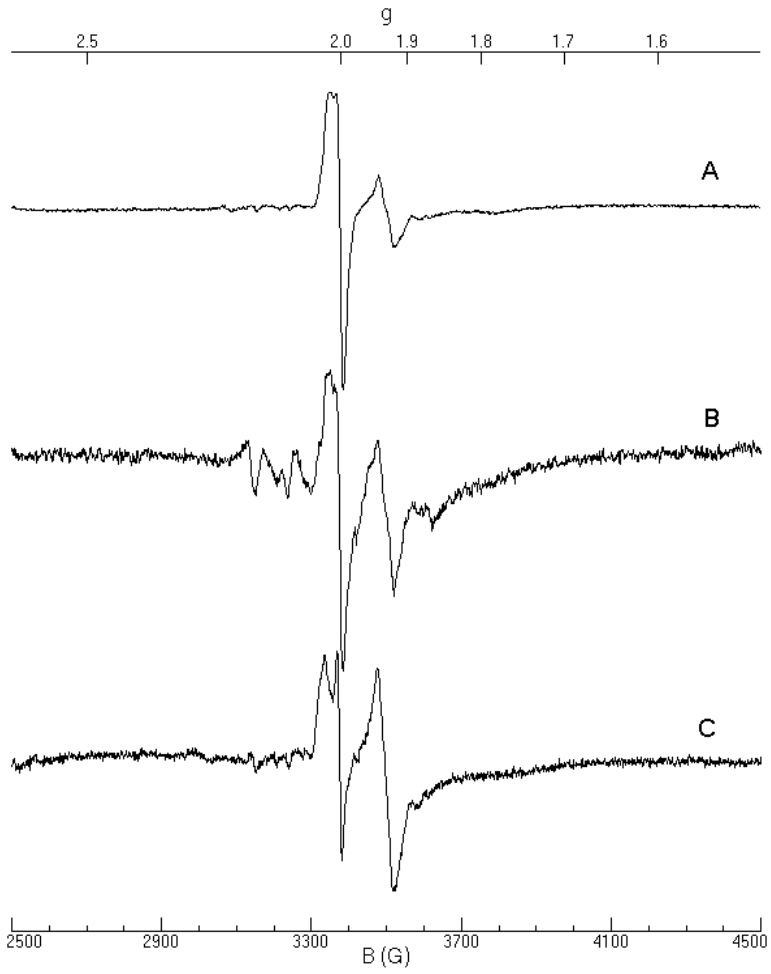

Figure 4-18. EPR spectral intensity diminishes over time and coincides with appearance of the Mn signal. Sample was originally stored in a Mössbauer cup, then crushed for EPR analysis three months later. Spectrum A was obtained within a few hours of crushing the sample into an EPR tube. The spectrum was collected at microwave power 0.2 mW, microwave, microwave frequency 9.44 GHz and 10 K. Spectrum B was obtained approximately two weeks later at the same power, temperature and gain. The sample was then taken into the anaerobic cold box and allowed to thaw. Once the sample thawed, it was diluted 2.5 fold with buffer 1 ST (pH 8.5), deoxycholate (1 % w/v final) and 1 mM dithionite. The sample was treated for 30 minutes before anaerobically freezing the sample and rerunning. Spectra were corrected for other variables including dilution, such that their intensities can be directly compared.

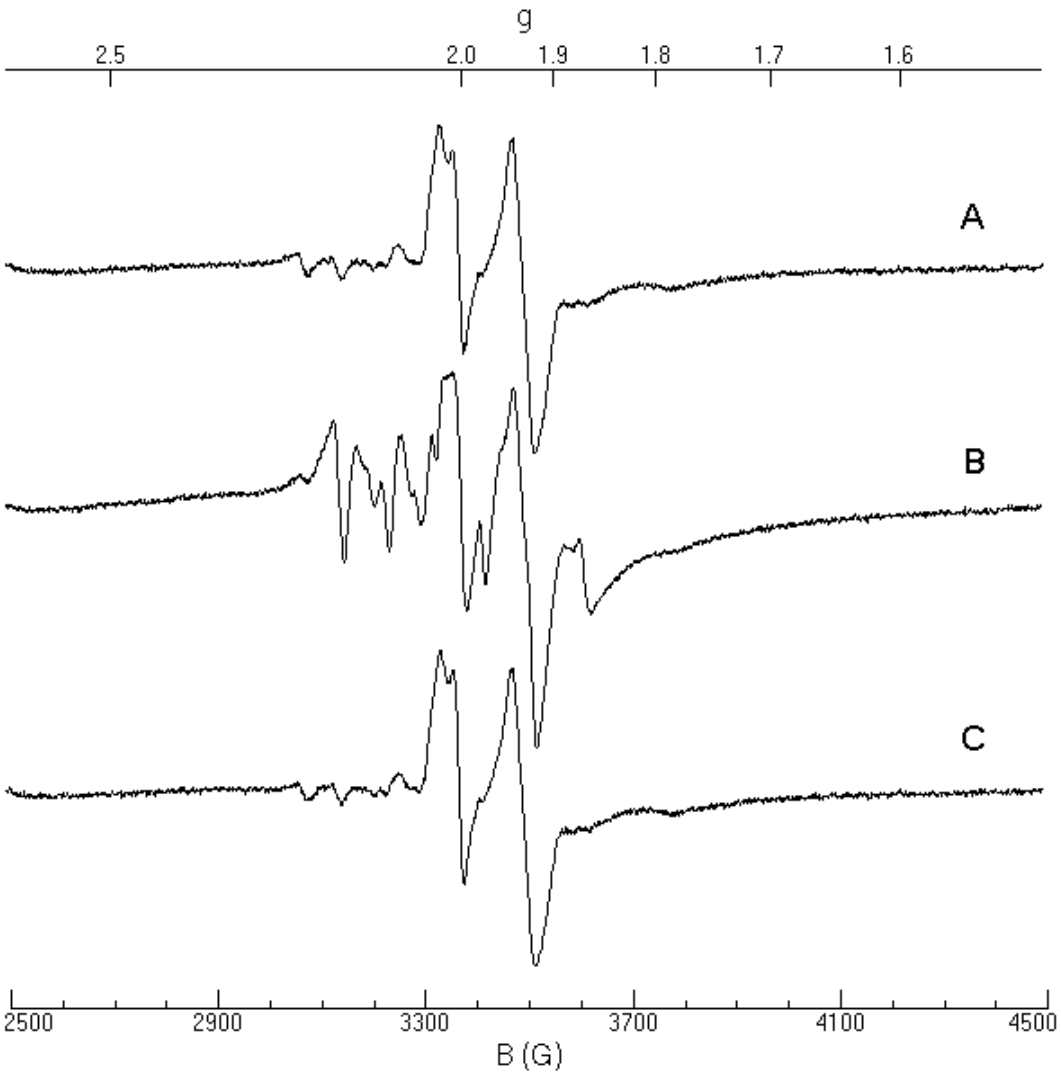

Figure 4-19. Mn signal can appear during storage and be removed by thawing. Spectra from mitochondria collected from cells grown on glycerol minimal media supplemented with 5 % YPG. Spectrum A was collected two weeks after the sample was isolated. Spectrum B was collected six days later with the same conditions. The sample was anaerobically thawed and allowed to incubate, without agitation for ~ 20 minutes. Spectrum C was collected within 3 hours of spectrum B. Spectra were collected at 10 K, microwave power 0.1 mW and microwave frequency 9.43 GHz.

in an anaerobic environment and then refrozen. The resulting spectra exhibited the original spectra (Figures 4-18C and 4-21C) except the g = 1.94 signal was increased to 10 ± 3 μM. Treatment with deoxycholate and dithionite also allowed recovery of the original sample features (Figure 4-18). The only changes seen in the spectral features of Mössbauer samples (Figure 4-20) is a decrease in the amount of Rieske protein. The Fe in this feature dropped from 14 % in freshly prepared samples to ~ 8 % in samples that had been stored for several months. This corresponds to the changes seen in our EPR samples.

The fact that the Mn signal can disappear by the anaerobic freeze/thaw treatment indicates that the process causing the feature's appearance (and subsequent removal) is due to some internal phenomenon from the samples themselves and not due to the growth or isolation protocol. Additionally, there may be a redox change that occurs in stored samples that causes its appearance. Although we have shown that treatment of isolated mitochondria with redox agents does not cause a shift in the Mn^{2+} EPR feature, this may only imply that the Mn is protected from redox treatment by a membrane. Whether the Mn is protected by mitochondrial membranes or by a contaminating organelle's membranes is still debatable. However, once the membranes are disrupted, by the freeze/thaw process (and subsequent addition of 1 % deoxycholate) the Mn is redox active. In addition, the intensity of other EPR signals diminish, which may also imply further error in calculating (by simulation) the spin concentrations of these spectra features. Since spectral features

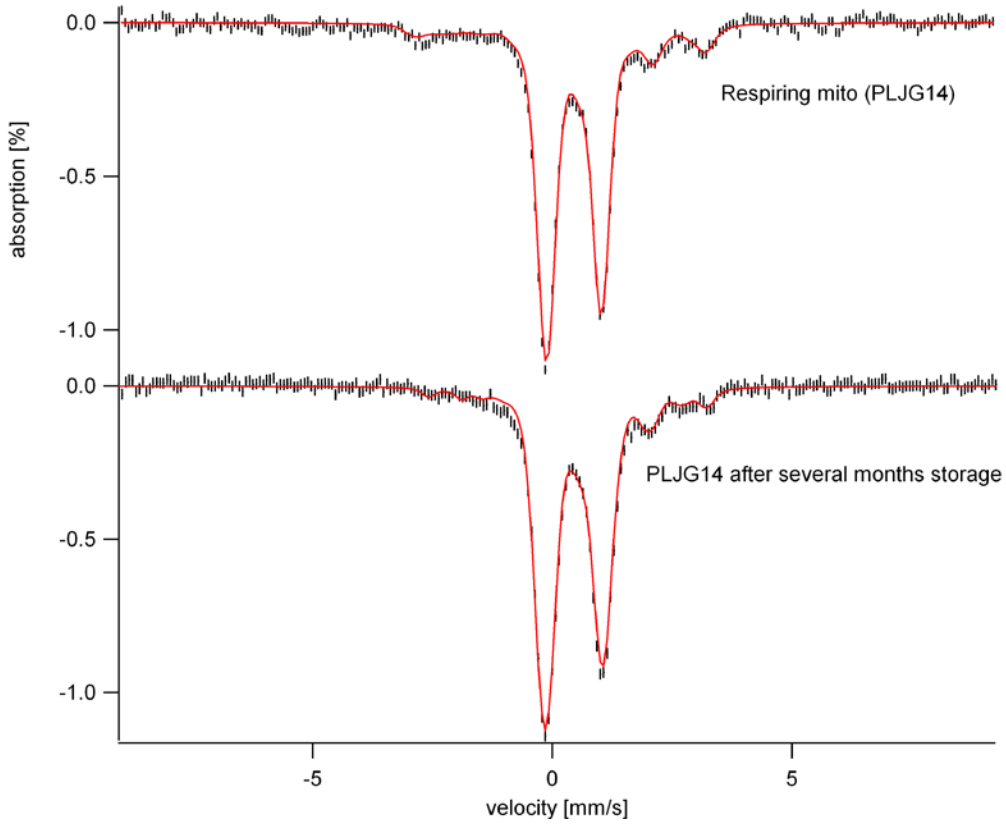

Figure 4-20. Mössbauer spectra undergo slight changes after long sample storage times. Both spectra are of the same sample obtained ~ 8 months apart. The top spectrum has an Fe distribution identical to that discussed in Chapter III, including 14 % Rieske protein. The later (bottom) spectrum was simulated with the same paramters except that there is now only 8 % Rieske protein.

change over time, the only way to accurately simulate spectra may be to do so immediately after sample isolation.

Discussion

We have reported on the iron-ome of respiring mitochondria in a preliminary study (139), and so it is useful to compare and contrast the results obtained from that study to the results in this and the previous chapter. The protein concentrations of packed mitochondria reported in the current study are higher by a factor of ~ 2, relative to that reported previously (139). Current samples were treated with deoxycholate rather than being sonicated prior to protein concentration determinations. The current metal/protein ratios (~ 4 nmol Fe/mg protein) for respiring and respirofermenting mitochondria are similar to those reported from other labs (134, 138, 141, 144, 240), and thus we consider our current protein concentrations to be more accurate.

We previously reported that ~ 22 % of total Fe was present as nonheme Fe^{2+} in respiring mitochondria (grown on lactate) (139). We now suspect that the majority of this was adventitious, as we no longer observe such features with this intensity in spectra of respiring mitochondria. Also, spectra reported in Hudder *et al.* (139) did not include a HS heme doublet, as we observe currently. Previous samples were not prepared as rapidly as are our current samples, and there may have been some heme and/or Fe/S cluster degradation that lead to the more intense nonheme HS Fe^{2+} doublet.

The Mn EPR signal once reported to be from adventitiously bound (and chelatable) ions (139) now appears to be inside a membrane, such as the IM of the mitochondria. The signal dominates the spectrum when present and may correlate to the absence of the $g_{ave} = 1.90$ and $g_{ave} = 1.94$ signals. The Mn signal is not correlated to mitochondrial Mn concentrations. It is still unclear what is causing a portion of the mitochondrial Mn to be EPR active. The Mn EPR signal is not correlated to media type, carbon source, oxygen flow rate during growth, OD_{600} of cell collection, and media Fe concentrations. Nor does the Mn species appear to be redox active.

The Mn EPR signal also appeared in stored samples. This occurred in samples which did not originally exhibit the Mn signal. This signal was not present in every sample, and its presence cannot be predicted. Packed and stored samples change redox states when stored in liquid N_2.

A similar phenomenon is seen with the intensity of EPR signals from stored samples. Samples that were stored for later analysis exhibit lower signal intensities in subsequent runs as compared to the initial spectrum collected for a sample. The signal intensity could be recovered by anaerobic thawing of the sample and incubation in an anaerobic atmosphere for 1 hour.

Early studies by our lab indicated that mitochondrial samples are susceptible to treatment with redox agents (139). Here we present evidence that samples undergo only slight changes when treated with dithionite. Treatment with a reductant did not change the heme concentrations detected by

Electron Absorption Spectroscopy. Reduced Mössbauer spectra had the same Fe distribution as as-isolated samples. Treatment with dithionite in the presence of a detergent still had no effect on Electron Absorption or Mössbauer spectra. EPR spectra of samples treated with dithionite showed a diminished g_{ave} = 2.0 signal due to an organic radical, perhaps from CoQH·, and exhibited no detectable ferric heme. The g_{ave} = 1.90 was unchanged by treatment with reductant while the g_{ave} = 1.94 signal intensity was unaffected in fermenting samples but increased by 20 % in respiring samples. This was still a minor change considering that in early preparations the g_{ave} = 1.94 signal intensity increased by 100 % upon treatment of dithionite alone (139).

Treatment of samples with molecular oxygen caused an increase in the NHHS Fe^{2+} doublet from ~ 3 % in as-isolated samples to ~ 20 %. This increase could be due to damage of Fe centers caused by O_2 followed by reduction of the Fe^{3+} ions by unidentified endogenous reductants. Mössbauer spectra of oxidized respiring mitochondria exhibited a feature due to ferric hemes. Since only 5 – 10 % of the Fe in our samples could be simulated in this feature, only a portion of the hemes were oxidized. This is most likely because the reduced heme centers are recovered quickly and it takes several minutes after oxidation to prepare and freeze a sample in a Mössbauer cup.

Oxidation of the samples with molecular oxygen is temporary. Mitochondrial samples that are isolated and prepared immediately for analysis are resistant to treatment with O_2. Although it is possible to oxidize the heme

centers in mitochondrial samples with molecular oxygen, the oxidation is temporary and the original electron absorption spectra and concentrations of reduced hemes are recovered after only a few minutes. Disruption of the mitochondrial membranes prior to redox treatment did not change this phenomenon.

These results seem to indicate that samples rest in a reduced state and have the ability to 'buffer' their redox state. We present a model in Figure 4-21 that explains this phenomenon. Mitochondria in an as-isolated state contain reduced heme centers and do not exhibit the Mn EPR feature. They contain unidentified endogenous reductants that allow for the recovery of reduced heme centers after treating samples with oxygen. Once frozen, samples are slowly oxidized, which results in the loss of the g_{ave} = 1.94 and g_{ave} = 1.90 signals. In addition, this is usually accompanied by an appearance of the Mn EPR signal. Thawing and freezing the sample anaerobically allows for the recovery of the as-isolated state. This tends to suggest that our samples have the ability to use endogenous reductants to prevent oxidation. This is most likely due to the mitochondrial roles of detoxifying ROS and preventing oxidative damage. Although further studies are needed, it also seems likely that the endogenous reductants are part of the citric acid cycle and may include succinate or pyruvate.

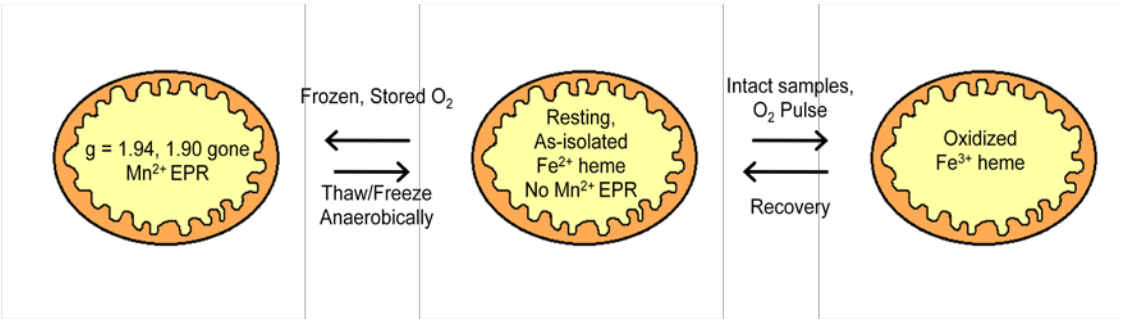

Figure 4-21. Model of redox changes occurring in samples.

CHAPTER V

SUMMARY AND FUTURE STUDIES

The goal of this dissertation was to probe the Fe-ome of yeast mitochondria collected from cells grown on fermenting and respiring carbon sources. The number of Fe-containing species makes the resolution of individual components difficult. However, we were able to develop a protocol that allowed for the large-scale isolation of mitochondrial samples followed by an integrated analysis of the Fe-ome.

The concentration of Fe in mitochondria did not change regardless of carbon source used for cell growth. Rather, it was the distribution of Fe that changed with metabolic mode. Respiring mitochondria contained higher concentrations of heme centers, Fe/S clusters and respiratory complexes. Fermenting cells do not require the same level of expression of those proteins. Indeed, fermenting cells have lower expression of proteins involved in oxidative phosphorylation, Fe metabolism and the citric acid cycle (28-29, 205, 218-219). It follows that the concentration of those Fe centers would also be lower. However, that mitochondria contain the same amount of Fe regardless of growth mode was unexpected, as was the dramatic shift in the Fe-ome.

One notable difference in our samples is that fermenting mitochondria contain approximately 20 % of Fe in a NHHS ferrous ‘pool.’ This is nearly 7-fold larger than the NHHS Fe^{2+} in respiring samples. This may be the labile Fe previously reported (135, 137-138). Estimations of labile Fe in isolated samples

range from 0.4 to 25 % of the total mitochondrial Fe. The higher estimate is based on a study where isolated mitochondria were disrupted before exposure to BPS. There was a dependence on whether reducing agents were added prior to estimating, indicating that most of the labile Fe was present as ferrous ions (138). However, this study may have overestimated the labile Fe for two reasons. First, there was no chelator included in the isolation protocol to remove any adventitiously bound Fe. Secondly, the study was destructive as mitochondria must be disrupted to obtain measurements. This disruption can potentially damage Fe-containing proteins causing additional labile Fe as well as loss of the *in vivo* state of the mitochondria. Studies which keep samples intact have a distinct advantage in measurements.

The lower estimation on the amount of labile Fe originates from studies on rat liver mitochondria incubated with fluorophores. These studies relied on fluorescent quenching to detect Fe chelation. Petrat *et al*. determined that the chelatable Fe in was approximately 16 µM (135). This study may have underestimated the labile Fe because it relies on the incorporation of the fluorophores into mitochondria.

The labile NHHS Fe^{2+} in our samples were similar to both previous estimates. The lower estimates originated from experiments done on rat liver mitochondria—mitochondria that are highly respiring. Respiring yeast mitochondria contained approximately 3 % NHHS ferrous ions. Since neat mitochondria contain ~ 700 µM Fe, approximately 20 µM is present as the

NHHS form. This is similar to the values reported by Petrat *et al*. (135) which may implicate a relationship between samples with similar respiration levels. In contrast, fermenting yeast mitochondria contain 20 % or ~ 150 µM NHHS. This estimate is similar to that seen by Tangeras *et al.* (138). The variation in the detected NHHS Fe may have metabolic implications.

It has been hypothesized that this Fe feeds into Fe/S cluster and heme biosynthesis (116, 122, 235). Since fermenting mitochondria do not have the same demand for Fe/S cluster or heme proteins, this reservoir may be stored until such a demand arises. In order for cells to undergo a diauxic shift (a change from growth on a fermenting carbon source such as glucose to growth on a respiring carbon source such as glycerol), it must be necessary to store some form of metabolically usable Fe for use when more Fe-containing proteins are required. Similarly, respiring mitochondria may not need to contain the same concentration of labile Fe, or may not be able to accumulate it, because Fe is constantly being used for production of respiratory complexes.

Fermenting mitochondria contain two other (potential) reservoirs of Fe In addition to the NHHS Fe. The first is the 20 % HS Fe^{3+}, the second is the 40 % of Fe is in the form of nanoparticles. Neither of these species is detected in respiring samples which may indicate a relationship between these three Fe classes. It may also implicate mechanistic details regarding Fe import, storage and metabolism. It seems likely that the build-up of the NHHS Fe^{2+} occurs because of reduced demand for Fe/S cluster and heme biosynthesis. However,

this hypothesis needs to be tested. For example, further analysis is necessary to confirm that Fe is imported at similar rates in respiring and fermenting samples. Additionally, it would be interesting to determine the fate of these three Fe pools when samples are allowed to shift metabolism. Is there an equilibrium relationship between these three types of Fe? Do nanoparticles and the HS Fe^{3+} shift to NHHS Fe^{2+} prior to feeding into Fe/S cluster or heme biosynthesis? These are some of the questions that should be answered in future studies.

In conclusion we have presented an analysis of the Fe-ome of mitochondrial samples. The concentrations of several individual proteins as well as classes of Fe centers have been determined. The shifts that occur as samples change metabolic mode can be at least partially explained by the cell's energetic requirements. Growth on a respiring carbon source dictates that oxidative phosphorylation will be the primary source of energy production. Therefore, respiring samples need to have higher expression of respiratory complexes. Our samples of respiring mitochondria contain 2 - 3 fold higher expression of heme centers, 4 fold more respiratory complexes (cytochrome bc1, cytochrome oxidase and succinate dehydrogenase) and virtually no Fe reservoirs. Samples exhibiting a mixture of respiration and fermentation had an iron-ome that was nearly identical to respiring samples indicating that it is repression of respiration by glucose (rather than diminished respiration) that causes the major shifts in the Fe distribution in fermenting samples.

We also present evidence that our samples have a default redox state that is buffered by endogenous reductants. Mitochondria are prone to oxidative damage by ROS (which can be generated from respiratory complexes). ROS production increases as mitochondria age. These endogenous reductants may provide insight to a biological strategy for dealing with this issue. Further investigations are needed to identify the endogenous reductants and their buffering capacity.

REFERENCES

1. Mannella CA (1992) The ins and outs of mitochondrial-membrane channels. *Trends Biochem. Sci.* 17(8):315-320.
2. Abe Y, Shodai T, Muto T, Mihara K, Torii H*, et al.* (2000) Structural basis of presequence recognition by the mitochondrial protein import receptor Tom20. *Cell* 100(5):551-560.
3. Koehler CM, Merchant S, & Schatz G (1999) How membrane proteins travel across the mitochondrial intermembrane space. *Trends Biochem. Sci.* 24(11):428-432.
4. Neupert W (1997) Protein import into mitochondria. *Annu. Rev. Biochem.* 66:863-917.
5. Frazier AE, Chacinska A, Truscott KN, Guiard B, Pfanner N, & Rehling P (2003) Mitochondria use different mechanisms for transport of multispanning membrane proteins through the intermembrane space. *Mol. Cell. Biol.* 23(21):7818-7828.
6. Rehling P, Model K, Brandner K, Kovermann P, Sickmann A*, et al.* (2003) Protein insertion into the mitochondrial inner membrane by a twin-pore translocase. *Science* 299(5613):1747-1751.
7. Endo T & Kohda D (2002) Functions of outer membrane receptors in mitochondrial protein import. *Biochim. Biophys. Acta-Mol. Cell Res.* 1592(1):3-14.

8. Alberts B, Johnson A, Lewis J, Raff M, Roberts K, & Walter P (1994) *Essential cell biology* (Garland Publishing, New York).

9. Bauer MF, Sirrenberg C, Neupert W, & Brunner M (1996) Role of Tim23 as voltage sensor and presequence receptor in protein import into mitochondria. *Cell* 87(1):33-41.

10. Komiya T, Rospert S, Koehler C, Looser R, Schatz G, & Mihara K (1998) Interaction of mitochondrial targeting signals with acidic receptor domains along the protein import pathway: Evidence for the 'acid chain' hypothesis. *EMBO J.* 17(14):3886-3898.

11. Bolliger L, Junne T, Schatz G, & Lithgow T (1995) Acidic receptor domains on both sides of the outer membrane mediate translocation of precursor proteins into yeast mitochondria. *EMBO J.* 14(24):6318-6326.

12. Moczko M, Bomer U, Kubrich M, Zufall N, Honlinger A, & Pfanner N (1997) The intermembrane space domain of mitochondrial Tom22 functions as a trans binding site for properties with N-terminal targeting sequences. *Mol. Cell. Biol.* 17(11):6574-6584.

13. Kovermann P, Truscott KN, Guiard B, Rehling P, Sepuri NB*, et al.* (2002) Tim22, the essential core of the mitochondrial protein insertion complex, forms a voltage-activated and signal-gated channel. *Mol. Cell* 9(2):363-373.

14. Pfanner N & Neupert W (1985) Transport of proteins into mitochondria - a potassium diffusion potential is able to drive the import of ADP/ATP carrier. *EMBO J.* 4(11):2819-2825.

15. Pfanner N & Neupert W (1987) Distinct steps in the import of ADP ATP carrier into mitochondria. *J. Biol. Chem.* 262(16):7528-7536.

16. Pfanner N, Tropschug M, & Neupert W (1987) Mitochondrial protein import - nucleoside triphosphates are involved in conferring import-competence to precursors. *Cell* 49(6):815-823.

17. Huser J & Blatter LA (1999) Fluctuations in mitochondrial membrane potential caused by repetitive gating of the permeability transition pore. *Biochem. J.* 343:311-317.

18. Sugrue MM & Tatton WG (2001) Mitochondrial membrane potential in aging cells. *Biol. Signal Recept.* 10(3-4):176-188.

19. Rehling P (2003) Protein insertion into the mitochondrial inner membrane by a twin-pore translocase (vol 299, pg 1747, 2003). *Science* 300(5617):251-251.

20. Schuller H-J (2003) Transcriptional control of nonfermentative metabolism in the yeast *Saccharomyces cerevisiae*. *Curr. Genet.* 43:139-160.

21. Vander Heiden MG, Chandel NS, Li XX, Schumacker PT, Colombini M, & Thompson CB (2000) Outer mitochondrial membrane permeability can regulate coupled respiration and cell survival. *Proc. Natl. Acad. Sci. U. S. A.* 97(9):4666-4671.

22. Scheffler IE (1999) *Mitochondria* (Wiley-Liss,New York).

23. Jensen RE & Dunn CD (2002) Protein import into and across the mitochondrial inner membrane: Role of the TIM23 and TIM22 translocons. *Biochim. Biophys. Acta-Mol. Cell Res.* 1592(1):25-34.

24. Hagen TM, Yowe DL, Bartholomew JC, Wehr CM, Do KL*, et al.* (1997) Mitochondrial decay in hepatocytes from old rats: Membrane potential declines, heterogeneity and oxidants increase. *Proc. Natl. Acad. Sci. U. S. A.* 94(7):3064-3069.

25. Sugrue MM, Wang Y, Rideout HJ, Chalmers-Redman RME, & Tatton WG (1999) Reduced mitochondrial membrane potential and altered responsiveness of a mitochondrial membrane megachannel in p53-induced senescence. *Biochem. Biophys. Res. Commun.* 261(1):123-130.

26. Stevens BJ (1977) Variation in number and volume of mitochondria in yeast according to growth-conditions - study based on serial sectioning and computer graphics reconstitution. *Biologie Cellulaire* 28(1):37-56.

27. Nunnari J, Marshall WF, Straight A, Murray A, Sedat JW, & Walter P (1997) Mitochondrial transmission during mating in *Saccharomyces cerevisiae* is determined by mitochondrial fusion and fission and the intramitochondrial segregation of mitochondrial DNA. *Mol. Biol. Cell* 8(7):1233-1242.

28. Gao J, Opiteck GJ, Friedrichs MS, Dongre AR, & Hefta SA (2003) Changes in the protein expression of yeast as a function of carbon source. *J. Proteome Res.* 2(643-649).

29. DeRisi JL, Iyer VR, & Brown PO (1997) Exploring the metabolic and genetic control of gene expression on a genomic scale. *Science* 278:680-686.

30. Klipp E, Heinrich R, & Holzhutter HG (2002) Prediction of temporal gene expression - metabolic optimization by re-distribution of enzyme activities. *Eur. J. Biochem.* 269(22):5406-5413.

31. Beinert H (2002) Spectroscopy of succinate dehydrogenases, a historical perspective. *Biochimica et Biophysica Acta-Bioenergetics* 1553(1-2):7-22.

32. Raha S, McEachern GE, Myint AT, & Robinson BH (2000) Superoxides from mitochondrial complex III: The role of manganese superoxide dismutase. *Free Radic. Biol. Med.* 29(2):170-180.

33. Dumont ME, Cardillo TS, Hayes MK, & Sherman F (1991) Role of cytochrome-C heme lyase in mitochondrial import and accumulation of cytochrome-c in *Saccharomyces cerevisiae*. *Mol. Cell. Biol.* 11(11):5487-5496.

34. Zitomer RS, Montgomery DL, Nichols DL, & Halo BD (1979) Transcriptional regulation of the yeast cytochrome c gene. *Proc. Natl. Acad. Sci. U. S. A.* 76(8):3627-3631.

35. Johnson DC, Dean DR, Smith AD, & Johnson MK (2005) Structure, function, and formation of biological iron-sulfur clusters. *Annu. Rev. Biochem.* 74(1):247-281.

36. Johnson MK (1998) Iron--sulfur proteins: New roles for old clusters. *Curr. Opin. Chem. Biol.* 2(2):173-181.

37. Lindahl PA, Day EP, Kent TA, Ormejohnson WH, & Munck E (1985) Mössbauer, electron-paramagnetic-res, and magnetization studies of the *Azobacter vinelandii* Fe protein - evidence for a 4Fe-4S 1+ cluster with spin S=3/2. *J. Biol. Chem.* 260(20):1160-1173.

38. Bulteau AL, Ikeda-Saito M, & Szweda LI (2003) Redox-dependent modulation of aconitase activity in intact mitochondria. *Biochemistry* 42(50):14846-14855.

39. Tong W-H & Rouault TA (2007) Metabolic regulation of citrate and iron by aconitases: Role of iron–sulfur cluster biogenesis. *BioMetals* 20:549-564.

40. Brown NM, Kennedy MC, Antholine WE, Eisenstein RS, & Walden WE (2002) Detection of a [3Fe-4S] cluster intermediate of cytosolic aconitase in yeast expressing iron regulatory protein 1 - insights into the mechanism of Fe-S cluster cycling. *J. Biol. Chem.* 277(9):7246-7254.

41. Regev-Rudzki N, Karniely S, Ben-Haim NN, & Pines O (2005) Yeast aconitase in two locations and two metabolic pathways: Seeing small amounts is believing. *Mol. Biol. Cell* 16(9):4163-4171.

42. Tong JJ & Feinberg BA (1994) Direct square-wave voltammetry of superoxidized [4Fe-4S](3+) aconitase and associated 3Fe/4Fe cluster interconversions. *J. Biol. Chem.* 269(40):24920-24927.

43. Lemire BD & Oyedotun KS (2002) The *Saccharomyces cerevisiae* mitochondrial succinate: Ubiquinone oxidoreductase. *Biochimica et Biophysica Acta-Bioenergetics* 1553(1-2):102-116.

44. Maguire JJ, Johnson MK, Morningstar JE, Ackrell BAC, & Kearney EB (1985) Electron-paramagnetic resonance studies of mammalian succinate-dehyrogenase detection of the tetranuclear cluster s2. *J. Biol. Chem.* 260(20):909-912.

45. Beinert H, Ackrell BAC, Kearney EB, & Singer TP (1974) EPR studies on mechanism of action of succinate dehydrogenase in activated preparations. *Biochem. Biophys. Res. Commun.* 58(3):564-572.

46. Peterson J, Vibat C, & Gennis RB (1994) Identification of the axial heme ligands of cytochrome b(556) in succinate - ubiquinone oxidoreductase from *Escherichia coli*. *FEBS Lett.* 355(2):155-156.

47. Hunte C, Koepke J, Lange C, Rossmanith T, & Michel H (2000) Structure at 2.3 angstrom resolution of the cytochrome bc(1) complex from the yeast *Saccharomyces cerevisiae* co-crystallized with an antibody Fv fragment. *Structure* 8(6):669-684.

48. Trumpower BL (1990) The protonmotive Q-cycle - energy transduction by coupling of proton translocation to electron-transfer by the cytochrome-bc1 complex. *J. Biol. Chem.* 265(20):11409-11412.

49. Ebert CE, Ghosh M, Wang YD, & Beattie DS (2003) Aspartate-186 in the head group of the yeast iron-sulfur protein of the cytochrome bc(1) complex contributes to the protein conformation required for efficient electron transfer. *Biochimica et Biophysica Acta-Bioenergetics* 1607(2-3):65-78.

50. Link TA, Hagen WR, Pierik AJ, Assmann C, & Vonjagow G (1992) Determination of the redox properties of the Rieske [2Fe-2S] cluster of bovine heart bc1 complex by direct electrochemistry of a water-soluble fragment. *Eur. J. Biochem.* 208(3):685-691.

51. Fee JA, Findling KL, Yoshida T, Hille R, Tarr GE*, et al.* (1984) Purification and characterization of the Rieske iron-sulfur protein from *Thermus-thermophilus* - evidence for a [2Fe-2S] cluster having non-cysteine ligands. *J. Biol. Chem.* 259(1):124-133.

52. Salerno JC (1984) Cytochrome electron-spin resonance line-shapes, ligand-fields, and components stoichiometry in ubiquinol-cytochrome-C oxidoreductase. *J. Biol. Chem.* 259(4):2331-2336.

53. Yu L, Dong JH, & Yu CA (1986) Characterization of purified cytochrome-c1 from *Rhodobacter-sphaeroides*-r-26. *Biochim. Biophys. Acta* 852(2-3):203-211.

54. Ormejohn.Nr, Hansen RE, & Beinert H (1971) EPR studies of cytochrome b-c1 segment of mitochondrial electron transfer system. *Biochem. Biophys. Res. Commun.* 45(4):871-&.

55. Lett CM & Guillemette JG (2002) Increasing the redox potential of isoform 1 of yeast cytochrome c through the modification of select haem interactions. *Biochem. J.* 362:281-287.

56. Brautigan DL, Feinberg BA, Hoffman BM, Margoliash E, Peisach J, & Blumberg WE (1977) Multiple low-spin forms of cytochrome-C ferrihemochrome - EPR-spectra of various eukaryotic and prokaryotic cytochromes-C. *J. Biol. Chem.* 252(2):574-582.

57. Murphy MEP, Nall BT, & Brayer GD (1992) Structure determination and analysis of yeast iso-2-cytochrome-C and a composite mutant protein. *J. Mol. Biol.* 227(1):160-176.

58. Daum G, Bohni PC, & Schatz G (1982) Import of proteins into mitochondria - cytochrome-b2 and cytochrome-C peroxidase are located in the intermembrane space of yeast mitochondria. *J. Biol. Chem.* 257(21):3028-3033.

59. Goodin DB & McRee DE (1993) The Asp-His-Fe triad of cytochrome-c peroxidase controls the reduction potential, electronic-structure, and coupling of the tryptophan free-radical to the heme. *Biochemistry* 32(13):3313-3324.

60. Goodin DB, Davidson MG, Roe JA, Mauk AG, & Smith M (1991) Amino-acid substitutions at tryptophan-51 of cytochrome-c peroxidase - effects on coordination, species preference for cytochrome-c, and electron-transfer. *Biochemistry* 30(20):4953-4962.

61. Svensson-Ek M, Abramson J, Larsson G, Tornroth S, Brzezinski P, & Iwata S (2002) The X-ray crystal structures of wild-type and EQ(I-286) mutant cytochrome c oxidases from *Rhodobacter sphaeroides*. *J. Mol. Biol.* 321(2):329-339.

62. Kojima N & Palmer G (1983) Further characterization of the potentiometric behavior of cytochrome-oxidase - cytochrome-a stays low-spin during oxidation and reduction. *J. Biol. Chem.* 258(24):4908-4913.

63. Babcock GT, Vickery LE, & Palmer G (1978) Electronic state of heme in cytochrome oxidase-II - oxidation-reduction potential interactions and heme iron spin state behavior observed in reductive titrations. *J. Biol. Chem.* 253(7):2400-2411.

64. Beinert H & Shaw RW (1977) On identity of high-spin heme components of cytochrome-C oxidase. *Biochim. Biophys. Acta* 462(1):121-130.

65. Gorbikova EA, Vuorilehto K, Wikstrom M, & Verkhovsky MI (2006) Redox titration of all electron carriers of cytochrome c oxidase by Fourier transform infrared spectroscopy. *Biochemistry* 45(17):5641-5649.

66. Schilke B, Voisine C, Beinert H, & Craig E (1999) Evidence for a conserved system for iron metabolism in the mitochondria of

Saccharomyces cerevisiae. *Proc. Natl. Acad. Sci. U. S. A.* 96(18):10206-10211.

67. Smith AD, Jameson GNL, Dos Santos PC, Agar JN, Naik S*, et al.* (2005) NifS-mediated assembly of [4Fe-4S] clusters in the N- and C-terminal domains of the NifU scaffold protein. *Biochemistry* 44(39):12955-12969.

68. Jensen LT & Culotta VC (2000) Role of *Saccharomyces cerevisiae* ISA1 and ISA2 in iron homeostasis. *Mol. Cell. Biol.* 20(11):3918-3927.

69. Picciocchi A, Douce R, & Alban C (2003) The plant biotin synthase reaction - identification and characterization of essential mitochondrial accessory protein components. *J. Biol. Chem.* 278(27):24966-24975.

70. Ugulava NB, Sacanell CJ, & Jarrett JT (2001) Spectroscopic changes during a single turnover of biotin synthase: Destruction of a [2Fe-2S] cluster accompanies sulfur insertion. *Biochemistry* 40(28):8352-8358.

71. Cosper MM, Jameson GNL, Hernandez HL, Krebs C, Huynh BH, & Johnson MK (2004) Characterization of the cofactor composition of *Escherichia coli* biotin synthase. *Biochemistry* 43(7):2007-2021.

72. Jameson GNL, Cosper MM, Hernandez HL, Johnson MK, & Huynh BH (2004) Role of the [2Fe-2S] cluster in recombinant *Escherichia coli* biotin synthase. *Biochemistry* 43(7):2022-2031.

73. Ollagnier-de Choudens S & Fontecave M (1999) The lipoate synthase from *Escherichia coli* is an iron-sulfur protein. *FEBS Lett.* 453(1-2):25-28.

74. Hoja U, Marthol S, Hofmann J, Stegner S, Schulz R*, et al.* (2004) HFA1 encoding an organelle-specific acetyl-CoA carboxylase controls mitochondrial fatty acid synthesis in *Saccharomyces cerevisiae*. *J. Biol. Chem.* 279(21):21779-21786.

75. Ollagnier-de Choudens S, Sanakis Y, Hewitson KS, Roach P, Baldwin JE*, et al.* (2000) Iron-sulfur center of biotin synthase and lipoate synthase. *Biochemistry* 39(14):4165-4173.

76. Velasco JA, Cansado J, Pena MC, Kawakami T, Laborda J, & Notario V (1993) Cloning of the dihydroxyacid dehydratase-encoding gene (ILV3) from *Saccharomyces cerevisiae*. *Gene* 137(2):179-185.

77. Flint DH, Emptage MH, Finnegan MG, Fu WG, & Johnson MK (1993) The role and properties of the iron-sulfur cluster in *Escherichia coli* dihydroxy-acid dehydratase. *J. Biol. Chem.* 268(20):14732-14742.

78. Branda SS, Cavadini P, Adamec J, Kalousek F, Taroni F, & Isaya G (1999) Yeast and human frataxin are processed to mature form in two sequential steps by the mitochondrial processing peptidase. *J. Biol. Chem.* 274(32):22763-22769.

79. He YN, Alam SL, Proteasa SV, Zhang Y, Lesuisse E*, et al.* (2004) Yeast frataxin solution structure, iron binding, and ferrochelatase interaction. *Biochemistry* 43(51):16254-16262.

80. Bou-Abdallah F, Adinolfi S, Pastore A, Laue TM, & Chasteen ND (2004) Iron binding and oxidation kinetics in frataxin CyaY of Escherichia coli. *J. Mol. Biol.* 341(2):605-615.

81. Petrova VY, Drescher D, Kujumdzieva AV, & Schmitt MJ (2004) Dual targeting of yeast catalase a to peroxisomes and mitochondria. *Biochem. J.* 380:393-400.

82. Bellei M, Jakopitsch C, Battistuzzi G, Sola M, & Obinger C (2006) Redox thermodynamics of the ferric-ferrous couple of wild-type synechocystis KatG and KatG(Y249F). *Biochemistry* 45(15):4768-4774.

83. Dawson JH, Bracete AM, Huff AM, Kadkhodayan S, Zeitler CM*, et al.* (1991) The active-site structure of *Escherichia coli* HPII catalase - evidence favoring coordination of a tyrosinate proximal ligand to the chlorin iron. *FEBS Lett.* 295(1-3):123-126.

84. Tegoni M, Silvestrini MC, Guigliarelli B, Asso M, Brunori M, & Bertrand P (1998) Temperature-jump and potentiometric studies on recombinant wild type and Y143F and Y254F mutants of *Saccharomyces cerevisiae* flavocytochrome b(2): Role of the driving force in intramolecular electron transfer kinetics. *Biochemistry* 37(37):12761-12771.

85. Capeillereblandin C, Bray RC, Iwatsubo M, & Labeyrie F (1975) Flavocytochrome b2 - kinetic studies by absorbance and electron-paramagnetic-resonance spectroscopy of electron-distribution among prosthetic groups. *Eur. J. Biochem.* 54(2):549-566.

86. Wu CSC, Brown WD, & Duffy P (1972) Interaction of myoglobin and cytochrome-c. *J. Biol. Chem.* 247(6):1899-&.

87. Franco R, Moura JJG, Moura I, Lloyd SG, Huynh BH*, et al.* (1995) Characterization of the iron-binding site in mammalian ferrochelatase by kinetic and Mössbauer methods. *J. Biol. Chem.* 270(44):26352-26357.

88. Glerum DM, Muroff I, Jin C, & Tzagoloff A (1997) Cox15 codes for a mitochondrial protein essential for the assembly of yeast cytochrome oxidase. *J. Biol. Chem.* 272(30):19088-19094.

89. Hederstedt L, Lewin A, & Throne-Holst M (2005) Heme a synthase enzyme functions dissected by mutagenesis of *Bacillus subtilis* CtaA. *J. Bacteriol.* 187(24):8361-8369.

90. Jonassen T, Proft M, Randez-Gil F, Schultz JR, Marbois BN*, et al.* (1998) Yeast clk-1 homologue (Coq7/Cat5) is a mitochondrial protein in coenzyme Q synthesis. *J. Biol. Chem.* 273(6):3351-3357.

91. Lill R & Kispal G (2001) Mitochondrial ABC transporters. *Res. Microbiol.* 152(3-4):331-340.

92. Rea S (2001) CLK-1/coq7p is a DMQ mono-oxygenase and a new member of the di-iron carboxylate protein family. *FEBS Lett.* 509(3):389-394.

93. Liu KE & Lippard SJ (1991) Redox properties of the hydroxylase component of methane monooxygenase from *Methylococcus capsulatus* -

effects of protein-b, reductase, and substrate. *J. Biol. Chem.* 266(20):12836-12839.

94. Fox BG, Hendrich MP, Surerus KK, Andersson KK, Froland WA*, et al.* (1993) Mössbauer, EPR, and ENDOR studies of the hydroxylase and reductase components of methane monooxygenase from *Methylosinus-trichosporium* OB3b. *J. Am. Chem. Soc.* 115(9):3688-3701.

95. Emptage MH, Kent TA, Kennedy MC, Beinert H, & Munck E (1983) Mössbauer and electron-paramagnetic-res studies of activated aconitase - development of a localized valence state at a subsite of the [4Fe-4S] cluster on binding of citrate. *Proc. Natl. Acad.Sci. U .S. A.* 80(15):4674-4678.

96. Wallace MA, Liou LL, Martins J, Clement MHS, Bailey S*, et al.* (2004) Superoxide inhibits 4Fe-4S cluster enzymes involved in amino acid biosynthesis - cross-compartment protection by CuZn-superoxide dismutase. *J. Biol. Chem.* 279(31):32055-32062.

97. Barros MH, Nobrega FG, & Tzagoloff A (2001) Mitochondrial ferredoxin is required for heme a synthesis in *Saccharomyces cerevisiae*. *J. Biol. Chem.* 277(12):9997-10002.

98. Schiffler B, Bureik M, Reinle W, Muller EC, Hannemann F, & Bernhardt R (2004) The adrenodoxin-like ferredoxin of *Schizosaccharomyces pombe* mitochondria. *J. Inorg. Biochem.* 98(7):1229-1237.

99. Cassanova N, O'Brien KM, Stahl BT, McClure T, & Poyton RO (2005) Yeast flavohemoglobin, a nitric oxide oxidoreductase, is located in both the cytosol and the mitochondrial matrix. *J. Biol. Chem.* 280(9):7645-7653.

100. Ioannidis N, Cooper CE, & Poole RK (1992) Spectroscopic studies on an oxygen-binding hemoglobin-like flavohaemoprotein from *Escherichia-coli*. *Biochem. J.* 288:649-655.

101. Macheroux P, Hill S, Austin S, Eydmann T, Jones T*, et al.* (1998) Electron donation to the flavoprotein NifL, a redox-sensing transcriptional regulator. *Biochem. J.* 332:413-419.

102. Voet D, Pratt CW, & Voet JG (2008) *Fundamentals of biochemistry : Life at the molecular level* (Wiley,Hoboken, NJ).

103. Johnson MK, Morningstar JE, Ackrell BAC, Kearney EB, & Maguire JJ (1985) Evidence for [2Fe-2S], [3Fe-XS], and [4Fe-4S] clusters in succinate dehydrogenase. *Federation Proceedings* 44(3):675-675.

104. Tzagoloff A, Nobrega M, Gorman N, & Sinclair P (1993) On the functions of the yeast COX10 and COX11 gene-products. *Biochemistry and Molecular Biology International* 31(3):593-598.

105. Sturgeon BE, Doan PE, Liu KE, Burdi D, Tong WH*, et al.* (1997) Non-Kramers ESEEM of integer-spin diferrous carboxylate-bridged clusters in proteins. *J. Am. Chem. Soc.* 119(2):375-386.

106. Hirota S, SvenssonEk M, Adelroth P, Sone N, Nilsson T*, et al.* (1996) A flash-photolysis study of the reactions of a caa(3)-type cytochrome

oxidase with dioxygen and carbon monoxide. *J. Bioenerg. Biomembr.* 28(6):495-501.

107. Johanssen S, Klee S, & Ungemach FR (1997) Studies on the role of cytosolic and mitochondrial glutathione depletion in hepatocellular cytotoxicity following oxidative stress. *Naunyn-Schmiedebergs Archives of Pharmacology* 355(4):604-604.

108. Marbois BN & Clarke CF (1996) The COQ7 gene encodes a protein in *Saccharomyces cerevisiae* necessary for ubiquinone biosynthesis. *J. Biol. Chem.* 271(6):2995-3004.

109. Macheroux P, Petersen J, Bornemann S, Lowe DJ, & Thorneley RNF (1996) Binding of the oxidized, reduced, and radical flavin species to chorismate synthase. An investigation by spectrophotometry, fluorimetry, and electron paramagnetic resonance and electron nuclear double resonance spectroscopy. *Biochemistry* 35(5):1643-1652.

110. Petrova VY, Rasheva TV, & Kujumdzieva AV (2002) Catalase enzyme in mitochondria of *Saccharomyces cerevisiae*. *Electronic Journal of Biotechnology* 5(1).

111. Buisson N & Labbe-Bois R (1998) Flavohemoglobin expression and function in *Saccharomyces cerevisiae* - no relationship with respiration and complex response to oxidative stress. *J. Biol. Chem.* 273(16):9527-9533.

112. Zhao XJ, Raitt D, Burke PV, Clewell AS, Kwast KE, & Poyton RO (1996) Function and expression of flavohemoglobin in *Saccharomyces cerevisiae* - evidence for a role in the oxidative stress response. *J. Biol. Chem.* 271(41):25131-25138.

113. Guiard B (1985) Structure, expression and regulation of a nuclear gene encoding a mitochondrial protein - the yeast l(+)-lactate cytochrome-C oxidoreductase (cytochrome-b2). *EMBO J.* 4(12):3265-3272.

114. Longo VD, Liou LL, Valentine JS, & Gralla EB (1999) Mitochondrial superoxide decreases yeast survival in stationary phase. *Arch. Biochem. Biophys.* 365(1):131-142.

115. Cook JD, Bencze KZ, Jankovic AD, Crater AK, Busch CN*, et al.* (2006) Monomeric yeast frataxin is an iron-binding protein. *Biochemistry* 45(25):7767-7777.

116. Gerber J, Muhlenhoff U, & Lill R (2003) An interaction between frataxin and Isu1/Nfs1 that is crucial for Fe/S cluster synthesis on Isu1. *EMBO Rep.* 4(9):906-911.

117. Adam AC, Bornhovd C, Prokisch H, Neupert W, & Hell K (2006) The Nfs1 interacting protein Isd11 has an essential role in Fe/S cluster biogenesis in mitochondria. *EMBO J.* 25:174-183.

118. Alves R, Herrero E, & Sorribas A (2004) Predictive reconstruction of the mitochondrial iron–sulfur cluster assembly metabolism: I. The role of the

protein pair ferredoxin–ferredoxin reductase (Yah1–Arh1). *Proteins: Struct., Funct., Bioinf.* 56:354-366.

119. Grandier-Vazeille X, Bathany K, Chaignepain S, Camougrand N, Manon S, & Schmitter JM (2001) Yeast mitochondrial dehydrogenases are associated in a supramolecular complex. *Biochemistry* 40(33):9758-9769.

120. Ruzicka FJ & Beinert H (1975) New membrane iron-sulfur flavoprotein of mitochondrial electron-transfer system - entrance point of fatty acyl dehydrogenation pathway. *Biochem. Biophys. Res. Commun.* 66(2):622-631.

121. Aisen P, Enns C, & Wessling-Resnick M (2001) Chemistry and biology of eukaryotic iron metabolism. *The International Journal of Biochemistry & Cell Biology* 33:940-959.

122. Craig EA, Voisine C, & Schilke B (1999) Mitochondrial iron metabolism in the yeast *Saccharomyces cerevisiae*. *Biol. Chem.* 380:1167-1173.

123. Kosman D (2003) Molecular mechanisms of iron uptake in fungi. *Mol. Microbiol.* 47(5):1185-1197.

124. Lill R & Muhlenhoff U (2008) Maturation of iron-sulfur proteins in eukaryotes: Mechanisms, connected processes, and diseases. *Annual Reviews Biochemistry* 77:669-700.

125. Yang M, Cobine PA, Molik S, Naranuntarat A, Lill R*, et al.* (2006) The effects of mitochondrial iron homeostasis on cofactor specificity of superoxide dismutase 2. *EMBO J.* 25(8):1775-1783.

126. Lange H, Kispal G, & Lill R (1999) Mechanism of iron transport to the site of heme synthesis inside yeast mitochondria. *J. Biol. Chem.* 274(27):18989-18996.

127. Foury F & Roganti T (2002) Deletion of the mitochondrial carrier genes MRS3 and MRS4 suppresses mitochondrial iron accumulation in a yeast frataxin-deficient strain. *J. Biol. Chem.* 277(27):24475-24483.

128. Muhlenhoff U, Stadler JA, Richhardt N, Seubert A, Eickhorst T*, et al.* (2003) A specific role of the yeast mitochondrial carriers Mrs3/4p in mitochondrial iron acquisition under iron-limiting conditions. *J. Biol. Chem.* 278(42):40612-40620.

129. Li LT & Kaplan J (1997) Characterization of two homologous yeast genes that encode mitochondrial iron transporters. *J. Biol. Chem.* 272(45):28485-28493.

130. Chaston TB & Richardson DR (2003) Iron chelators for the treatment of iron overload disease: Relationship between structure, redox activity, and toxicity. *American Journal of Hematology* 73(3):200-210.

131. Kalinowski DS & Richardson DR (2005) The evolution of iron chelators for the treatment of iron overload disease and cancer. *Pharmacological Reviews* 57(4):547-583.

132. Prus E & Fibach E (2008) The labile iron pool in human erythroid cells. *British Journal of Haematology* 142(2):301-307.

133. Jacobs A (1977) Low-molecular weight intracellular iron transport compounds. *Blood* 50(3):433-439.

134. Cobine PA, Ojeda LD, Rigby KM, & Winge DR (2004) Yeast contain a non-proteinaceous pool of copper in the mitochondrial matrix. *J. Biol. Chem.* 279(14):14447-14455.

135. Petrat F, de Groot H, Sustmann R, & Rauen U (2002) The chelatable iron pool in living cells: A methodically defined quantity. *Biol. Chem.* 383(3-4):489-502.

136. Petrat F, Weisheit D, Lensen M, de Groot H, Sustmann R, & Rauen U (2002) Selective determination of mitochondrial chelatable iron in viable cells with a new fluorescent sensor. *Biochem. J.* 362:137-147.

137. Rauen U, Springer A, Weisheit D, Petrat F, Korth HG*, et al.* (2007) Assessment of chelatable mitochondrial iron by using mitochondrion-selective fluorescent iron indicators with different iron-binding affinities. *ChemBioChem* 8(3):341-352.

138. Tangeras A, Flatmark T, Backstrom D, & Ehrenberg A (1980) Mitochondrial iron not bound in heme and iron-sulfur centers - estimation, compartmentation and redox state. *Biochim. Biophys. Acta* 589(2):162-175.

139. Hudder BN, Morales JG, Stubna A, Münck E, Hendrich MP, & Lindahl PA (2007) Electron paramagnetic resonance and Mössbauer spectroscopy of

intact mitochondria from respiring *Saccharomyces cerevisiae Journal of Biological Inorganic Chemistry* 12(7):1029-1053.

140. Naranuntarat A, Jensen LT, Pazicni S, Penner-Hahn JE, & Culotta VC (2009) The interaction of mitochondrial iron with manganese superoxide dismutase. *J. Biol. Chem.* 284(34):22633-22640.

141. Babcock M, deSilva D, Oaks R, DavisKaplan S, Jiralerspong S*, et al.* (1997) Regulation of mitochondrial iron accumulation by Yfh1p, a putative homolog of frataxin. *Science* 276(5319):1709-1712.

142. Lesuisse E, Santos R, Matzanke BF, Knight SAB, Camadro JM, & Dancis A (2003) Iron use for haeme synthesis is under control of the yeast frataxin homologue (Yfh1). *Hum. Mol. Genet.* 12(8):879-889.

143. Gerber J, Neumann K, Prohl C, Muhlenhoff U, & Lill R (2007) The yeast scaffold proteins Isu1p and Isu2p are required inside mitochondria for maturation of cytosolic Fe/S proteins. *Mol. Cell. Biol.* 24(11):4848-4857.

144. Kispal G, Csere P, Prohl C, & Lill R (1999) The mitochondrial proteins Atm1p and Nfs1p are essential for biogenesis of cytosolic Fe/S proteins. *EMBO J.* 18(14):3981-3989.

145. Biederbick A, Stehling O, Rosser R, Niggemeyer B, Nakai Y*, et al.* (2006) Role of human mitochondrial Nfs1 in cytosolic iron-sulfur protein biogenesis and iron regulation. *Mol. Cell. Biol.* 26(15):5675-5687.

146. Pondarre C, Antiochos BB, Campagna DR, Greer EL, Deck KM*, et al.* (2006) The mitochondrial ATP-binding cassette transporter Abcb7 is

essential in mice and participates in cytosolic iron-sulfur cluster biogenesis. *Hum. Mol. Genet.* 15(6):953-964.

147. Rutherford JC, Ojeda L, Balk J, Muhlenhoff U, Lill R, & Winge DR (2005) Activation of the iron regulon by the yeast Aft1/Aft2 transcription factors depends on mitochondrial but not cytosolic iron-sulfur protein biogenesis. *J. Biol. Chem.* 280(11):10135-10140.

148. Miao R, Kim H, Koppolu UMK, Ellis EA, Scott RA, & Lindahl PA (2009) Biophysical characterization of the iron in mitochondria from Atm1p-depleted *Saccharomyces cerevisiae*. *Biochemistry* 48(40):9556-9568.

149. Andrew AJ, Dutkiewicz R, Knieszner H, Craig EA, & Marszalek J (2006) Characterization of the interaction between the J-protein Jac1p and the scaffold for Fe-S cluster biogenesis, Isu1p. *J. Biol. Chem.* 281(21):14580-14587.

150. Gordon DM, Lyver ER, Lesuisse E, Dancis A, & Pain D (2006) GTP in the mitochondrial matrix plays a crucial role in organellar iron homoeostasis. *Biochem. J.* 400:163-168.

151. Vozza A, Blanco E, Palmieri L, & Palmieri F (2004) Identification of the mitochondrial GTP/GDP transporter in *Saccharomyces cerevisiae*. *J. Biol. Chem.* 279(20):20850-20857.

152. Amutha B, Gordon DM, Dancis A, & Pain D (2009) Nucleotide-dependent iron-sulfur cluster biogenesis of endogenous and imported apoproteins in isolated intact mitochondria. *Methods Enzymol.* 456:247-266.

153. Kuhnke G, Neumann K, Muehlenhoff U, & Lill R (2006) Stimulation of the ATPase activity of the yeast mitochondrial ABC transporter Atm1p by thiol compounds. *Mol. Membr. Biol.* 23(2):173-184.

154. Hausmann A, Samans B, Lill R, & Muhlenhoff U (2008) Cellular and mitochondrial remodeling upon defects in iron-sulfur protein biogenesis. *J. Biol. Chem.* 283(13):8318-8330.

155. Wilkins RG (1991) *Kinetics and mechanism of reactions of transition metal complexes* (VCH Publishers,New York).

156. Barja G (1998) Mitochondrial free radical production and aging in mammals and birds. eds Harman D, Holliday R, & Meydani M (Acad Sciences, New York), pp 224-238.

157. Turrens JF (1997) Superoxide production by the mitochondrial respiratory chain. *Biosci. Rep.* 17(1):3-8.

158. Barrientos A (2003) Yeast models of human mitochondrial diseases. *IUBMB Life* 55:85-95.

159. Irazusta V, Moreno-Cermeño A, Cabiscol E, Ros J, & Tamarit J (2008) Major targets of iron-induced protein oxidative damage in frataxin-deficient yeasts are magnesium-binding proteins. *Free Radic. Biol. Med.* 44(9):1712-1723.

160. Rouault TA & Tong W-H (2008) Iron–sulfur cluster biogenesis and human disease. *Trends Genet.* 24(8):398-407.

161. Schonauer MS & Dieckmann CL (2004) Mitochondrial genomics and proteomics. *Curr. Genomics* 5(7):575-588.

162. Lodi R, Tonon C, Calabrese V, & Schapira AHV (2006) Friedreich's ataxia: From disease mechanisms to therapeutic interventions *Antioxidants and Redox Signaling* 8(3-4):438-443.

163. Carraway MS, Suliman HB, Madden MC, Piantadosi CA, & Ghio AJ (2006) Metabolic capacity regulates iron homeostasis in endothelial cells. *Free Radic. Biol. Med.* 41(11):1662-1669.

164. Napoli E, Taroni F, & Coropassi GA (2006) Frataxin, iron–sulfur clusters, heme, ros, and aging. *Antioxidants and Redox Signaling* 8(3-4):506-516.

165. Hare D, Reedy B, Grimm R, Wilkins S, Volitakis I*, et al.* (2009) Quantitative elemental bio-imaging of Mn, Fe, Cu and Zn in 6-hydroxydopamine induced Parkinsonism mouse models. *Metallomics* 1(1):53-58.

166. Lee DW, Kaur D, Chinta SJ, Rajagopalan S, & Andersen JK (2009) A disruption in iron-sulfur center biogenesis via inhibition of mitochondrial dithiol glutaredoxin 2 may contribute to mitochondrial and cellular iron dysregulation in mammalian glutathione-depleted dopaminergic cells: Implications for Parkinson's disease. *Antioxid. Redox Signaling* 11(9):2083-2094.

167. Gerhardsson L, Blennow K, Lundh T, Londos E, & Minthon L (2009) Concentrations of metals, beta-amyloid and tau-markers in cerebrospinal

fluid in patients with Alzheimer's disease. *Dementia and Geriatric Cognitive Disorders* 28(1):88-94.

168. Jiang DL, Li XJ, Williams R, Patel S, Men LJ*, et al.* (2009) Ternary complexes of iron, amyloid-beta, and nitrilotriacetic acid: Binding affinities, redox properties, and relevance to iron-induced oxidative stress in Alzheimer's disease. *Biochemistry* 48(33):7939-7947.

169. Camaschella C, Campanella A, De Falco L, Boschetto L, Merlini R*, et al.* (2007) The human counterpart of zebrafish shiraz shows sideroblastic-like microcytic anemia and iron overload. *Blood* 110(4):1353-1358.

170. Lill R & Muhlenhoff U (2008) Maturation of iron-sulfur proteins in eukaryotes: Mechanisms, connected processes, and diseases. *Annu. Rev. Biochem.* 77:669-700.

171. Kielley WW & Kielley RK (1953) A specific adenosinetriphosphatase of liver mitochondria. *J. Biol. Chem.* 200:213-222.

172. Siekevitz P & Potter V (1953) The adenylate kinase of rat liver mitochondria. *J. Biol. Chem.* 200:187-196.

173. Sanger F, Air G, Barrell B, Brown N, Coulson A*, et al.* (1977) Nucleotide sequence of bacteriophage phi x174 DNA. *Nature* 265(5596):687-695.

174. Wilkins MR, Pasquali C, Appel RD, Ou K, Golaz O*, et al.* (1996) From proteins to proteomes: Large scale protein identification by two-dimensional electrophoresis and arnino acid analysis. *Nat Biotech* 14(1):61-65.

175. Ghaemmaghami S, Huh W, Bower K, Howson RW, Belle A*, et al.* (2003) Global analysis of protein expression in yeast. *Nature* 425(6959):737-741.

176. Huh WK, Falvo JV, Gerke LC, Carroll AS, Howson RW*, et al.* (2003) Global analysis of protein localization in budding yeast. *Nature* 425(6959):686-691.

177. Fiehn O (2001) Combining genomics, metabolome analysis, and biochemical modelling to understand metabolic networks. *Comp. Funct. Genomics* 2(3):155-168.

178. Gavin CE, Gunter KK, & Gunter TE (1999) Manganese and calcium transport in mitochondria: Implications for manganese toxicity. *Neurotoxidty.*20(2-3):445-453.

179. Tuckey RC, McKinley AJ, & Headlam MJ (2001) Oxidized adrenodoxin acts as a competitive inhibitor of cytochrome P450scc in mitochondria from the human placenta. *Eur. J. Biochem.* 268(8):2338-2343.

180. Hewitson KS, Ollagnier-de Choudens S, Sanakis Y, Shaw NM, Baldwin JE*, et al.* (2002) The iron-sulfur center of biotin synthase: Site-directed mutants. *Journal of Biological Inorganic Chemistry* 7(1-2):83-93.

181. Haile DJ, Rouault TA, Tang CK, Chin J, Harford JB, & Klausner RD (1992) Reciprocal control of RNA-binding and aconitase activity in the regulation of the iron-responsive element binding-protein - role of the iron-sulfur cluster. *Proc. Natl. Acad. Sci. U. S. A.* 89(16):7536-7540.

182. Henze K & Martin W (2003) Evolutionary biology: Essence of mitochondria. *Nature* 426(6963):127-128.

183. Muhlenhoff U & Lill R (2000) Biogenesis of iron-sulfur proteins in eukaryotes: A novel task of mitochondria that is inherited from bacteria. *Biochimica et Biophysica Acta-Bioenergetics* 1459(2-3):370-382.

184. Brito OM & Scorrano L (2008) Mitofusin 2 tethers endoplasmic reticulum to mitochondria *Nature* 456(7222):605-610.

185. Toyoshima S, Watanabe F, Saido H, Miyatake K, & Nakano Y (1995) Methylmalonic acid inhibits respiration in rat-liver mitochondria. *J. Nutr.* 125(11):2846-2850.

186. *Mössbauer Spectroscopy Consultants. www.mossbauer.com Accessed 2010.*

187. *Royal Academy of Chemistry .Introduction to Mössbauer Spectroscopy. http://www.rsc.org/Membership/Networking/InterestGroups/MossbauerSpect/intro.asp Accessed 2010.*

188. Altshuler SA & Kozirev BM (1964) *Electron paramagnetic resonance* (Academic Press,New York).

189. Lindahl PA, Morales JG, Miao R, & Holmes-Hampton G (2009) Chapter 15 isolation of *Saccharomyces cerevisiae* mitochondria for Mössbauer, EPR, and electronic absorption spectroscopic analyses. *Methods Enzymol.* 456:267-285.

190. Sherman F (1991) Getting started with yeast. *Methods Enzymol.* 194:3-21.

191. Glick BS & Pon LA (1995) Isolation of highly purified mitochondria from *Saccharomyces cerevisiae*. *Mitochondrial biogenesis and genetics, pt a, Methods Enzymol*. 260: 213-223.

192. Diekert K, de Kroon A, Kispal G, & Lill R (2001) Isolation and subfractionation of mitochondria from the yeast *Saccharomyces cerevisiae*. Methods Cell Biol. 65:37-51.

193. Pelley JW, Garner CW, & Little GH (1978) Simple rapid biuret method for estimation of protein in samples containing thiols. *Anal. Biochem.* 86(1):341-343.

194. Guldutuna S, Zimmer G, Leuschner M, Bhatti S, Elze A*, et al.* (1999) The effect of bile salts and calcium on isolated rat liver mitochondria. *Biochimica et Biophysica Acta-Molecular Basis of Disease* 1453(3):396-406.

195. Polcic P, Sabova L, & Kolarov J (1997) Fatty acids induced uncoupling of *Saccharomyces cerevisiae* mitochondria requires an intact ADP/ATP carrier. *FEBS Lett.* 412(1):207-210.

196. Boyle GM, Roucou X, Nagley P, Devenish RJ, & Prescott M (1999) Identification of subunit g of yeast mitochondrial F1F0-ATP synthase, a protein required for maximal activity of cytochrome c oxidase. *Eur. J. Biochem.* 262(2):315-323.

197. Soubannier V, Vaillier J, Paumard P, Coulary B, Schaeffer J, & Velours J (2002) In the absence of the first membrane-spanning segment of subunit

4(b), the yeast ATP synthase is functional but does not dimerize or oligomerize. *J. Biol. Chem.* 277(12):10739-10745.

198. Olsen B & Markwell J (2007) Assays for the determination of protein concentration. *Current Protocols in Protein Science* 3.4:1-29.

199. Morales JG, Holmes-Hampton G, Miao R, Guo Y, Munck E, & Lindahl PA (2010) The iron-ome of mitochondria isolated from respiring and fermenting *Saccharomyces cerevisiae*. *Biochemistry. Accepted.*

200. Liao GL & Palmer G (1996) The reduced minus oxidized difference spectra of cytochromes a and a(3) *Biochimica et Biophysica Acta-Bioenergetics* 1274(3):109-111.

201. Teissier P, Perret B, Latrille E, Barillere JM, & Corrieu G (1996) Yeast concentration estimation and prediction with static and dynamic neural network models in batch cultures. *Bioprocess Eng.* 14(5):231-235.

202. Fiechter A & Seghezzi W (1992) Regulation of glucose metabolism in growing yeast cells. *J. Biotechnol.* 27:27-42.

203. Stoimenova M, Igamberdiev A, Gupta K, & Hill R (2007) Nitrite-driven anaerobic ATP synthesis in barley and rice root mitochondria. *Planta* 226(2):465-474.

204. Bro C, Regenberg B, Lagniel G, Labarre J, Montero-Lomeli M, & Nielsen J (2003) Transcriptional, proteomic, and metabolic responses to lithium in galactose-grown yeast cells. *J. Biol. Chem.* 278(34):32141-32149.

205. Meunier JR & Choder M (1999) *Saccharomyces cerevisiae* colony growth and ageing: Biphasic growth accompanied by changes in gene expression. *Yeast* 15(12):1159-1169.

206. Gao J, Opiteck GJ, Friedrichs MS, Dongre AR, & Hefta SA (2003) Changes in the protein expression of yeast as a function of carbon source. *J. Proteome Res.* 2(6):643-649.

207. Usaite R, Wohlschlegel J, Venable JD, Park SK, Nielsen J*, et al.* (2008) Characterization of global yeast quantitative proteome data generated from the wild-type and glucose repression *Saccharomyces cerevisiae* strains: The comparison of two quantitative methods. *J. Proteome Res.* 7(1):266-275.

208. Velagapudi VR, Wittmann C, Schneider K, & Heinzle E (2007) Metabolic flux screening of *Saccharomyces cerevisiae* single knockout strains on glucose and galactose supports elucidation of gene function. *J. Biotechnol.* 132:395-404.

209. Westergaard SL, Oliveira AP, Bro C, Olsson L, & Nielsen J (2007) A systems biology approach to study glucose repression in the yeast *Saccharomyces cerevisiae*. *Biotechnol. Bioeng.* 96(1):134-145.

210. Fuge EK, Braun EL, & Wernerwashburne M (1994) Protein-synthesis in long-term stationary-phase cultures of *Saccharomyces-cerevisiae*. *J. Bacteriol.* 176(18):5802-5813.

211. Jazwinski SM (2002) Growing old: Metabolic control and yeast aging. *Annual Reviews in Microbiology* 56:769-792.

212. Sellick CA, Campbell RN, & Reece RJ (2008) Galactose metabolism in yeast - structure and regulation of the leloir pathway enzymes and the genes encoding them. *International Review of Cell and Molecular Biology* 269:111-150.

213. Lopez-Lazaro M (2008) The Warburg effect: Why and how do cancer cells activate glycolysis in the presence of oxygen? *Anti-Cancer Agents Med. Chem.* 8(3):305-312.

214. Spurway NC (1992) Aerobic exercise, anaerobic exercise and the lactate threshold. *Br. Med. Bull.* 48(3):569-591.

215. Bertram JS (2000) The molecular biology of cancer. *Molecular Aspects of Medicine* 21(6):167-223.

216. Pelicano H, Martin DS, Xu RH, & Huang P (2006) Glycolysis inhibition for anticancer treatment. *Oncogene* 25(34):4633-4646.

217. Kim J-W & Dang CV (2006) Cancer's molecular sweet tooth and the Warburg effect. *Cancer Res.* 66(18):8927-8930.

218. McCammon MT, Epstein CB, Przybyla-Zawislak B, McAlister-Henn L, & Butow RA (2003) Global transcription analysis of Krebs tricarboxylic acid cycle mutants reveals an alternating pattern of gene expression and effects on hypoxic and oxidative genes. *Mol. Biol. Cell* 14:958-972.

219. Ohlmeier S, Kastaniotis AJ, Hiltunen JK, & Bergmann U (2004) The yeast mitochondrial proteome, a study of fermentative and respiratory growth. *J. Biol. Chem.* 279(6):3956-3979.

220. Usaite R, Nielsen J, & Olsson L (2008) Physiological characterization of glucose repression in the strains with SNF1 and SNF4 genes deleted. *J. Biotechnol.* 133(1):73-81.

221. Polakis ES, Bartley W, & Meek GA (1964) Changes in structure + enzyme activity of *Saccharomyces cerevisiae* in response to changes in environment. *Biochemical Journal* 90(2):369-&.

222. Polakis ES & Bartley W (1965) Changes in enzyme activities of *Saccharomyces cerevisiae* during aerobic growth on different carbon sources. *Biochemical Journal* 97(1):284-&.

223. Polakis ES, Bartley W, & Meek GA (1965) Changes in activities of respiratory enzymes during aerobic growth of yeast on different carbon sources. *Biochemical Journal* 97(1):298-&.

224. Egner A, Jakobs S, & Hell SW (2002) Fast 100-nm resolution three-dimensional microscope reveals structural plasticity of mitochondria in live yeast. *Proc. Natl. Acad. Sci. U. S. A.* 99(6):3370-3375.

225. Holmes-Hampton G, Garber-Morales J, Guo Y, Münck E, & PA L (2010) A nonheme high-spin ferrous pool in mitochondria from fermenting *Saccharomyces cerevisiae*. *Biochemistry Submitted*.

226. Wang H, Sauke T, Debrunner PG, & Chan SI (1988) The CO adduct of yeast cytochrome-C oxidase - Mössbauer and photolysis studies. *J. Biol. Chem.* 263(30):15260-15263.

227. Pikus JD, Studts JM, Achim C, Kauffmann KE, Munck E*, et al.* (1996) Recombinant toluene-4-monooxygenase: Catalytic and Mössbauer studies of the purified diiron and Rieske components of a four-protein complex. *Biochemistry* 35(28):9106-9119.

228. Swanson MA, Usselman RJ, Frerman FE, Eaton GR, & Eaton SS (2008) The iron-sulfur cluster of electron transfer flavoprotein-ubiquinone oxidoreductase is the electron acceptor for electron transfer flavoprotein. *Biochemistry* 47(34):8894-8901.

229. Dickson DPE & Berry FJ (1986) *Mossbauer spectroscopy* (Cambridge University Press,Cambridge).

230. Wikstrom M, Krab K, & Saraste M (1981) Proton-translocating cytochrome complexes. *Annu. Rev. Biochem.* 50:623-655.

231. Kent TA, Munck E, Dunham WR, Filter WF, Findling KL*, et al.* (1982) Mossbauer study of a bacterial cytochrome-oxidase - cytochrome c1aa3 from *Thermus thermophilus*. *J. Biol. Chem.* 257(21):2489-2492.

232. Miao R, Martinho M, Morales JG, Kim H, Ellis EA*, et al.* (2008) EPR and Mössbauer spectroscopy of intact mitochondria isolated from Yah1p-depleted *Saccharomyces cerevisiae*. *Biochemistry* 47(37):9888-9899.

233. Perkins GA, Song JY, Tarsa L, Deerinck TJ, Ellisman MH, & Frey TG (1998) Electron tomography of mitochondria from brown adipocytes reveals crista junctions. *J. Bioenerg. Biomembr.* 30(5):431-442.

234. Costa V, Amorim MA, Reis E, Quintaniha A, & Moradas-Ferreira P (1979) Mitochondrial superoxide dismutase is essential for ethanol tolerance of *Saccharomyces cerevisiae* in the post-diauxic phase. *Microbiology* 143:1649-1656.

235. Zhang Y, Lyver ER, Knight SAB, Pain D, Lesuisse E, & Dancis A (2006) Mrs3p, Mrs4p, and frataxin provide iron for Fe-S cluster synthesis in mitochondria. *J. Biol. Chem.* 281(32):22493-22502.

236. Courel M, Lallet S, Camadro JM, & Blaiseau PL (2005) Direct activation of genes involved in intracellular iron use by the yeast iron-responsive transcription factor Aft2 without its paralog Aft1. *Mol. Cell. Biol.* 25(15):6760-6771.

237. Paradkar PN, Zumbrennen KB, Paw BH, Ward DM, & Kaplan J (2009) Regulation of mitochondrial iron import through differential turnover of mitoferrin 1 and mitoferrin 2. *Mol. Cell. Biol.* 29(4):1007-1016.

238. Sivakumar R, Babu PVA, & Shyamaladevi CS (2008) Protective effect of aspartate and glutamate on cardiac mitochondrial function during myocardial infarction in experimental rats. *Chem.-Biol. Interact.* 176(2-3):227-233.

239. Lang G, Herbert D, & Yonetani T (1968) Mössbauer spectroscopy of cytochrome c. *J. Chem. Phys.* 49(2):944-&.

240. Foury F & Cazzalini O (1997) Deletion of the yeast homologue of the human gene associated with Friedreich's ataxia elicits iron accumulation in mitochondria. *FEBS Lett.* 411(2-3):373-377.

VITA

Jessica Hope Garber Morales

Contact:

Department of Chemistry
Mail Stop 3255
Texas A&M University
College Station, TX 77843

jgarber@mail.chem.tamu.edu

Education:

Ph.D. Chemistry, Texas A&M University. College Station, Texas. 2010.

B.S. Chemistry and Anthropology & Sociology, Virginia Commonwealth University. Richmond, Virginia. 2004.

Publications:

Morales, JG.; Holmes-Hampton, G; Miao, R.; Lindahl, PA. Comparison of the 'Fe-ome' of Mitochondria Isolated from Media Containing Glycerol, Galactose or Glucose. 2010. *Biochemistry. Submitted.*

Holmes-Hampton, GP.; Miao, R.; Morales, JG.; Guo, Y; Münck, E.; Lindahl PA. Analysis of a High Spin Fe2+ Pool in Mitochondria from *Saccharomyces cerevisiae*. 2010. Biochemistry. *Accepted.*

Lindahl, PA.; Morales, JG.; Miao, R.; Holmes-Hampton, GP. Isolation of *Saccharomyces cerevisiae* Mitochondria for Mössbauer, EPR and Electronic Absorption Spectroscopic Analyses. *Methods of Enzymology.* 2009. 456: 267-285.

Miao, R.; Morales, JG.; Martinho, M.; Stubna, A.; Lill, R.; Hendrich, MP.; Munck, E.; Lindahl, PA. EPR and Mössbauer spectroscopy of intact mitochondria isolated from Yah1p-depleted *Saccharomyces cerevisiae*. *Biochemistry.* 2008. 47(37): 9888-9899.

Hudder, BN.; Morales, JG.; Stubna, A.; Munck, E.; Hendrich, MP.; Lindahl, PA. Electron paramagnetic resonance and Mössbauer spectroscopy of intact mitochondria from respiring *Saccharomyces cerevisiae*. *Journal of Biological Inorganic Chemistry*. 2007. 12(7): 1029-1053.